Efficiency of floating floors on CLT or concrete plate in the low frequency region

Master's thesis in Master Programme Sound and Vibration

ANTON HERMANSSON

Department of Architechture and Civil Engineering
Chalmers University of Technology
Gothenburg, Sweden 2018

BOMX02-18-01

Efficiency of floating floors on CLT or concrete plate in the low frequency region

ANTON HERMANSSON

CHALMERS
UNIVERSITY OF TECHNOLOGY

Department of Architechture and Civil Engineering
Division of Sound and Vibration
Chalmers University of Technology
Gothenburg, Sweden 2018

Efficiency of floating floors on CLT or concrete plate in the low frequency region
ANTON HERMANSSON

Supervisor: Pontus Thorsson, Akustikverkstan, Lidköping
Examiner: Jens Forssén, Applied Acoustics, Chalmers, Gothenburg

BOMX02-18-01
Department of Architechture and Civil Engineering
Division of Sound and Vibration
Chalmers University of Technology
SE-412 96 Gothenburg
Telephone +46 31 772 1000

Cover: Floating floor construction

Typeset in LaTeX
Gothenburg, Sweden 2018

Efficiency of floating floors on CLT or concrete plate in the low frequency region
ANTON HERMANSSON
Department of Architechture and Civil Engineering
Chalmers University of Technology

Abstract

In order to fulfil requirements regarding impact sound insulation between two vertically adjacent rooms, a floating floor construction is a commonly used technique. However the understanding of the acoustical performance of the floor construction at low frequencies is limited. This thesis aims to evaluate which physical parameters in the different layers of a floating floor construction that are important for the improvement of impact sound insulation below 200 Hz. Two different kinds of base floors are tested, concrete and cross laminated timber, CLT.

The impact sound insulation improvement is evaluated using a numerical model developed in the finite element software COMSOL Multiphysics for extraction of vibration levels below the floor. The floor is considered being placed in an infinite baffle and the sound radiation is calculated using the Rayleigh integral.

Applying a floating floor to a structural plate of either concrete or CLT changes the radiated sound power from the floor in different ways. Below the mass-spring-mass resonance frequency created by the three layers, the efficiency of the floating floor is mainly controlled by how the modal content of the floor is changed, both in frequency and amplitude. Above the resonance the efficiency of the floating floor follows expected theoretical improvements to different extent.

The most important physical parameters in a floating floor construction are according to this study the stiffness of the interlayer as well as the density and thickness of the floating floor slab. The study shows that the density of the interlayer as well as the damping of the floating slab is less important for the efficiency of the floating floor.

When increasing the thickness or the density of the floating floor slab, the sound insulation improvement at the lowest frequencies ($f < 30$ Hz) is better for the CLT plate, attenuating the radiated sound power to almost the same amplitudes as for the corresponding concrete case. Above the floating floor resonance the slope of the sound insulation improvement is in general steeper for the concrete cases. However no other general tendency can be seen when studying the difference between applying the same floating floor construction to the different structural plates.

Keywords: Building acoustics, Impact sound insulation, Floating floor, Concrete, Cross laminated timber.

Acknowledgements

I want to express my gratitude to my supervisor Pontus Thorsson for his positive approach in general, but in particular for his inspiration and encouragement during the work with this thesis. A great thank you also to my fellow students and the staff at Applied Acoustics, including examiner Jens Forssén. My last two years at Chalmers have been characterized by collaboration "over the boarders" with a flat hierarchy, creating a great social working environment.

Anton Hermansson, Gothenburg, February 2018

Contents

1
Introduction

Building houses using wood has grown to be a common technique in construction. Several benefits arise from using a renewable and hence an environmentally sustainable source as material for houses. In Sweden where most parts are covered by forest, a particular opportunity show up to meet the needs of climate-friendly engineering. Since 1994 it is in Sweden allowed to use wooden structures for dwellings with 2 floors or more [8].

A lot of benefits follow the use of lightweight materials such as timber in construction compared to e.g. concrete or steel. A more sustainable way of building houses can be achieved as wood enables storage for carbon dioxide, the material is renewable and compared to other materials the energy needed for production is small. Instead of constructing a whole building with its parts on site, prefabrication of walls and floors etc. create shorter building times which are not as dependent on weather conditions. The cost for construction is also reduced thanks to this in addition to reduced waste on sites. The quality of the building parts can also be more controlled when produced in an industrial environment.

The acoustical behaviour of a lightweight wood floor has some drawbacks. Due to the low mass, both the airborne and impact sound insulation is poor at low frequencies. In addition when using timber floors in constructions, frequencies below 50 Hz are very important for disturbances from impact sounds. The peak energy of a footstep is typically around 15-30 Hz where a light weight wood floor often has its first resonance [4]. Recent inquiries on subjectively perceived impact sound level has indicated that frequencies down to 20 Hz is important for lightweight floors [3], and prediction methods for such low frequencies are needed. The building code and the standards used during construction and verification was developed at a time when lightweight material for construction purposes was not an option for residents with two floors or more [10]. The fact that standard measurements does not take into account frequencies below 50 Hz, makes the comparison between a heavy and a light construction with the same objective measurement irrelevant [14].

In many floor constructions for dwellings a floating floor construction is needed to fulfil the requirements regarding both airborne sound insulation and impact sound level. In the literature there exists many simplified models that can be used to predict the efficiency of floating floors at medium to high frequencies, but their precision is substantially reduced when moving to low frequencies.

In the literature there are also measurements of floating floor's efficiency down to 50 Hz. However, the efficiency is not correctly predicted at low frequencies by the simplified models mentioned above. This is due to shortcomings in theoretical assumptions in the models, material data, and in practical laboratory work (e.g. the limited size of laboratory floors with regards to important wavelengths at low frequencies). More understanding of the efficiency of floating floors at low frequencies is needed, and preferably with as few theoretical assumptions as possible.

1.1 Purpose

In order to gain understanding of the vibration and radiation behaviour, the purpose of this thesis is to investigate and evaluate the influence of different parameters on floating floor constructions with poor impact sound insulation.

1.2 Main objective

The main objective of the thesis is to show which physical parameters that are important for a floating floor's acoustic efficiency for frequencies below 200 Hz.

1.2.1 Intermediate objectives

- Show the floating floor's efficiency on different base floors, including orthotropic behaviour of the base floor.
- Show the difference of different floating floor materials.
- Relate the floating floor's efficiency to physical properties of the different parts (base floor, elastic interlayer, floating floor).
- Correlate the calculation model to measurements.

1.2.2 Limitations

- The frequency range to be studied is limited to frequencies below 200 Hz.
- The base plate is resting on its short edges with a simply supported boundary condition.

1.3 Floating floor constructions

A common way of improving the impact sound insulation, both vertically as well as horizontally for two adjacent rooms is to use a floating floor. The principle is that the top floor is "floating" on the base floor with an elastic layer in between. No adhesive or similar is used. Figure 1.1 shows two configurations of a floating floor. a) with a continuous elastic layer and b) with point bearing elastic mounts. The general terminology when discussing the floating floor construction and its different parts in the thesis is the one in case a).

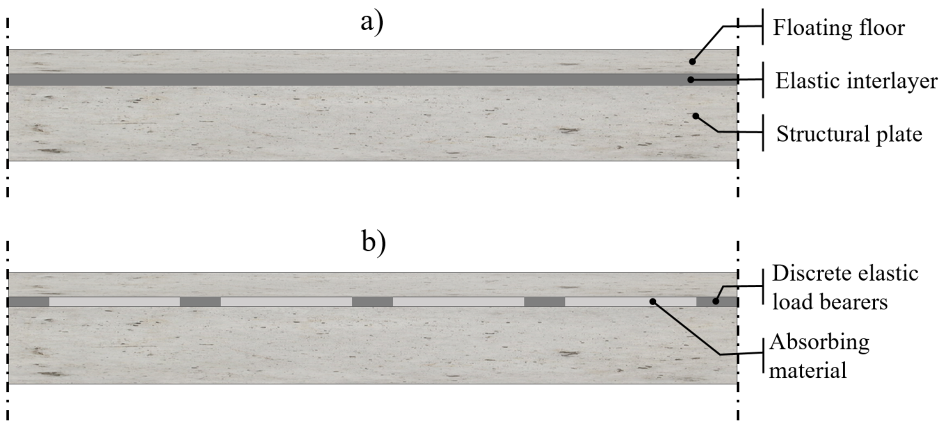

Figure 1.1: Two configurations of floating floors on concrete primary floor. Only a) is considered in the thesis, where a continuous elastic interlayer is used.

The elastic layer does usually consist of mineral wool of some kind, but also more rubber-like materials can be used. The floating floor can be a concrete plate, a gypsum board, chip board or another floorboard or parquet [20].

Theoretically the top layer, from now on termed the floor, can react to an input force in two ways, either locally or resonantly. Locally reacting means that the force is transmitted down to the primary floor only in the near of the point of excitation, while resonant reaction implies that a resonant bending wave field is created in the floor, causing transmission to the primary floor. Typically a lightweight floor such as gypsum boards is acting as a locally reacting floor due to its low stiffness and high internal losses. In that case the wave caused by the input force is quickly attenuated before arriving to boundaries of the floor and no resonance occur. A concrete floor however can be modeled as resonant reacting. A higher stiffness and lower losses causes the attenuation of waves much lower, and a resonant field can more easily be created [20].

Steindor Gudmundsson presents three different ways of modelling a floating floor in his report from 1984 [9]. The first two are the same previously discussed, locally reacting as well as resonant transmission. He compares measurements of impact sound insulation improvements from floating floors with the improvement formula stated by Cremer seen in Equation 1.1.

$$\Delta L = 40 \cdot \log\left(\frac{f}{f_0}\right) \tag{1.1}$$

where ΔL is the sound insulation improvement, i.e. the efficiency of the floating floor, and f_0 is the resonance frequency of the primary floor and the floating floor according to

$$f_0 = \frac{1}{2\pi}\sqrt{\frac{s}{m_1} + \frac{s}{m_2}} \tag{1.2}$$

where m_1 and m_2 are the mass per unit area of the two plates and s the stiffness of the interlayer. Equation 1.1 implies an increase of improvement of 12 dB/oct. Note that Equation 1.1 though only is valid for frequencies above f_0 and should not be expected to be applicable for the whole frequency range studied in the thesis. The derivation of Equation 1.1 is done assuming an infinite floor construction where the influence of resonances and near fields are not present [20].

When considering effects of the floating floor to be resonantly reacting as well as finite in size creating near field effects at boundaries, a corrected formula often cited is the one stated by Vér in 1969 shown in Equation 1.3.

$$\Delta L = 30 \cdot \log\left(\frac{f}{f_0}\right) \tag{1.3}$$

Considering Equation 1.3 the improvement of the floating floor is expected to increase by 9 dB/oct. Again this is however only expected above the double resonance frequency f_0.

The third way of evaluating the efficiency of a floating floor according to [9] is to see the elastic interlayer as a wave medium, i.e. the interlayer is not seen as only an ideal spring, but wave propagation in the layer is considered. The conclusion from this study is that "The most interesting properties are the loss factors of the different slabs and of the resilient layer, together with the dynamic stiffness of that layer".

Gudmundsson also presents a series of measurements for different configurations of all three layers in a floating floor construction. The results show quite good agreement with the analytical equations 1.1 and 1.3. However at low frequencies, i.e. in the frequency range studied in the thesis, various examples of measurements showing negative efficiency of the floating floor occur which indicate a worse impact sound insulation at these frequencies when adding a floating floor [9]. A reason proposed for this is that the resilience of the floating floor implies a slower rise of the input energy to the plate causing more low frequency energy getting in to the system [4].

The performance of the floating floor construction below and at the double resonance frequency is discussed in [17]. Below the double resonance the sound field created by the floating floor construction is to a large extent dependent on the bending wave field in the structural plate, hence the changes obtained by adding the floating floor is the changes in modal content of the plate. At the double resonance the vibrations are amplified, potentially causing more sound radiation at that frequency.

1.4 Cross laminated timber

Cross laminated timber, CLT, is a massive wood product built up by layers of single sawn timber panels. The layers are perpendicularly bonded together with the layer above and below most often using adhesive [19]. In the 2000's the product has been used for construction more and more. The product is lighter compared to brick or concrete with a density of about $470\,\mathrm{kg/m^3}$ [18]. The thickness of the plate is variable by choosing different number of layers. An odd number of layers is usually used, making the outer layers end up in the same direction for better strength, and high static stiffness in all directions can be achieved. The standard range of thickness is about 60-500 mm, maximum width of 3 m and length of 24 m. The plates can be used as both floors and walls bearing loads. The principle build up of a CLT plate is shown in Figure 1.2.

Figure 1.2: CLT plate construction [13].

2

Theory

This section starts with the most fundamental parts of structural acoustics, i.e. the oscillation of a simple mass-spring system with one degree of freedom. Thereafter applied plate and wave theory is treated, along with phenomena as damping and sound radiation. Lastly a brief description of the finite element method, FEM, is included.

2.1 Mass-spring system

The most elemental dynamic system is the one of a mass-spring system of one degree of freedom containing a mass, a spring and an exciting force, see Figure 2.1.

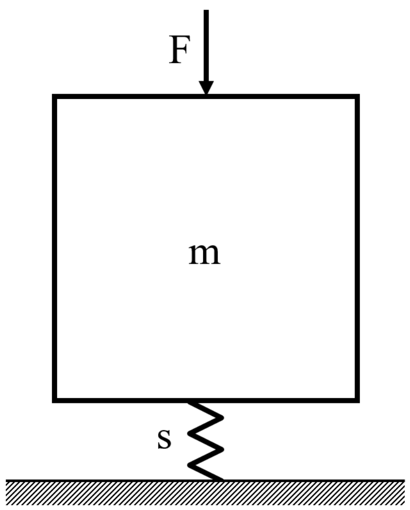

Figure 2.1: Mass spring system with one degree of freedom with exciting force.

Writing down the equation of the force balance for such a system the following is obtained [15].

$$m\ddot{\xi}(t) + s\xi(t) = F(t) \tag{2.1}$$

where m is the mass, ξ the vertical displacement, s the stiffness and F the force. Assuming harmonic excitation on the form $F = \hat{F}e^{j\omega t}$ and hence harmonic displacement $\xi = \hat{\xi}e^{j\omega t}$ together with Equation 2.1 and the fact that a derivative is equivalent to multiplication with $j\omega$ in the frequency domain, the following is obtained.

$$-m\omega^2\xi + s\xi = F \tag{2.2}$$

The relation between the exciting force F and the resulting displacement can now be formulated. This ratio is known as the receptance and is shown in Equation 2.3.

$$\frac{\xi(\omega)}{F(\omega)} = \frac{1}{-\omega^2 m + s} \tag{2.3}$$

The receptance is a frequency response function that reveals the displacement response for each frequency given a certain excitation force. In the thesis however the quantity that will be used for expressing the dynamic behaviour of a system will be the mobility, $Y(\omega)$, which is obtained by taking the first derivative of the receptance. The mobility is hence the ratio between the exciting force and the resulting velocity according to Equation 2.4. This is also the inverse of the mechanical impedance $Z = \frac{F}{v}$ [15].

$$Y(\omega) = \frac{v(\omega)}{F(\omega)} = \frac{1}{j\omega m + \frac{s}{j\omega}} \tag{2.4}$$

In order to introduce losses in the system, different models can be used. The damping can e.g. be modelled as dependent on velocity of the mass, i.e. a viscous damper, or the displacement of the mass. A damping model depending on the displacement of the solid is used by making the stiffness complex according to

$$s' = s(1 + j\eta) \tag{2.5}$$

where η is the loss factor, used extensively in the thesis. Applying the complex stiffness to the mobility ratio the following is obtained

$$Y(\omega) = \frac{v(\omega)}{F(\omega)} = \frac{1}{j\omega m + \frac{s}{j\omega}(1 + j\eta)} \tag{2.6}$$

At some frequencies the velocity amplitude gets very high even with a small input force. These frequencies are called resonance frequencies. Mathematically these occur when the imaginary part in the denominator of the mobility expression is zero. The amplitudes at the resonances depend on the amount of damping in the system, the more damping the smaller amplitude and vice versa.

The half power bandwidth method can be used to estimate the loss factor using Equation 2.7

$$\eta = \frac{\Delta f}{f_n} \tag{2.7}$$

where Δf is the size of the frequency interval where a 3 dB attenuation is obtained from a resonance top with its peak at frequency f_n.

2.2 Kirchhoff plate theory

For a thin plate the theory presented by Kirchhoff can be applied. It is based on the same assumptions as Euler theory for beams, i.e. no rotational inertia occur and the cross sections occur straight during deformation [1]. The wave equation for a Kirchhoff plate is shown in Equation 2.8.

$$B_x \frac{\partial^4 \eta}{\partial x^4} + B_{xy} \frac{\partial^2 \eta}{\partial x \partial y} + B_y \frac{\partial^4 \eta}{\partial y^4} + m \frac{\partial^2 \eta}{\partial t^2} = 0 \tag{2.8}$$

where B_x and B_y is the bending stiffness of the plate in the x and y direction respectively and B_{xy} is a mixed stiffness-term, η is the vertical displacement on the plate located in the x-y-plane and m is the mass per unit area.

The bending stiffness is dependent on the material i.e. the Youngs modulus, E, and the inertia I according to

$$B = \frac{EI}{(1 - \mu^2)} \tag{2.9}$$

where $I = \frac{h^3}{12}$ with h as the thickness of the plate. μ is the Poissons number and can be different in different directions.

The stiffness of an isotropic material is the same in all directions, hence B_x and B_y is the same. However an anisotropic material can have different stiffness in different directions. A special case concerning this is an orthotropic material where the stiffness is different in perpendicular directions, B_x, B_y and B_z [15].

The solution to the wave equation gives a wave field consisting of bending waves, which is the most important type of wave in solids when it comes to acoustics. This is because of the displacement in normal direction of the plate, causing sound radiation [7]. The bending wave speed of the plate is shown in Equation 2.10.

$$c_B = \sqrt[4]{\frac{B}{\rho h} \omega^2} \tag{2.10}$$

where ρ is the density and h is the thickness of the plate. As seen in Equation 2.10 the bending wave speed are dependent on frequency, i.e. the waves are dispersive.

Apart from the bending wave field on the plate the total wave field also consist of bending near fields, which occur at boundaries and other discontinuities such as excitation points.

2.3 Modes in rectangular plates

To describe the wave field on a thin plate, e.g. the velocity distribution over all x and y coordinates, the modal components of the structure can be summed up. A modal component is a combination of a mode shape function, Φ_n, and corresponding resonance frequency, ω_n (eigenfrequency). These parameters are dependent on the combination of geometry, boundary conditions and material properties of the structure. To describe the wave field of a structure using modal components is convenient, since the contribution from each mode can be summed up to a total resulting wave field. This is possible because of the orthogonal property of the modes, i.e. the energy in one mode is independent of energy in another mode. For a rectangular plate simply supported on all four sides the mode shape functions can be obtained analytically according to Equation 2.11.

$$\Phi_n(x,y) = sin\left(\frac{n_1 \pi x}{W}\right) sin\left(\frac{n_2 \pi y}{L}\right) \tag{2.11}$$

where n_1 and n_2 are integers from 1, 2, 3... representing every mode. W and L are the dimensions of the plate. The corresponding eigenfrequency can be obtained using the same set of integers n_1 and n_2 according to Equation 2.12.

$$\omega_n = \sqrt{\frac{B}{m}} \left[sin\left(\frac{n_1 \pi}{W}\right)^2 sin\left(\frac{n_2 \pi}{L}\right)^2 \right] \tag{2.12}$$

where B is the bending stiffness and m is the mass per unit area of the plate. Using the expressions in Equation 2.11 and 2.12 the total velocity field on the plate can be obtained including damping, η, and a point excitation F on the location (x_0, y_0) according to Equation 2.13.

$$v(x,y,\omega) = j\omega \frac{4}{mWL} \sum_n \frac{F sin\left(\frac{n_1 \pi x_0}{W}\right) sin\left(\frac{n_2 \pi y_0}{L}\right) sin\left(\frac{n_1 \pi x}{W}\right) sin\left(\frac{n_2 \pi y}{L}\right)}{\omega_n^2 (1 + j\eta) - \omega^2} \tag{2.13}$$

Figure 2.2 shows the summation of the four first modes in a rectangular plate. Note that the graphs only plot the amplitude and not the phase, whereas the summation is done including the phase.

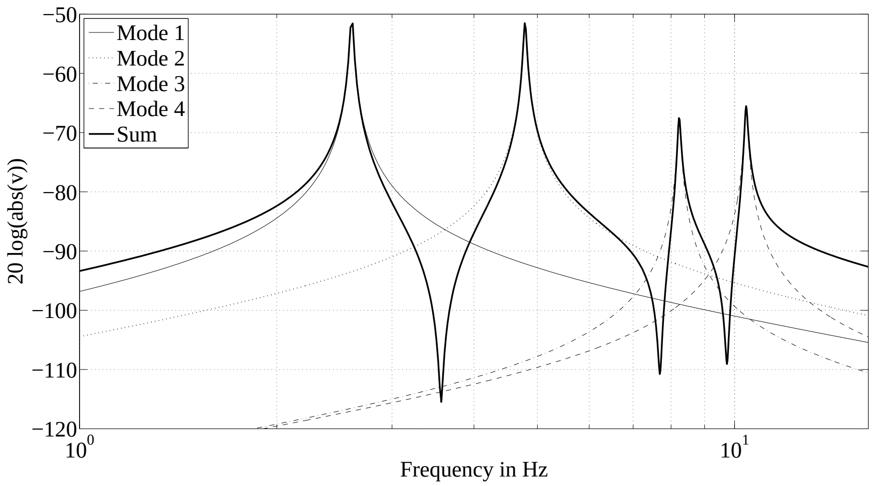

Figure 2.2: Summation of the four first modes in rectangular simply supported plate.

2.4 Sound radiation

The radiated sound from a plate is highly dependent on frequency. This has to do with the previously mentioned fact that the wave speed in the plate is dependent on frequency. There is one frequency where the bending wave speed in the plate is equal to the speed of sound in air, the critical frequency, f_c. This can be obtained by replacing the bending wave speed with the speed of sound in air, c_0, according to Equation 2.14 [7].

$$f_c = \frac{c_0^2}{2\pi}\sqrt{\frac{m''}{B}} \tag{2.14}$$

where m'' is the mass per unit area of the plate. Below the critical frequency the sound radiation is zero for an infinite plate. This is because the wavelength in air in that case is shorter than the bending wavelength on the plate and only cancellation of air close to the plate occurs. However for a finite plate the boundaries and other discontinuities and their consequence bending near fields still contribute to radiated sound, since cancellation of air cannot be completed at these locations [2].

For the case when having an orthotropic plate, i.e. different stiffness in different directions, there are two critical frequencies, $f_{c,x}$ and $f_{c,y}$ respectively [12]. A common way of treating this is to calculate an effective critical frequency $f_{c,eff}$ according to Equation 2.15.

$$f_{c,eff} = \sqrt{f_{c,x} f_{c,y}} \tag{2.15}$$

A convenient way of describing the radiation from a structure is using the radiation efficiency, σ. When using σ the actual radiated power, W_{rad}, is compared to the power radiated from a baffle with the same size S, moving with the space averaged velocity, $\langle v_{rms}^2 \rangle$, of the considered plate according to

$$\sigma = \frac{W_{rad}}{\rho c S \langle v_{rms}^2 \rangle} \tag{2.16}$$

where ρ and c is the density and speed of sound in air. The radiation efficiency for an infinite and a finite plate is shown in Figure 2.3. As observed, no radiation occurs below the critical frequency for an infinite plate, but for a finite plate some radiation occur below the critical frequency.

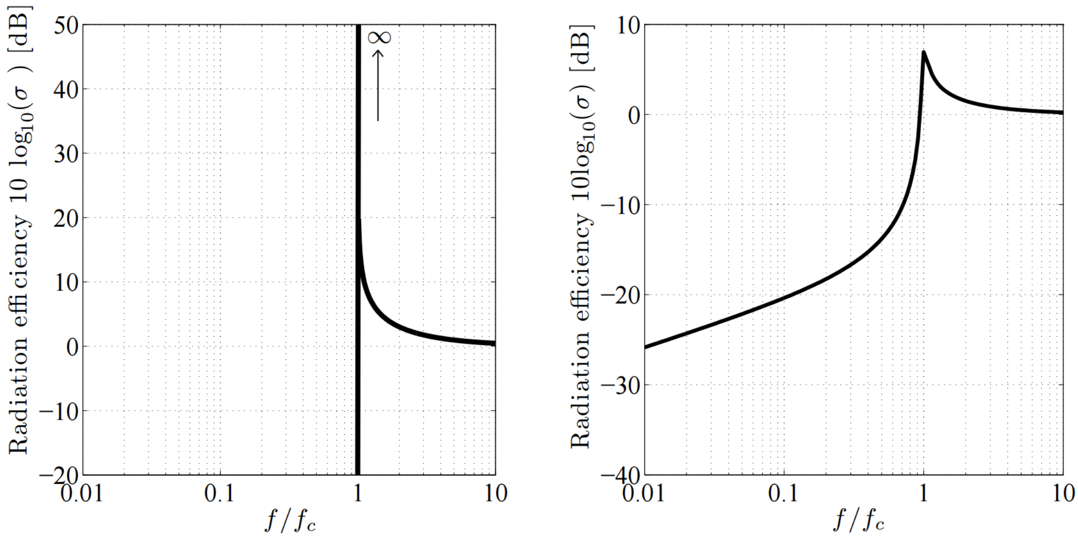

Figure 2.3: Radiation efficiency of an infinite plate (*left*), no radiation occurs below critical frequency. Radiation efficiency of a finite plate (*right*), radiation below critical frequency occurs. Figures from [2].

The frequency range studied in the thesis is mainly located below the critical frequency for the plates considered. The radiation efficiency can be hard to estimate in this region, therefore in the thesis the Rayleigh integral is used to calculate the radiated sound pressure from the plate, see Equation 2.17.

$$p(r) = \frac{j\omega\rho}{2\pi} \sum_i \frac{q_i}{r_i} e^{-jkr_i} \tag{2.17}$$

where $p(r)$ is the pressure at some distance r from the plate. The plate is (as later explained) divided into several volume sources. As seen in Equation 2.17 the contribution from each source q_i [m^3/s] with its unique distance to the receiver r_i is summed up to a total pressure. Note that this is the case for a baffled plate, since the denominator only contain 2π instead of 4π [6]. An illustration of the different variables included in Equation 2.17 is shown in Figure 3.11.

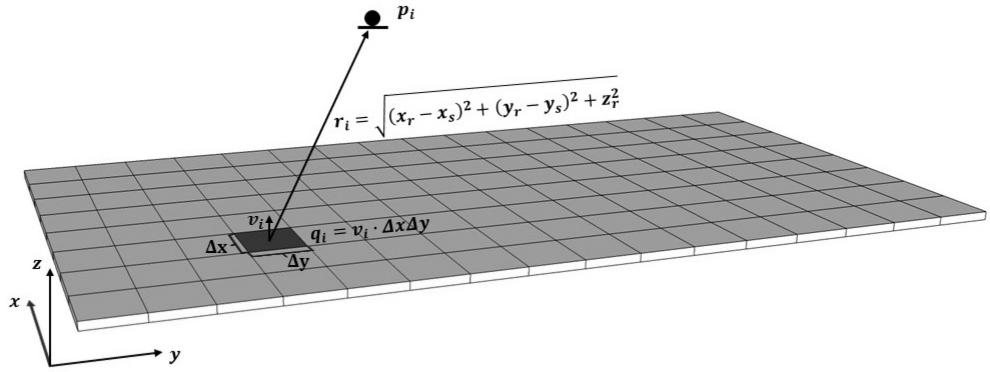

Figure 2.4: Illustration of Rayleigh integral variables. The plate is divided into discrete sections with dimensions Δx and Δy. Index r is referring to receiver and index s is referring to source.

The radiated sound intensity, I [W/m^2], can then be calculated from the radiated pressure using

$$I(r) = \frac{|p|^2}{\rho c} \tag{2.18}$$

where ρ and c are the density and speed of sound in air. In order to obtain the radiated sound power the intensity is multiplied by the area representing each receiver according to Equation 2.19, where S_i is the area for each receiver.

$$P = \sum_i I(r)_i S_i = \sum_i \frac{|p_i|^2}{\rho c} S_i \tag{2.19}$$

Observe also that the Rayleigh integral is a way of evaluating the sound pressure in the acoustic far field for a source with the characteristic size L. Three conditions have to be fulfilled in order for the receiver position to be in the far field [11].

- $r >> L$: The receiver has to be on a distance from the source much larger than the size of the source.
- $\frac{r}{L} > \frac{L}{\lambda_{air}}$: The phase of the sound wave coming from two different sources has to be the same.
- $r > \lambda_{air}$: The receiver has to be on a distance from the source such that plane wave impedance, ρc, is obtained.

2.5 Efficiency

In the thesis the main quantity evaluated is the so called efficiency, ΔL. Every floating floor construction is compared to the corresponding case when having only the structural plate. The efficiency is a measure of the improvement or the insertion loss of the floating floor according to Equation 2.20. The quantity compared is the radiated power to the space below the floor construction, with and without the floating floor.

$$\Delta L = 10 \cdot \log \left(\frac{P_{rad,withoutfloatingfloor}}{P_{rad,withfloatingfloor}} \right) \tag{2.20}$$

A positive efficiency is hence an improvement of the impact sound insulation.

2.6 FEM

The vibrational behaviour of the floor construction is evaluated using FEM, Finite Element Method. The general idea of FEM is to divide a large problem into a number of discrete sub-problems, finite elements, at which the exact solution is known. In between the known solutions at the nodes, the solution is approximated using interpolation of some degree that could be e.g. linear or quadratic. Furthermore these sub-problems are assembled applying continuity and equilibrium along with boundary conditions to solve a system of equations. In the thesis the commercial FEM software COMSOL Multiphysics is used for evaluating vibrations on different floor structures.

3

Implementation

The objectives of the thesis is reached by using a FEM model in the commercial software Comsol Multiphysics along with a sound radiation calculation script created by the author. The calculated results are compared to measurements conducted by the author and existing measurements as well as analytical calculations.

3.1 140 mm CLT-plate

The project starts by only studying one 140 mm CLT-plate in an attempt to find material properties for that specific plate. Later comparison with previous measurements on floating floors for that specific plate is conducted, making this initial study relevant.

Measurements of mobility

A series of measurements were conducted the 2nd of March 2016 at Akustikverkstan's acoustical laboratory in Skultorp, Skövde, Sweden. The purpose of the measurements was to investigate the vibrational behaviour of a simply supported CLT-plate. The input mobility at two different points were measured along with some transfer mobilities.

The objective is to gain an idea of what mobility levels can be expected in the corresponding modelled plate and in what direction the model should be adjusted in order to fit to a real case. I.e. the intention is not to do a full modal analysis of the plate, only to get an idea what kind of response that can be expected.

The mobility was measured using an impulse force hammer together with two accelerometers and a data acquisition system consisting of a sound interface and a computer with MATLAB. The input mobility was measured by exciting the structure with the hammer as close as possible, in this case 4 cm, to the accelerometer without risking hitting it directly. Hence a small phase difference between the force and acceleration can be expected. However at the frequencies considered this is negligible.

To investigate if the plate can be regarded as a thin plate, i.e. if it follows Kirchhoff plate theory, the acceleration was measured on the top of the plate as close as possible to the excitation point as well as at the corresponding x- and y-coordinates on the bottom of the plate.

The measurement setup is shown in Figure 3.1. Two excitation points were used together with two accelerometer points respectively. During the first measurement the transfer mobility was measured directly below the excitation as previously explained. When excitation point 2 was used, the transfer mobility accelerometer was kept at the same position, i.e. directly below the first excitation point. As seen in Figure 3.1 the plate is resting on two legs along the short sides. The legs are connected to the plate by two angle irons on each side.

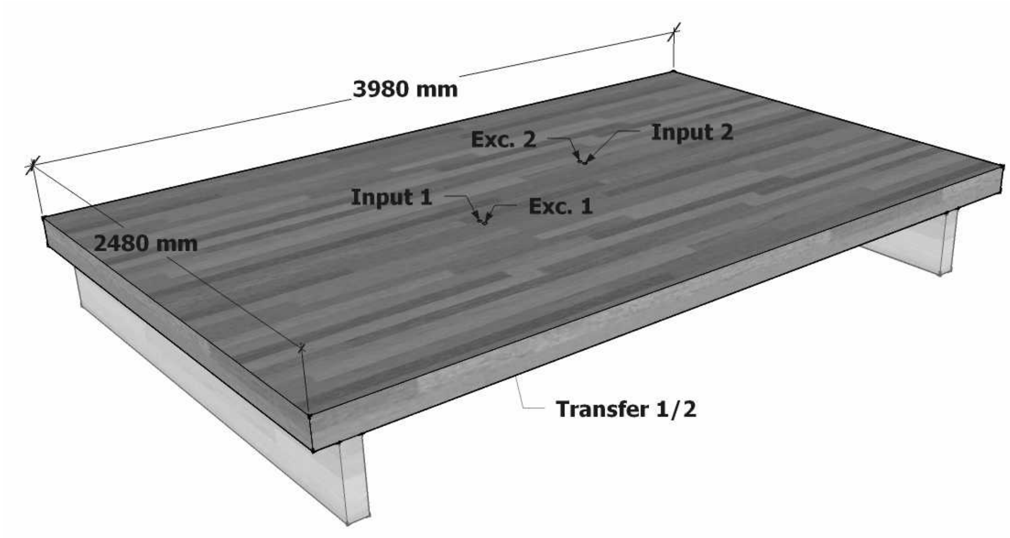

Figure 3.1: Plate dimensions, excitation points Exc. 1 and 2, as well as accelerometer points Input/Transfer 1 and 2.

The equipment used during the measurements is shown in Table 3.1.

Table 3.1: Measurement equipment specifications.

Item	Model	Serial no.	Last cal.
Impulse hammer	PCB Piezotronics 086D05	31461	2014-10-23
Accelerometer	B&K Type 4507	30845	2015-06-16
Accelerometer	B&K Type 4507	30990	2015-06-16
Sound interface	National Instruments NI 9234/NI cDAQ-9171	190DB0B	2016-02-17
Computer	HP ZBook 15		

The impulse force hammer comes with optional configurations depending on investigated surface and frequency range of interest. In this case the upper frequency limit is set to 200 Hz and therefore the choice ended up being the ”Super Soft” rubber tip together with a steel extender making the hammer heavier. Using this configuration the frequency response can be expected to be even up to 200 Hz where a -5 dB gain is found and further decreasing gain with increasing frequency.

A time bounded recording of 30 s was used where three impacts and the signals from the accelerometers were recorded into `MATLAB` with a spacing of approximately 4-5 s. The signals were then post processed in order to obtain mobilities.

In addition a measurement of the static deflection was made in order to estimate the stiffness of the plate in the long direction. This was made by measuring the distance from the plate to the floor with and without a man with the mass 108 kg standing on the plate.

Measurement data & results

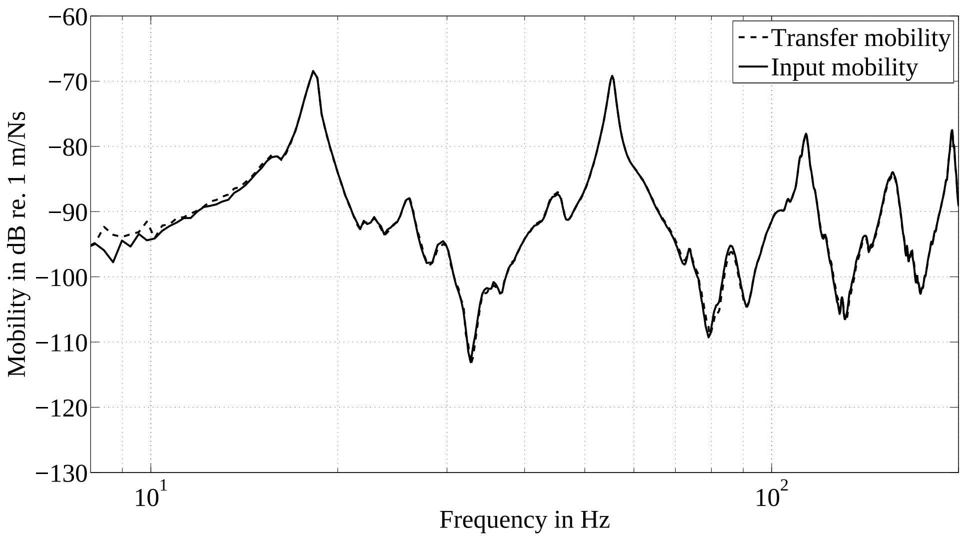

Figure 3.2: Input mobility 1 and transfer mobility 1 from excitation in point 1.

Figure 3.2 shows the mobility for the simply supported CLT plate. As seen there are clear resonances occurring at 18 Hz, 55 Hz and 113 Hz with anti-resonances and smaller resonances in between. The relative small decrease in amplitude when going up in frequency indicate low damping in the structure.

When comparing the two graphs in Figure 3.2 the input mobility correspond very well to the transfer mobility on the bottom of the plate. This indicate that the plate behaves homogeneously throughout the thickness and hence it holds as a Kirchoff plate.

Another indication of the Kirchhoff plate behaviour is the phase comparison between the input and transfer mobility in excitation point 1 shown in Figure 3.3 which shows a very good agreement of the phase from the two accelerometers.

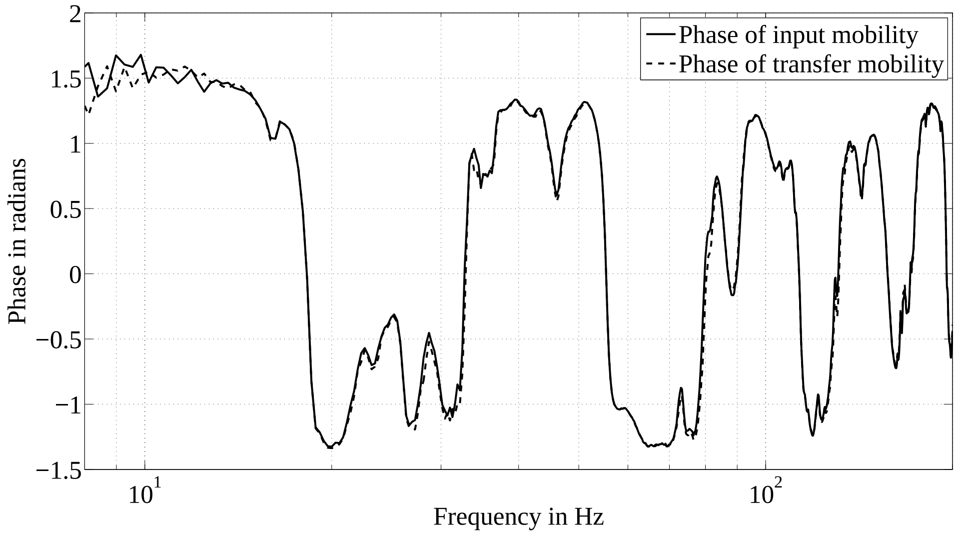

Figure 3.3: Phase of the input and transfer mobility from excitation point 1.

The loss factor of the CLT-plate is estimated using the half power bandwidth method for the different resonance tops of the input and transfer mobilities using Equation 2.7. The result is shown in Table 3.2.

Table 3.2: Calculation of loss factor using half power bandwidth method.

f_n **[Hz]**	Δf **[Hz]**	η [-]
18.2	0.7	0.039
55.4	1.2	0.022
113.4	2.6	0.023
156.5	6.8	0.044
196.9	3.1	0.016

As seen in Table 3.2 the damping is although different for different frequencies in general low. A mean value of the investigated frequencies would turn up to

$$\frac{0.039 + 0.022 + 0.023 + 0.044 + 0.016}{5} = 0.029 = 2.9\,\%$$

which indicate in what range the damping in the plate is located. This value is somewhat stretched in the following comparisons with the FEM calculations.

The static deflection test is used in order to get an idea of the value of the stiffness of the plate in the long direction, i.e. the y-direction. The measurement showed a deflection of the plate of 0.25 mm when adding a mass (person) of 108 kg. The plate is hence modelled as a beam in order to obtain the stiffness in the length direction. The conditions used for the calculation are listed in Table 3.3.

Table 3.3: Calculation conditions for static stiffness evaluation.

$P = mg = 108 \cdot 9.81\,\mathrm{N}$
$w = 0.25\,\mathrm{mm} = 0.25 \cdot 10^{-3}\,\mathrm{m}$
$L = 3.43\,\mathrm{m}$
$I = \frac{bh^3}{12}$
$h = 0.140\,\mathrm{m}$
$b = 2.48\,\mathrm{m}$

The vertical deflection in the middle of the plate is given by elemental case for simply supported beam. The stiffness is calculated using the measured deflection according to

$$w = \frac{PL^3}{48EI} \Rightarrow E = \frac{PL^3}{48wI} = \frac{108 \cdot 9.81 \cdot 3.43^3}{48 \cdot 0.25 \cdot 10^{-3} \cdot \frac{2.48 \cdot 0.140^3}{12}} = 6.29 \cdot 10^9\,\mathrm{Pa}$$

As seen in the stiffness investigation of the static deflection this deviate significantly from the expected value from tables on $12 \cdot 10^9$ Pa. However this goes in the "right" direction when it comes to the mobility measurement where the resonances are found lower in frequency in the measurements than calculations show.

3.2 COMSOL model

The FEM calculations in the thesis is conducted in the commercial software COMSOL Multiphysics, in which the Structural mechanics module is used. All models are built up using the 3D solid mechanics interface using linear elastic materials, which is based on solving Navier's equations for acquiring of displacements, stresses and strains [5].

In the thesis the extractions from the FEM calculations are the complex velocities on a discrete number of points forming a grid with a certain resolution on the underside of the floor construction. The excitation used in all cases is a point force with the amplitude 1 N applied on the upper side of the floor, see Figure 3.4. When modelling several layers, such as a floating floor construction, the different layers are modelled as a union, i.e. they are stuck together and will not be separated when exciting the floor with a force. The layers however can be modelled as different materials. In the thesis the most common way is to treat every layer as isotropic, i.e. the same properties hold for all directions x, y and z. The CLT plate model is however deviating from this principle, as it is modelled as orthotropic with different stiffness, i.e. Young's modulus as well as shear modulus, in x, y and z directions. Figure 3.4 shows the general model setup.

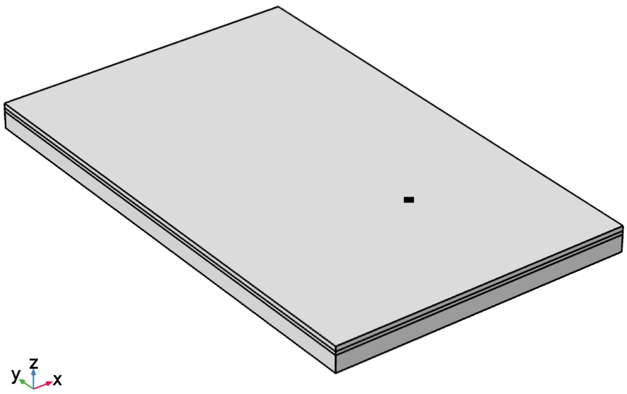

Figure 3.4: General model setup in COMSOL. The black dot indicate location of the point force applied on the upper side of the floor.

The resolution of the mesh as well as the resolution of the extraction grid of the velocity field on the underside of the floor is chosen with regards to a 10 elements-per-wavelength principle. In the frequency ranges studied the wavelength is checked for both bending waves in the floor as well as the sound waves in air. The shortest wavelength sets the largest element size allowed in the mesh. The velocity field grid is constructed so that a whole number of elements fit to the plate dimension, rounded up to the safe side so that the 10 elements-per-wavelength is not violated. Figure 3.5 shows an example of a floating floor construction meshed with a resolution fulfilling the demand for a frequency range up to 200 Hz.

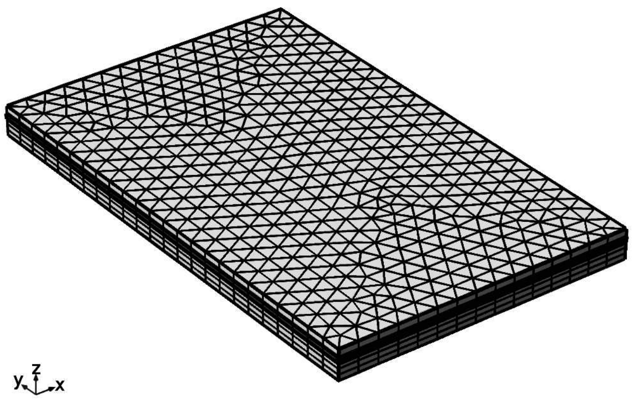

Figure 3.5: Meshed floating floor construction in COMSOL. The elastic interlayer is shown as thick black.

As stated in the limitations the boundary conditions for parameter study is for the plate simply supported only on its short edges. Hence the long edges are modelled as free - free. Specifically the simply supported boundary condition is set up as prescribed displacements along the lower edges. On one of the sides no translation is allowed, however on the opposite side translation is allowed in one direction, in this case the y-direction, see Figure 3.6. Rotation around the x-axis is allowed on both sides, hence the supports does not contribute with any torque on the plate. However when comparing the FEM model to both analytical calculations and existing measurements the boundary conditions are adapted to the corresponding cases, i.e. simply supported on all four sides of the floor construction. The boundary conditions on the two top layers are free -free on all sides, hence the model relies on the only boundary condition set on the bottom plate.

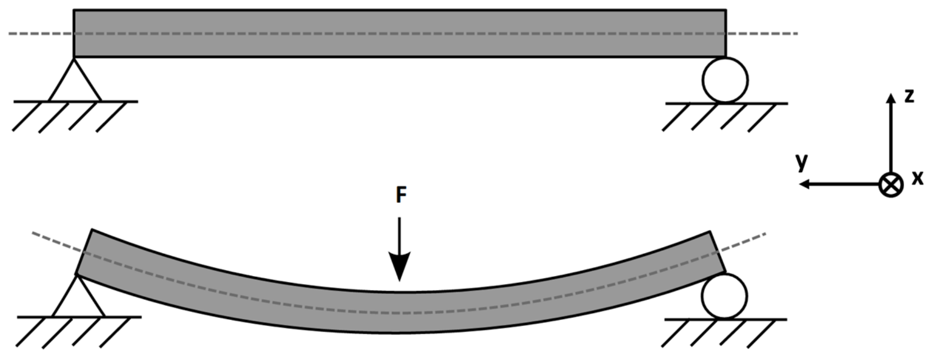

Figure 3.6: Simply supported beam. Rotation is allowed on both sides as well as translation in y-direction on one of the sides (rolling support).

COMSOL provides several models for introducing damping into the system. As mentioned in the theory section the damping model used in the thesis is a complex stiffness with an isotropic loss factor, η.

When using the frequency range 8-200 Hz as in most cases in the thesis, a resolution of 1 Hz is used when not stated differently.

3.2.1 Comparison FEM model, measurements and analytical model

An attempt to adapt the material properties as well as the boundary conditions of the plate is done using parametric sweeps in COMSOL. Each individual material property of the CLT-plate is tried in a reasonable interval to see the effect on the input mobilities in the two measurement points. The boundary conditions are also changed and tried in different configurations. As seen in Figure 3.1 the measured plate is resting on two legs with the same thickness as the plate itself. The model is tried both by including the legs and when not including the legs. A lot of uncertainty is included regarding the connection between the legs and the plate when it comes to e.g. torque coupling.

The results from this study show both satisfying and not so satisfying results. The measurement shows in general a less stiffer/heavier behaviour than the modelled results. The lowest resonance always end up below the calculated one and without going to unreasonable low stiffness in the plate a good adaptation to the measurement was not found. Figure 3.7 shows the resulting comparison between the mobility measurements made by the author and calculations. The boundary conditions are in this case applied to the included legs as simply supported against the floor, i.e. they are allowed to tilt when exciting the floor. The coupling between the legs and the plate are modelled as a union, i.e. they are stuck together.

The material properties used in the calculation are shown in Table 3.4.

Table 3.4: Material parameters of the CLT plate and the two legs used in calculation for comparison with the mobility measurements.

Parameter	**Value**
ρ	$450\,\mathrm{kg/m^3}$
(ν_x,ν_y,ν_z)	(0.1 0.1 0)
(E_x,E_y,E_z)	(1e9, 5e9, 1e9) Pa
(G_x,G_y,G_z)	$\frac{E}{2(1+\nu)}$ Pa
η [-]	0.035

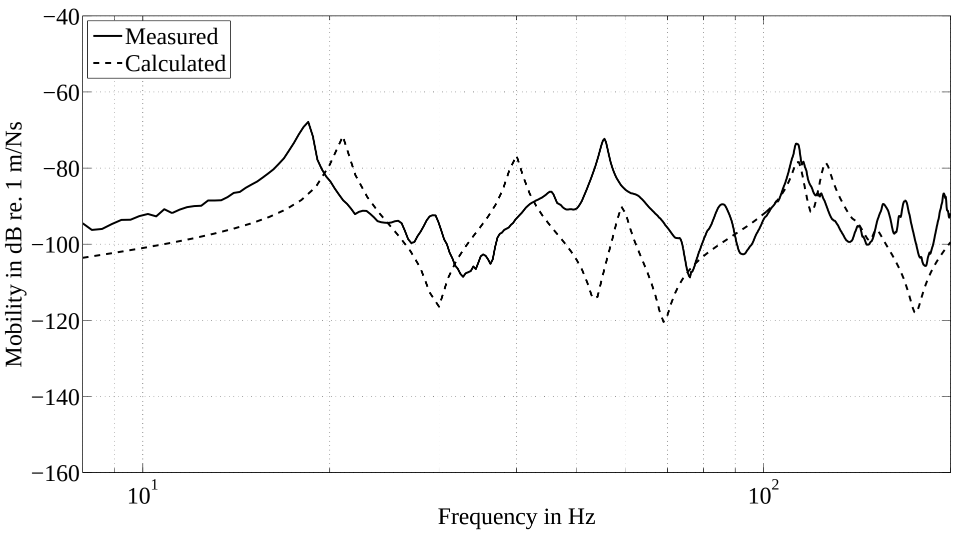

Figure 3.7: Comparison between best agreement achieved in modelling the CLT plate with the measurement results from excitation point 2.

The main reason for deviations when comparing the measured mobility and FEM-model is believed to be the coupling between the legs and the plate. The model treats the connections as rigid, while the real plate is attached to the legs using only two brackets on each side. This could explain the relatively lower amplitudes and the mismatch obtained in the model at the resonance at ca 60 Hz. This in addition to the material uncertainties can explain the overall deviations.

However it can be concluded that the modelled mobilities is in the correct range when it comes to levels and the overall resonant behaviour. Values of density, stiffness and damping in the CLT plate is believed to be reasonably found. After time consuming trial and error calculations, it was decided to move on with the model of an added covering floating floor.

Because of the partly not so satisfying agreement between mobility measurements and the FEM model, the model is also compared to an analytical case using modal superposition explained in the theory section. The case compared is a rectangular plate simply supported on all four sides. The analytical calculation is simplified in the sense that the plate is considered to be a 2-dimensional isotropic using a combination of the x and y stiffness of the FEM-model plate according to

$$E_{isotropic} = \sqrt{E_x E_y}$$

A frequency independent force with magnitude 1 N is used. Hence when using Equation 2.13 the resulting velocity is actually the same as the mobility. The same excitation point (x_0,y_0) and evaluation point (x,y) are used in the analytical model as well as the FEM model. Unlike the measurement comparison case, the boundary conditions in this case is simply supported on all four sides of the plate.

The material parameters used is shown in Table 3.5.

Table 3.5: Material parameters used in the comparison between FEM-model and analytical model.

FEM	*CLT plate*
ρ_{plate}	$450\,\mathrm{kg/m^3}$
ν_{plate} [X Y Z]	[0.1 0.1 0]
E_{plate} [X Y Z]	[1e9 5e9 1e9]Pa
G_{plate}	$\frac{E}{2(1+\nu)}$
η_{plate}	0.035
Analytical	*CLT plate*
ρ_{plate}	$450\,\mathrm{kg/m^3}$
ν_{plate}	0.1
E_{plate}	$\sqrt{5e9 \cdot 1e9}\,\mathrm{Pa}$
η_{plate}	0.035

The result is shown in Figure 3.8.

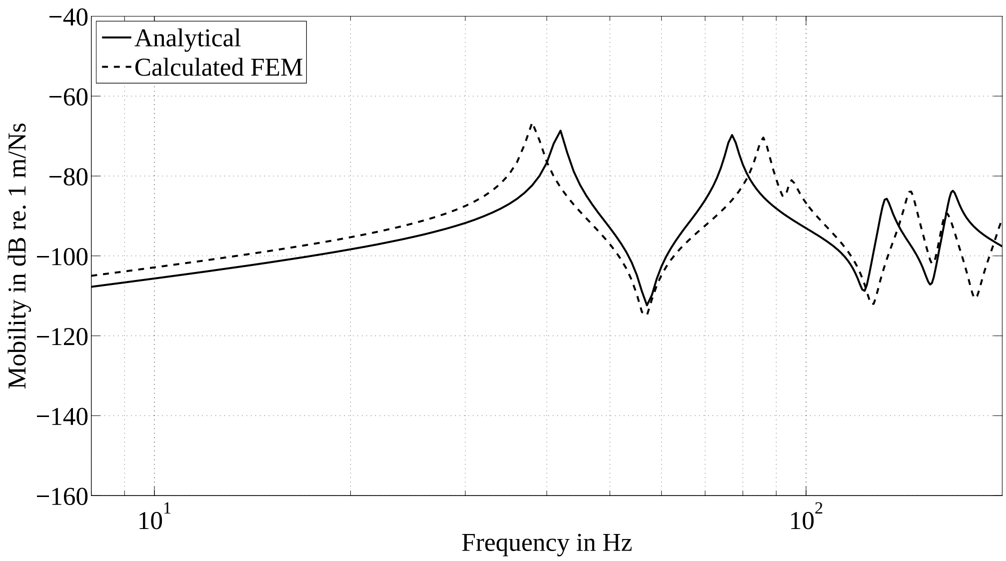

Figure 3.8: Comparison between FEM model of the CLT plate with analytical case.

As seen in Figure 3.8 the resonances are shifted up in frequency when having the boundary conditions set to simply supported on all four sides of the plate. The agreement is better when comparing the FEM result with the analytical case. The resonance frequencies as well as the resulting amplitudes show good agreement, which indicate that the exported results from the COMSOL model is reliable and can hence be used as is further in the study.

3.2.2 Excitation point study

When exciting a plate only on one position it is very unlikely that all modes in the plate are excited. To get a more complete picture of the vibrational behaviour of the plate, more excitation points are needed. In order to reduce the calculation time of the parameter study, an excitation point study is conducted to find a number of excitation points giving a representative response, firstly for the CLT plate only and secondly for the complete floating floor construction. The model is symmetric along the mid y-axis, hence only half the plate is required in the test. Figure 3.9 shows the resulting set of excitation points used in the rest of the study. Three x-direction points and seven y-direction points create a 21-point grid of excitation points. Different combinations of points are tried and compared to the case when averaging the response when having all excitation points.

The following material parameters are used for the three layers:

Table 3.6: Material parameters used in the excitation point study.

Plate	*CLT*
ρ_{plate}	$450\,\mathrm{kg/m^3}$
ν_{plate} [X Y Z]	[0.1 0.1 0]
E_{plate} [X Y Z]	[1e9 5e9 1e9]Pa
G_{plate}	$\frac{E}{2(1+\nu)}$
η_{plate}	0.035
Interlayer	
$\rho_{elastic}$	$50\,\mathrm{kg/m^3}$
$\nu_{elastic}$	0.3
$E_{elastic}$	7e6 Pa
$t_{elastic}$	3 cm
$\eta_{elastic}$	0.25
Floor	*Concrete*
ρ_{top}	$2300\,\mathrm{kg/m^3}$
ν_{top}	0.15
E_{top}	29e9 Pa
t_{top}	4 cm
η_{top}	0.006

The total difference in average velocity level on the plate is investigated for the different cases in order to conclude how many excitation points is needed and not needed (due to e.g. symmetry). The average difference in velocity level, $\bar{L}_{v^2}$, as well as the standard deviation, σ, are evaluated according to Equation 3.1 and 3.2.

$$\bar{L}_{v^2} = \frac{\sum \Delta L_{v^2}(f)}{N_f} = \frac{\sum(L_{v^2,exc1}(f) - L_{v^2,exc2}(f))}{N_f} \tag{3.1}$$

$$\sigma = \sqrt{\frac{\sum(\Delta L_{v^2}(f) - \bar{L}_{v^2})^2}{N_f}} \tag{3.2}$$

where $L_{v^2,exc1}(f)$ and $L_{v^2,exc2}(f)$ is the average velocity level for each frequency for two different excitation points according to

$$L_{v^2} = 10 \cdot \log(|v|^2) \tag{3.3}$$

and N_f is the number of frequencies. A tolerance of 1 dB is set to acceptable deviation of the average difference in velocity level as well as standard deviation.

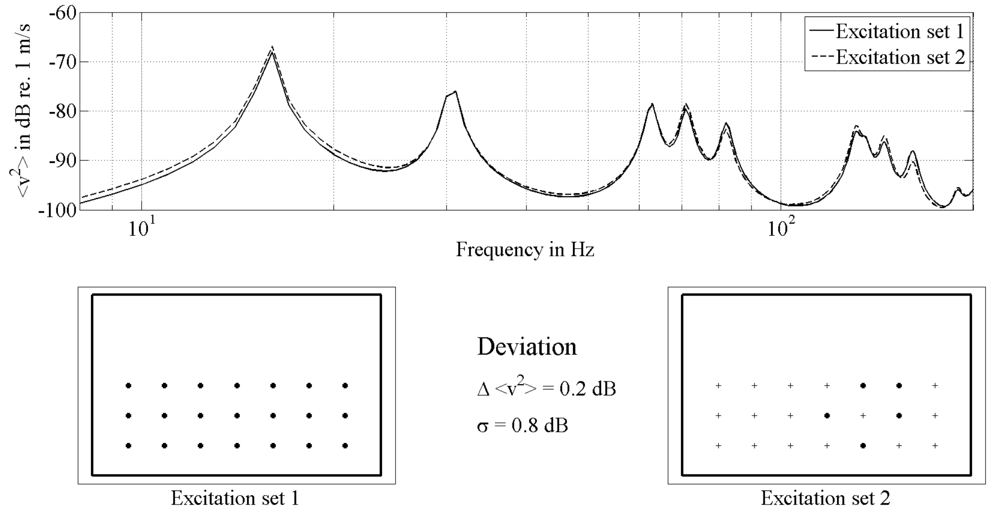

Figure 3.9: Space average velocity levels for different sets of excitation points on CLT plate. Highlighted bold points at plate are the active excitation points.

To the left in Figure 3.9 all excitation points are highlighted and the space averaged velocity level are plotted as a solid black line. On the right side the final set of excitation points are highlighted. The corresponding space averaged velocity level is plotted as a dashed black line in the same plot. The result shows that even though the boundary conditions are slightly different on each side, symmetry is obtained around the x-axis as well as the y-axis, hence only one quarter of the plate needs to be excited. The combination shown to the right in Figure 3.9 gives a tolerated response using 5 excitation points and is hence the excitation point set used from now on. Figure 3.10 shows the corresponding result from the floating floor case.

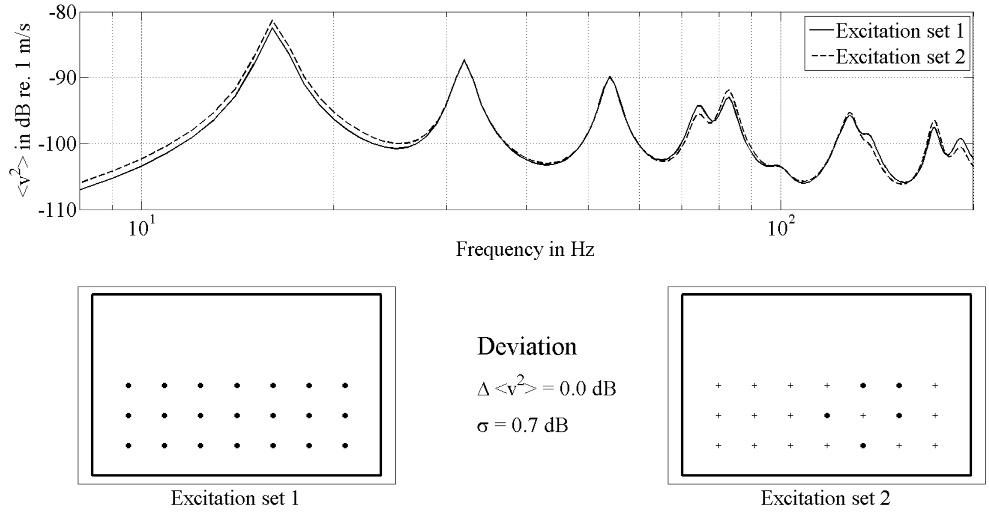

Figure 3.10: Average velocity levels on plate using different excitation point sets for floating floor construction.

The same set of excitation points ends up in the satisfying tolerance and is hence also used in the parameter study.

3.3 Sound radiation calculation

The sound radiation is calculated using a Rayleigh integral, see Equation 3.11, to a half sphere of receivers evenly spread out on a radius of 35 m which fulfil all requirements on far field positions stated in Section 2.4. The floor is regarded as being baffled, i.e. it is placed in an infinite rigid wall. The pressure at each receiver is summed up from the contribution from all sources on the plate. The plate itself is divided into several rectangular sources fulfilling a principle of 10 elements per wavelengths resolution. The requirement is checked both against the bending wavelength in the plate as well as the wavelength of sound waves in air. The resulting resolution for validity up to 200 Hz implies a grid of 24x15 sources on the plate. Figure 3.11 shows an illustration plot of the sound radiation calculation.

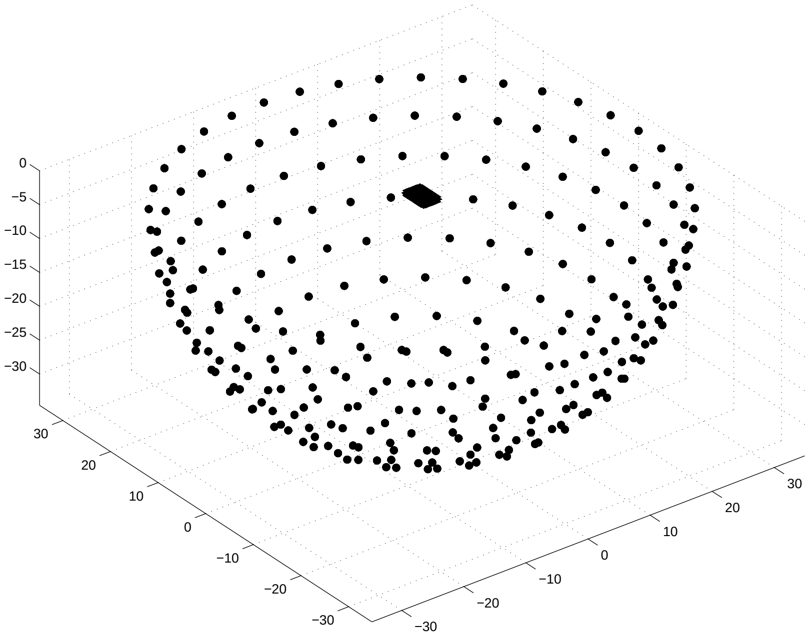

Figure 3.11: Illustration of the sound radiation calculation. The rectangular field in the middle is the velocity field points on the plate in a 24x15 grid. The black dots visualises the receiver points on a half sphere with radius 35 m.

The resulting pressure at each receiver is used to calculate the sound intensity using Equation 2.18. The half sphere of receivers is constructed such that every receiver has the same area, hence the sound power calculation can be conveniently calculated using the total intensity for the half sphere multiplied with the total area according to

$$P = S_{tot} \sum_i I(r)_i = 2\pi R^2 \sum_i I(r)_i \tag{3.4}$$

Each case for the floating floor construction is examined in comparison to the case when only considering radiation from the plate. The efficiency is hence the difference in radiated sound power for the two cases according to Equation 2.20.

3.4 Comparison floating floor constructions with analytical models and measurements

To correlate the calculation model to existing measurements of floating floor constructions, the corresponding setups and floor constructions used in measurements are applied in the COMSOL model. Firstly a model valid for an extended frequency range is developed to which measurements made by Gudmundsson [9] are compared. Secondly measurements made by Thorsson are compared in the frequency range studied in the thesis. The latter measurements are made using the same 140 mm CLT plate as in the measurements made by the author.

Gudmundsson measurements

A high resolution version of the parameter study model was developed using significantly more elements in the FEM-calculation as well as the sound radiation calculation. The frequency range was also extended in order to see how the floating floor behaves at frequencies up to 4 kHz. As this case took a lot more of calculation time, only three comparisons were made using a concrete plate as well as a concrete floating floor with an interlayer of mineral wool with three different thicknesses. The corresponding cases in Gudmundssons report [9] are found in cases I.3.9-I.3.11 in the appendix of that report. The parameters used in the calculation is shown in Table 3.7.

Table 3.7: Parameters used in calculation to compare with measurements and analytical models.

Plate	*Concrete*
W	2980 mm
L	4080 mm
t	160 mm
E	3e10 Pa
η	0.014
ρ	2400 kg/m^3
Interlayer	*Mineral wool*
t	***Case 1:*** 30 mm, ***Case 2:*** 60 mm, ***Case 3:*** 120 mm
E	0.4e6 Pa
η	0.2
ρ	50 kg/m^3
Floor	*Concrete*
t	50 mm
E	3e10 Pa
η	0.014
ρ	2400 kg/m^3

The results from the calculation are shown using 1/3 octave bands in Figures 3.12-3.14 along with measurements and analytical model stated by Vér found in Equation 1.3.

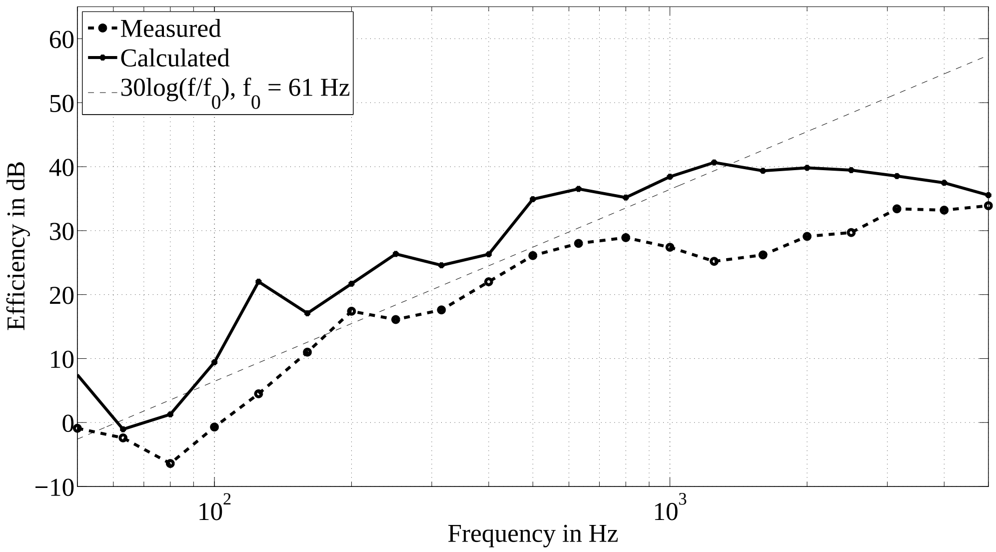

Figure 3.12: Case 1. Efficiency of the floating floor. FEM/Rayleigh calculation in comparison with analytical formula stated by Vér as well as measurement I.3.9 by Gudmundsson [9].

As seen in Figure 3.12 the model seems to behave reasonable for frequencies above the double resonance, f_0, where it follows the expected improvement of the impact sound insulation with 9 dB/oct which indicate some validity of the model. However the effect of applying the floating floor to the concrete plate is overestimated in the calculation when compared to the measurement over all frequencies. One believed reason for this could be that the interlayer is modelled as too soft compared to the real case, causing the double resonance ending up too low in frequency. As concluded later in the parameter study, the location of the double resonance is highly influencing the efficiency above it. A higher resonance would be pushing the calculated efficiency giving a better fit to the measurements.

Both the FEM results and the measurements deviate from the analytical expectations at about 1 kHz where the improvement flattens out. A proposed reason for this behaviour is that a standing wave resonance is created when the bending wavelength fits to the thickness of the elastic interlayer, causing transmission to a higher extent.

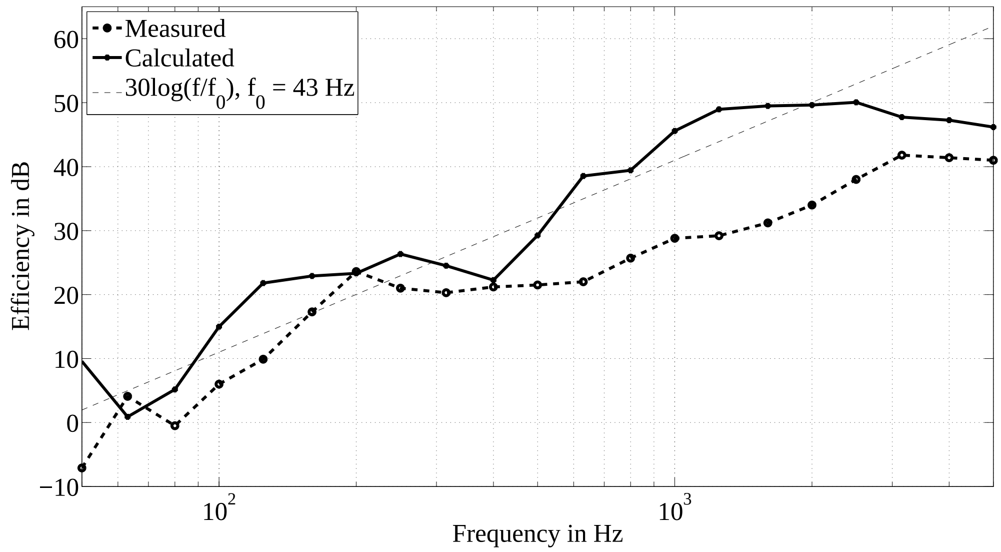

Figure 3.13: Case 2. Efficiency of the floating floor. FEM/Rayleigh calculation in comparison with analytical formula stated by Vér as well as measurement I.3.10 by Gudmundsson [9].

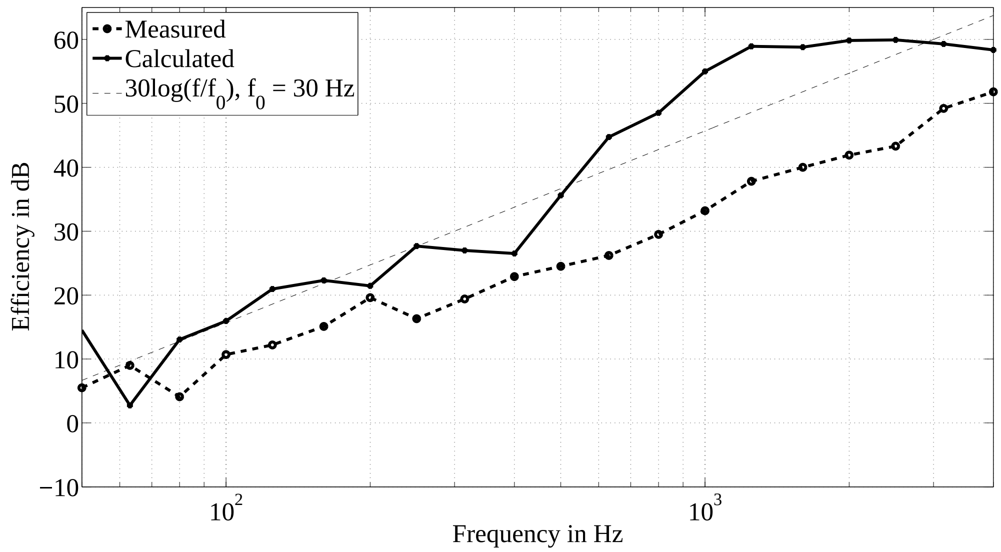

Figure 3.14: Case 3. Efficiency of the floating floor. FEM/Rayleigh calculation in comparison with analytical formula stated by Vér as well as measurement I.3.11 by Gudmundsson [9].

The two last cases show the same result where the FEM calculations overestimate the efficiency of the floating floor, especially for frequencies above 500 Hz. The calculated result agree better with the expected improvement of 9 dB/oct found in the analytical formula.

Thorsson measurements

Three different cases are investigated when comparing calculations to measurements made by Thorsson in the acoustical laboratory of Akustikverkstan in Skultorp, Skövde. The properties of each layer used in the calculations are shown in Table 3.8. Note that the FEM model is built up covering the whole structural plate with the floating floor construction, whereas the measurements was conducted covering only parts of the plate around the point of excitation. Deviations from the measurements can hence be explained partly for this reason.

Table 3.8: Parameters used in calculation to compare with measurements made by Thorsson. The three different cases have different thickness on the interlayer and the floor.

Plate	*CLT (Orthotropic)*
t	140 mm
$(E_x,\, E_y,\, E_z)$	(1e9, 5e9, 1e9) Pa
η	0.035
ρ	450 kg/m^3
$(G_x,\, G_y,\, G_z)$	$\frac{E}{2(1+\nu)}$ Pa
Interlayer	*Isover TDPT*
t	***Case 1:*** 20 mm, ***Case 2:*** 20 mm, ***Case 3:*** 45 mm
E	3e5 Pa
η	0.1
ρ	100 kg/m^3
Floor	*Concrete*
t	***Case 1:*** 50 mm, ***Case 2:*** 60 mm, ***Case 3:*** 60 mm
E	29e9 Pa
η	0.006
ρ	2300 kg/m^3
f_0	***Case 1:*** 97 Hz, ***Case 2:*** 94 Hz, ***Case 3:*** 62 Hz

The results are presented in 1/3 octave bands for the three cases in Figures 3.15-3.17.

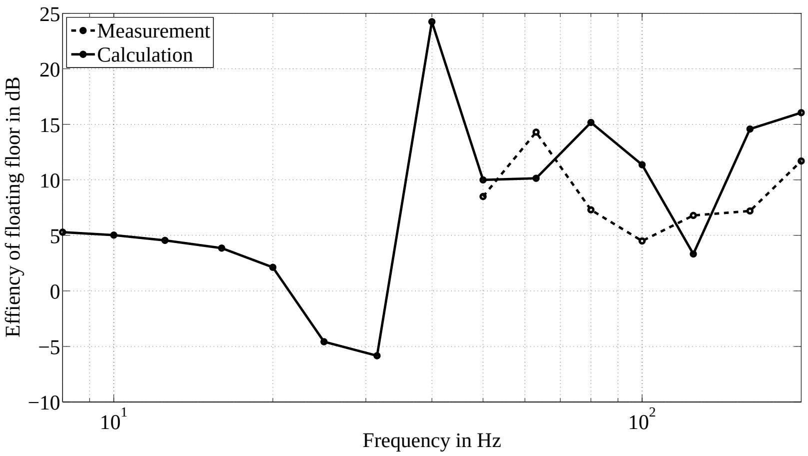

Figure 3.15: Calculations compared to measurements by Thorsson, case 1. See Table 3.8 for material parameters.

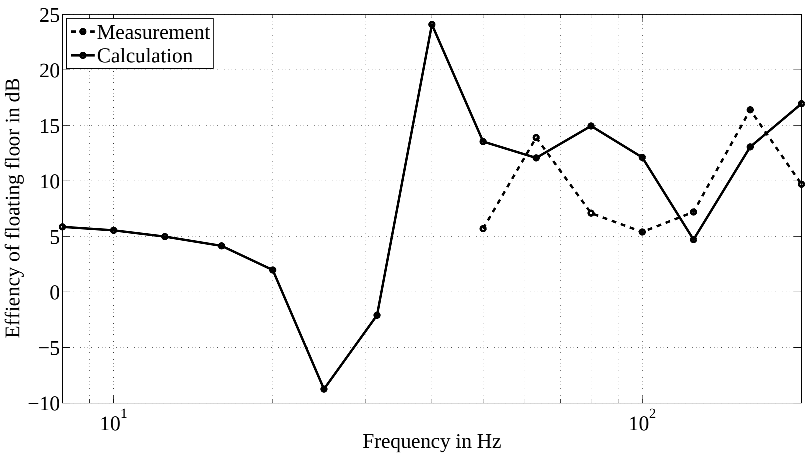

Figure 3.16: Calculations compared to measurements by Thorsson, case 2. See Table 3.8 for material parameters.

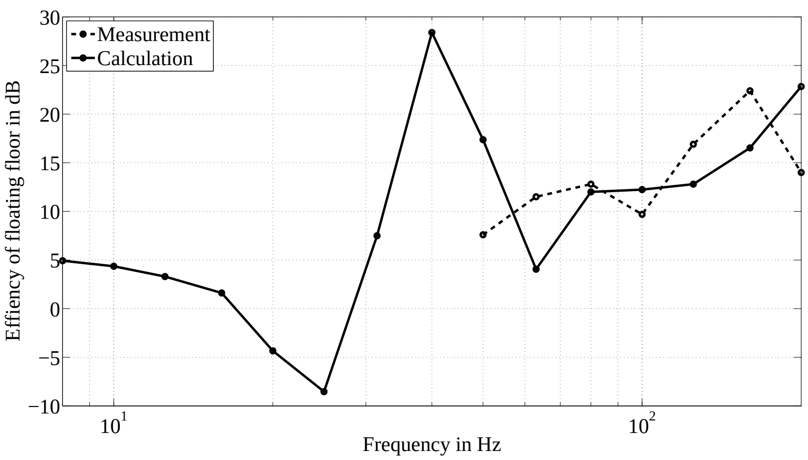

Figure 3.17: Calculations compared to measurements by Thorsson, case 3. See Table 3.8 for material parameters.

As seen in Figure 3.15-3.17 the calculated result agree fairly well with the measured improvement when it comes to expected amplitudes. The deviations can partly be explained by previously discussed differences between the measurement methods and the model. The agreement between measurements and calculations is regarded as satisfying for the scope of this thesis.

3.5 Parameter study and choice of material

The parameter study is divided into two parts using different plate materials, i.e. CLT and concrete respectively. The only parameter varied for the plate is the thickness, t. Hence the other properties density, ρ, Young´s modulus, E and loss factor, η are kept constant and is not further investigated. The studied parameters are listed to the left in Figure 3.18.

Figure 3.18: Floating floor construction. Parameters investigated are listed to the left.

The choice of material parameters for the parameter study is in general chosen using a $log5$ principle originating from the center parameter, although a number of exceptions from this principle can be seen. The chosen parameters are shown in Table 3.10. Material parameters for the floating floor are in general chosen so that both the properties of a gypsum board and a concrete floor are covered. Typical values of concrete and gypsum boards are shown in Table 3.9 [15].

Table 3.9: Typical values found in literature over material properties of concrete and gypsum boards.

Material property	**Concrete**	**Gypsum**
ρ	2300 kg/m^3	1200 kg/m^3
E	3e10 Pa	7e9 Pa
η	0.008	0.006
t	30-70 mm	13 mm (single board)

Table 3.10: Material properties used in parameter study calculations.

Plate					
CLT t_{plate} [mm]		140	**220**	320	
Concrete t_{plate} [mm]		130	**200**	300	
Interlayer					
$t_{elastic}$ [mm]		10	**30**	50	
$E_{elastic}$ [Pa]	0.08e5	0.4e5	**2e5**	1e6	5e6
$\eta_{elastic}$ [-]	0.01	0.05	**0.25**	0.5	0.7
$\rho_{elastic}$ [kg/m^3]	40	60	**90**	135	200
Floating floor					
t_{floor} [mm]	6	12	**24**	48	96
E_{floor} [Pa]	2e9	6e9	**1.8e10**	5.4e10	1.62e11
η_{floor} [-]	0.01	0.025	**0.06**	0.15	0.4
ρ_{floor} [kg/m^3]	600	1100	**2200**	4000	7800

The parameter study is conducted by scripting a set of calculations in COMSOL. All material parameters are kept at the center parameter (in bold in Table 3.10) except from the parameter under investigation. I.e. only one parameter at a time is varied while all other are kept constant. The only exception from this principle is the thickness t and the stiffness E of the floating floor. In these cases all the different values of the stiffness is tried in combination with all thicknesses. This result in 56 variants of material combinations for each plate material (CLT and concrete) giving in total 112 cases for evaluation. The different cases and its variant-number are shown in Table 3.11.

Table 3.11: The calculated cases and its belonging variant number.

Material property	**Variant no.**
t_{plate}	1-3
$t_{elastic}$	4-6
$E_{elastic}$	7-11
$\eta_{elastic}$	12-16
$\rho_{elastic}$	17-21
E_{floor} for $t_{floor} = 6\,\text{mm}$	22-26
E_{floor} for $t_{floor} = 12\,\text{mm}$	27-31
E_{floor} for $t_{floor} = 24\,\text{mm}$	32-36
E_{floor} for $t_{floor} = 48\,\text{mm}$	37-41
E_{floor} for $t_{floor} = 96\,\text{mm}$	42-46
η_{floor}	47-51
ρ_{floor}	52-56

Each and every variant is in addition calculated and averaged over 5 different excitation points on the floor. The calculation time on the computer used is for each of the CLT and concrete cases about 15 h respectively.

4

Results and discussion

Various results from the parameter study are presented in this section firstly in a general sense and secondly with comments and discussion around every parameter. The section is divided into results from calculations using concrete as structural plate and CLT as structural plate respectively.

In order to get an overview of the large amount of data to be analysed in the result, table 4.1 shows the total efficiency of the floating floor, E_{tot}, in the studied frequency range 8-200 Hz for all cases using CLT and concrete as base plate respectively. The total efficiency is calculated by adding the radiated sound power from every frequency with and without the floating floor and subtracting the two cases from each other according to Equation 4.1. The results from varying each individual parameter are then presented in separate figures in the following subsections. Table 4.1 should be considered as giving only a rough picture of the performance of the floating floor.

$$E_{tot} = 10 \cdot \log\left(\sum_f W_{rad,structuralonly}\right) - 10 \cdot \log\left(\sum_f W_{rad,floatingfloor}\right) \tag{4.1}$$

Table 4.1: Total efficiency, E_{tot}, in dB in the frequency range 8-200 Hz of all 56 variants for CLT case and concrete case respectively.

	Var.	CLT	Concrete	Var.	CLT	Concrete	
	1	9.3	10.4	27	5.4	5.8	
t_{plate}	2	8.0	9.9	28	4.8	5.4	
	3	6.9	5.9	29	3.9	5.0	E_{floor2}
				30	5.7	4.5	
				31	6.9	5.5	
	4	6.2	6.5	32	10.3	9.7	
$t_{elastic}$	5	8.0	9.9	33	9.7	9.8	
	6	9.7	10.9	34	8.0	9.9	E_{floor3}
				35	9.1	10.1	
				36	12.0	9.6	
	7	21.0	19.1	37	15.7	13.5	
	8	14.6	14.4	38	14.8	12.8	
$E_{elastic}$	9	8.0	9.9	39	12.6	14.0	E_{floor4}
	10	6.2	6.2	40	12.7	15.3	
	11	6.0	4.5	41	16.8	13.7	
	12	1.1	3.0	42	21.3	20.0	
	13	4.2	5.8	43	19.9	19.4	
$\eta_{elastic}$	14	8.0	9.9	44	17.2	18.2	E_{floor5}
	15	10.0	11.6	45	18.9	22.5	
	16	10.1	12.2	46	24.5	21.7	
	17	8.0	9.9	47	6.7	9.8	
	18	8.0	9.9	48	7.2	9.8	
$\rho_{elastic}$	19	8.0	9.9	49	8.0	9.9	η_{floor}
	20	8.0	9.8	50	9.1	10.1	
	21	8.0	9.6	51	10.5	10.6	
	22	1.3	1.6	52	3.1	3.5	
	23	0.9	1.4	53	4.4	3.3	
E_{floor1}	24	1.2	1.3	54	8.0	9.9	ρ_{floor}
	25	2.4	2.9	55	13.7	13.6	
	26	4.2	2.0	56	19.8	19.0	

The correlation between all cases for the concrete plate and CLT plate respectively is compared in Figure 4.1, where the efficiency of the floating floor for the concrete case is plotted on the x-axis against the corresponding case for CLT-plate on the y-axis.

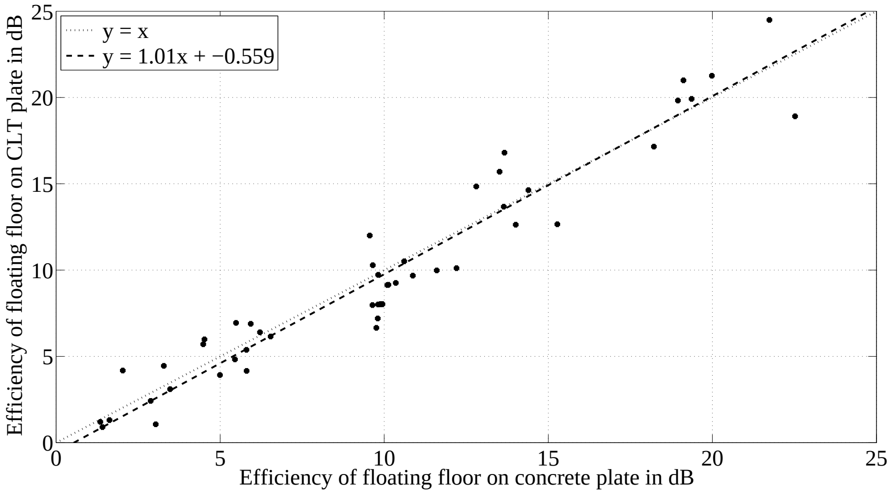

Figure 4.1: Concrete and CLT cases plotted together along with a linear regression line on the form y = kx + m.

As seen in Figure 4.1 the general result is that no tendency in difference between applying the floating floor to a CLT base floor rather than the concrete base floor can be observed. Although the relative increase of mass is higher for the CLT case the results show that the influence of the floating floor is in principle equally good. However as later discussed the impact sound insulation improvement of the floating floor is highly dependent on e.g. where the double resonance frequency is located and the individual cases should be analysed separately.

Mass-spring-mass resonance

As discussed earlier in the report, the simple analytical formulas for the sound insulation improvement of the floating floor is valid only above the resonance frequency f_0 in the mass-spring-mass system formed by the three layers in the floating floor construction. Above this frequency an increase by 9-12 dB/oct is expected. For all cases this frequency is calculated and shown in the corresponding figure. The general observation is that the double resonance frequency appears in the radiated sound power not as a clear peak, but as a smooth increase in amplitude around this frequency. This is believed to be due to the high damping in the elastic interlayer chosen as a default value of 0.25. As later observed when decreasing this damping, the radiated sound at and around the double resonance clearly increases. Depending on the location of the double resonance, modal resonances in the floor construction is attenuated to different extents.

A general observation is also that the radiated sound power below the double resonance frequency is dependent on the mode content of the plate. Hence the efficiency of the floating floor is dependent of how the movement of the plate is changed, as discussed in [17]. Above the double resonance the results differ from each case significantly. Reasons for this are discussed as follows. Another general observation is that the floating floor starts to act as an improvement at about the $f = 2 \cdot f_0$ rather than directly above it as often stated in the literature.

Critical frequency

For finite plates it is expected to get sound radiated below the critical frequency. In addition an increased radiated sound power is expected to be found at the critical frequency. However no effect of an increased sound power is noticed at the critical frequency in any of the studied cases in the thesis. For most cases the critical frequency is located at around 90 Hz for both the concrete and the CLT cases. The wavelength at these frequencies are about 4 m which is in the same order as the size of the plate. In order to see effects of the critical frequency, several bending wavelengths in the plate must be present which thus is not the case. In addition the match between bending waves and sound waves in air is more favourable when the waves in the plate is plane. When exciting the plate in a point as in the thesis more circular shaped waves are obtained, increasing the mismatch between bending waves and sound waves.

4.1 Concrete base floor

The parameter study results from the case when having a concrete base floor is shown and discussed here. Except from the first three variants, only the radiated sound power is shown. Separate figures for each individual variant with both radiated sound power as well as efficiency is shown in Appendix A.1.

Thickness plate

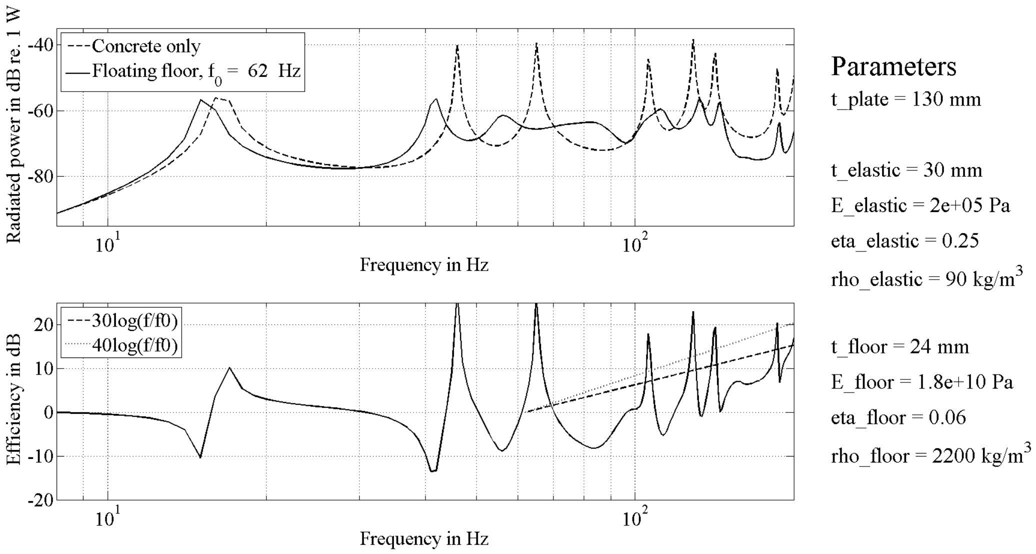

Figure 4.2: Parameter study result from variant 1. The thickness of the concrete plate is varied and radiated sound power is calculated for the floating floor cases along with plate only case. See Figure 4.3 and 4.4 for the other thicknesses.

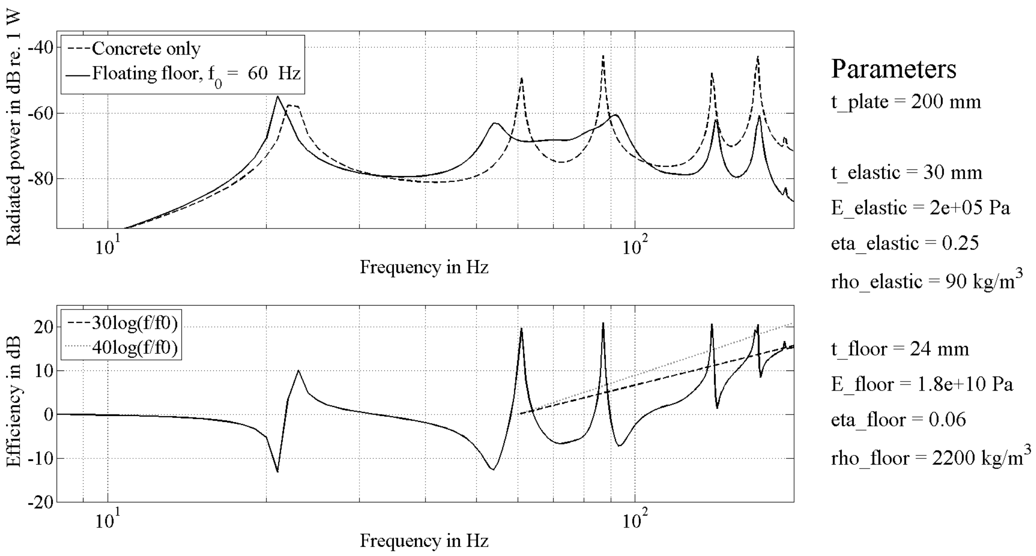

Figure 4.3: Parameter study result from variant 2. The thickness of the concrete plate is varied and radiated sound power is calculated for the floating floor cases along with plate only case. See Figure 4.2 and 4.4 for the other thicknesses.

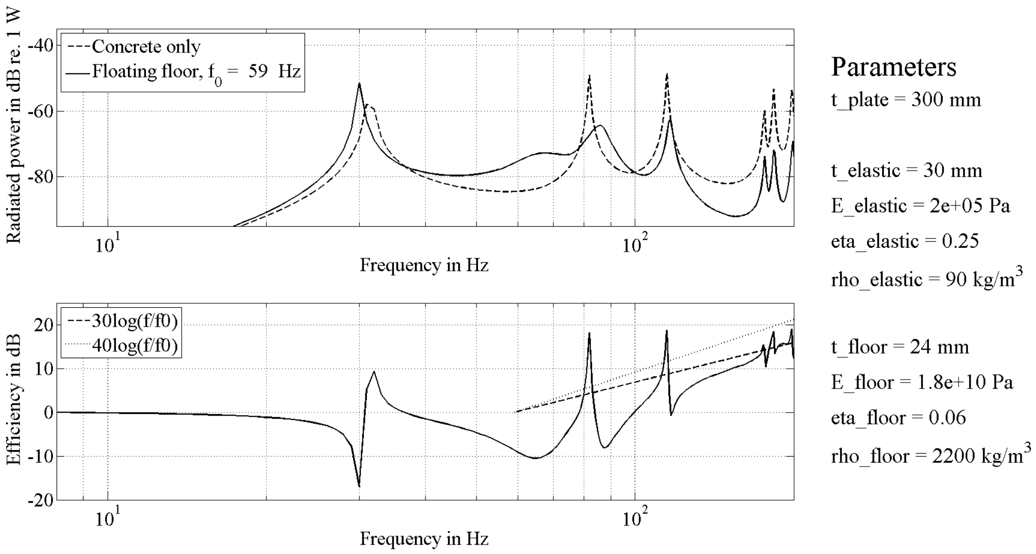

Figure 4.4: Parameter study result from variant 3. The thickness of the concrete plate is varied and radiated sound power is calculated for the floating floor cases along with plate only case. See Figure 4.2 and 4.3 for the other thicknesses.

As seen in Figure 4.2-4.4 the radiated sound power is highly dependent on the thickness of the structural plate both when considering amplitudes but especially when comparing the frequency dependence. The resonances are shifted upwards in frequency when making the plate thicker, although the double resonance is about the same for all three cases. Therefore the efficiency of the floating floor is quite similar in the three cases with general increase of sound insulation of about 12 dB/oct when interpolating between 100 Hz and 200 Hz.

Thickness interlayer

Figure 4.5 shows the result when varying the thickness of the elastic interlayer. When having a very thin interlayer of 10 mm the double resonance goes up above 100 Hz causing the effect of the floating floor to decrease. The three first resonances are just shifted in frequency causing alternating improvements and impairments. According to [9] a doubling of the thickness of the interlayer should result in an increase of the efficiency of 6 dB. When comparing the two latter cases this seem to be correct here as well when looking above 100 Hz between the resonances.

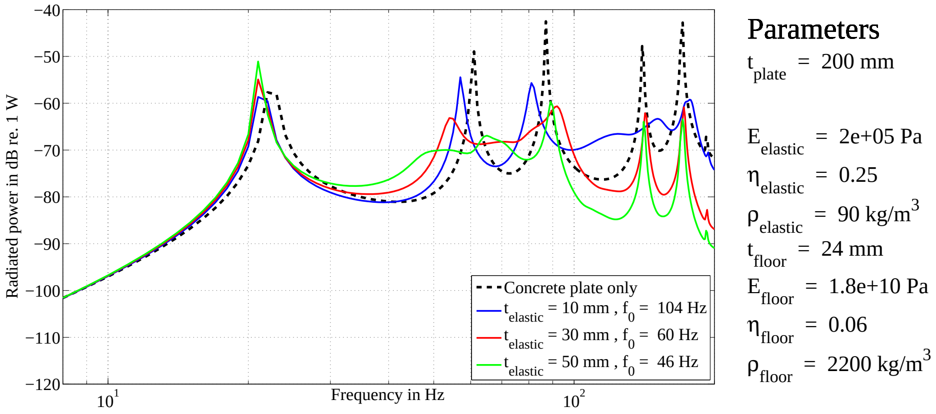

Figure 4.5: Parameter study result from variant 4-6. The thickness of the interlayer is varied and radiated sound power is calculated for the different cases along with plate only case.

Stiffness interlayer

As the function of the elastic interlayer is much like a spring, changing the stiffness of the layer changes the effect of the floating floor drastically. Firstly the resonance is shifted with about a factor 2 with a change of the stiffness with a factor 5. The double resonance of the floor construction clearly appears seen as a smooth peak around that frequency. It is beneficial to have as low stiffness as possible for the sake of the efficiency as the isolating effect is made used of to a large extent. Obviously the practical implications when it comes to static deflection and sense of springiness of the floor have to be considered.

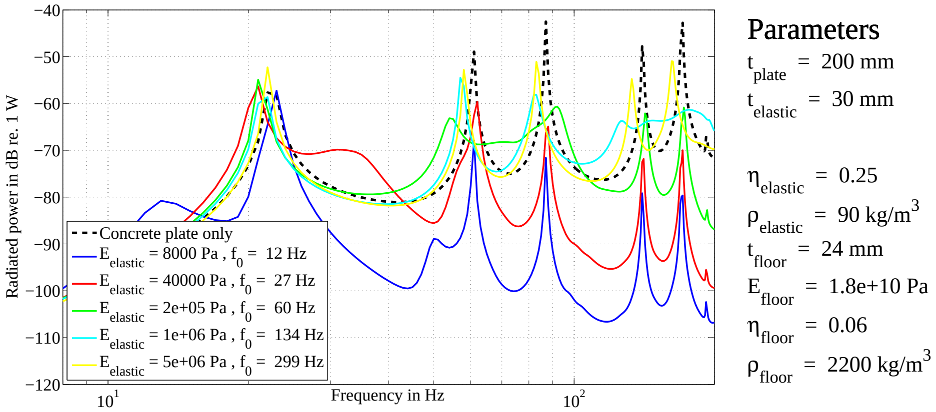

Figure 4.6: Parameter study result from variant 7-11. The stiffness of the interlayer is varied and radiated sound power is calculated for the different cases along with plate only case.

Damping interlayer

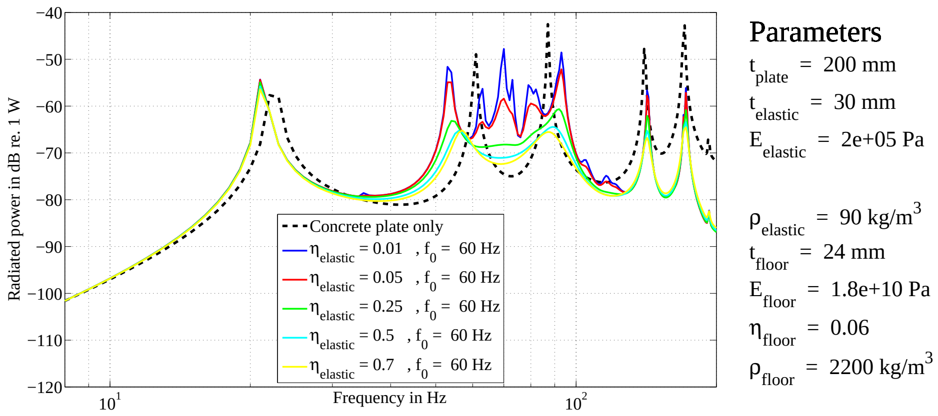

Figure 4.7: Parameter study result from variant 12-16. The damping of the interlayer is varied and radiated sound power is calculated for the different cases along with plate only case.

The amplitudes at especially the double resonance frequency is highly dependent on the damping in the elastic interlayer as expected. When decreasing the damping the amplitudes at and around the resonance goes up. The amplitudes are also affected above f_0 where a higher damping is beneficial.

Density interlayer

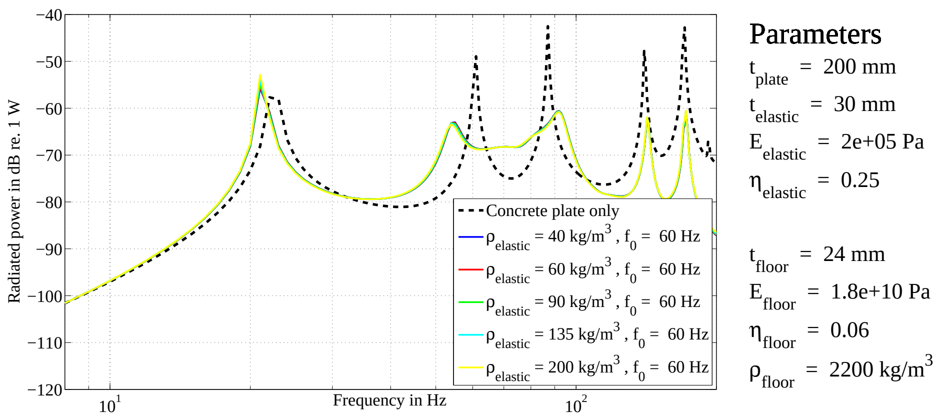

Figure 4.8: Parameter study result from variant 17-21. The density of the interlayer is varied and radiated sound power is calculated for the different cases along with plate only case.

A parameter that does not seem to have any changing effects on the efficiency of the floating floor is the density of the interlayer. More or less the same result is obtained even when studying the difference when changing the mass with a factor

5. The reason for this is probably because the interlayer functions a lot like an ideal spring. The contribution to the total mass of the floor construction is very small.

Stiffness floor for $t_{floor} = 6$ mm

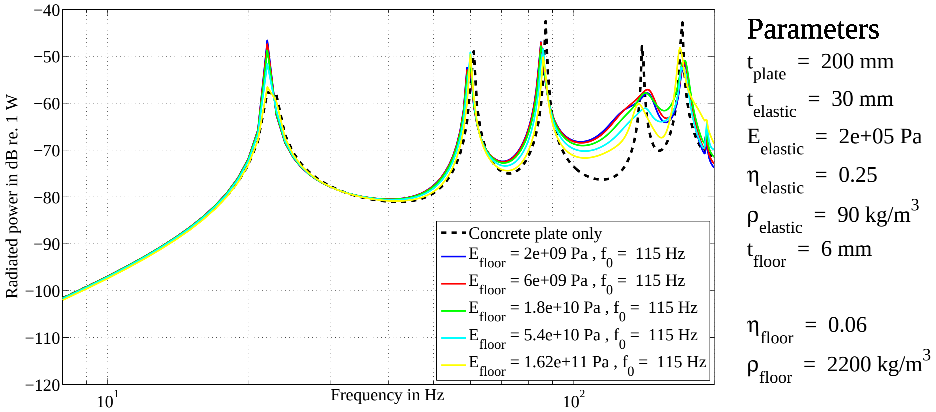

Figure 4.9: Parameter study result from variant 22-26. The stiffness of the floor is varied and radiated sound power is calculated for the different cases along with plate only case.

When decreasing the thickness of the floor to 6 mm the general efficiency of the floating floor goes down to almost having no effect at all for the studied frequency range. At and below the double resonance the tendency when increasing the stiffness is that the efficiency is improved. However when approaching 200 Hz the a softer floor give a better result, although the differences are very small.

Stiffness floor for $t_{floor} = 12$ mm

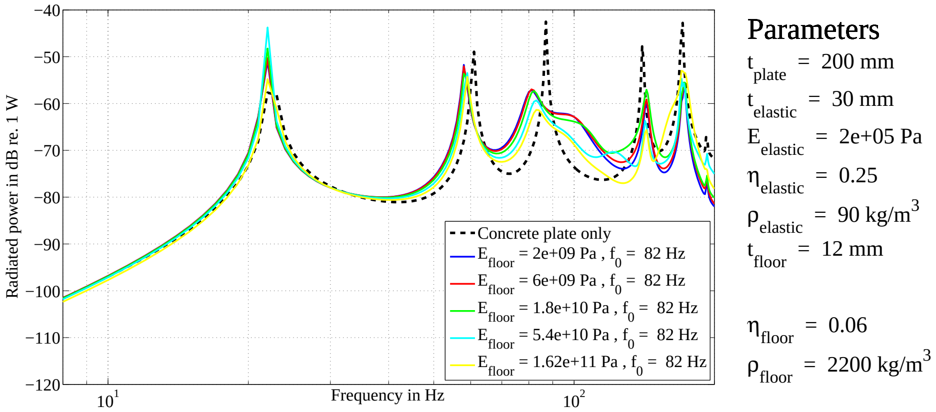

Figure 4.10: Parameter study result from variant 27-31. The stiffness of the floor is varied and radiated sound power is calculated for the different cases along with plate only case.

Doubling the thickness from the previous case have no significant effect on the efficiency. A general increase with 1 dB on the total efficiency in the studied frequency range can be observed in Table 4.1. Otherwise the same observation as in previous case can be made.

Stiffness floor for t_{floor} = 24 mm

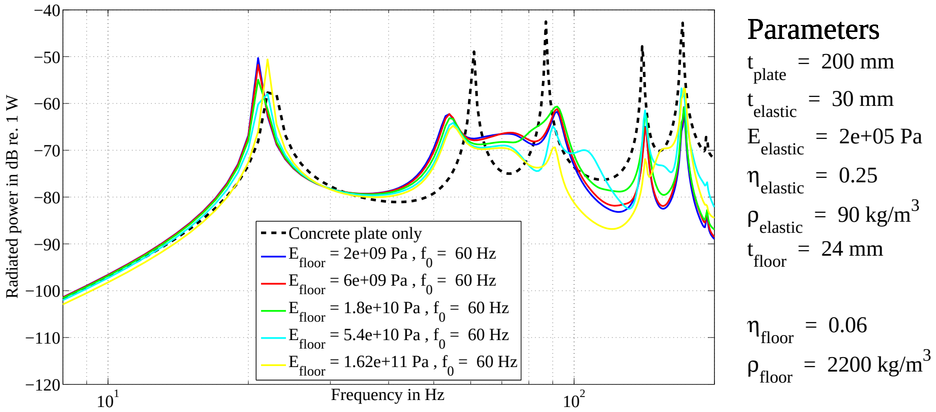

Figure 4.11: Parameter study result from variant 32-36. The stiffness of the floor is varied and radiated sound power is calculated for the different cases along with plate only case.

Increasing the thickness of the floor is good for the efficiency, since the double resonance is shifted down in frequency and some improvement at higher frequencies is obtained. It is not obvious that a stiffer floor is better for the efficiency. The last case when having a very stiff floor is beneficial for the frequency range just above the resonance, however when looking further up in frequency that is not the case.

Stiffness floor for t_{floor} = 48 mm

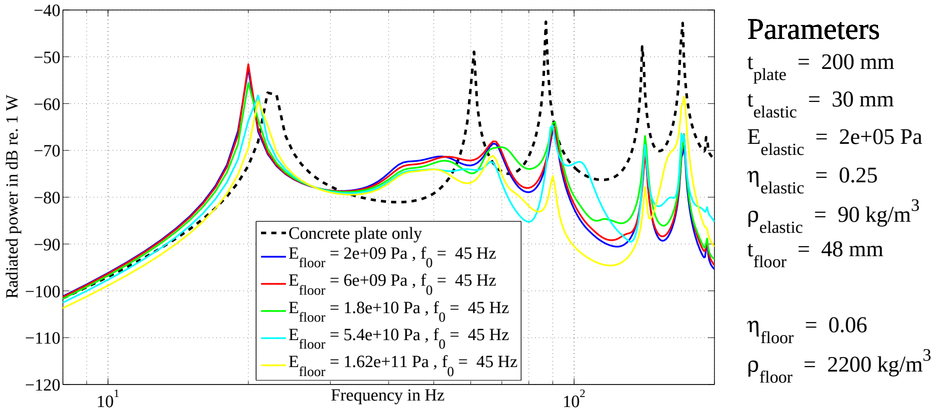

Figure 4.12: Parameter study result from variant 37-41. The stiffness of the floor is varied and radiated sound power is calculated for the different cases along with plate only case.

When increasing the thickness of the floor to 48 mm some more effect is observed in the efficiency. The resonance peaks are attenuated with up to 15 dB and the overall improvement is significant. The stiffness is as previously mentioned wanted as high as possible to attenuate the impact sound insulation for frequencies below the double resonance, however higher up in frequency the same trend is not seen.

Stiffness floor for t_{floor} = 96 mm

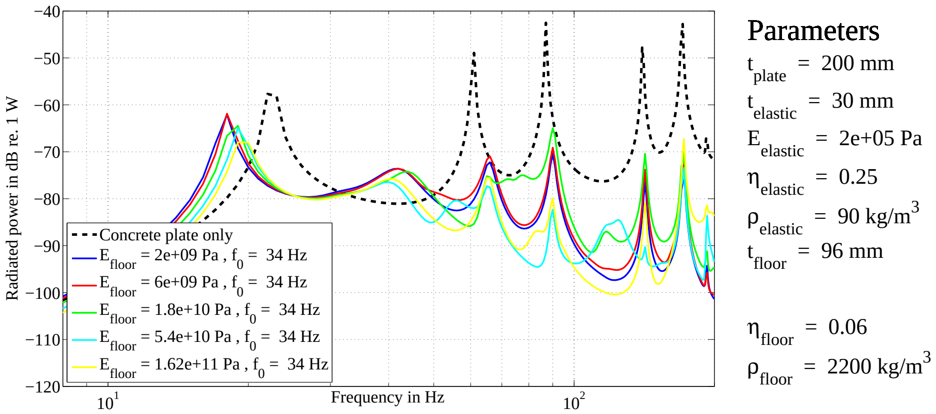

Figure 4.13: Parameter study result from variant 42-46. The stiffness of the floor is varied and radiated sound power is calculated for the different cases along with plate only case.

The best result overall when studying the concrete plate cases, is obtained when having the thickest floating floor. The resonance peaks get highly attenuated and the total efficiency of the floating floor is reaching almost 23 dB for the second highest stiffness. It is not obvious if a stiffer floor is beneficial for the efficiency. The resulting improvement is highly dependent on where in frequency the evaluation is done.

Damping floor

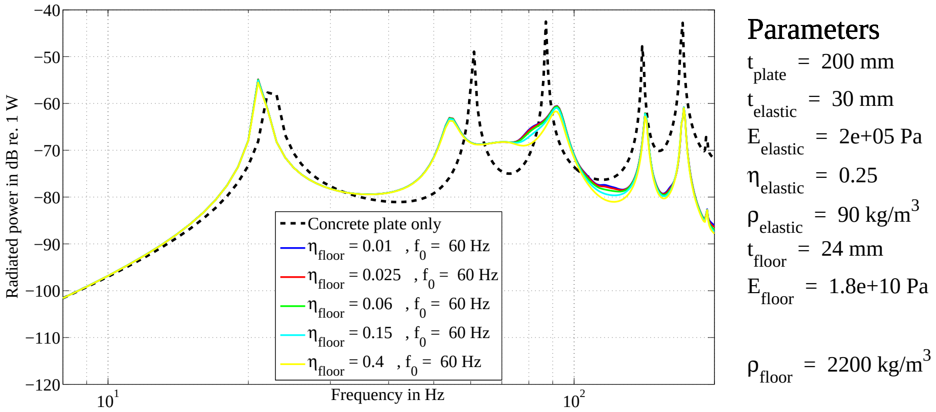

Figure 4.14: Parameter study result from variant 47-51. The damping of the floating floor is varied and radiated sound power is calculated for the different cases along with plate only case.

Changing the damping of the floor gives insignificant effect on the efficiency of the floating floor. The amplitudes at the resonance peaks goes slightly down the higher loss factor used. The effect of locally/globally reacting floors can hence not be observed. Even when going up to a quite large loss factor at 0.4 the effect is limited. This could indicate the choice of damping model might be inadequate for the study.

Density floor

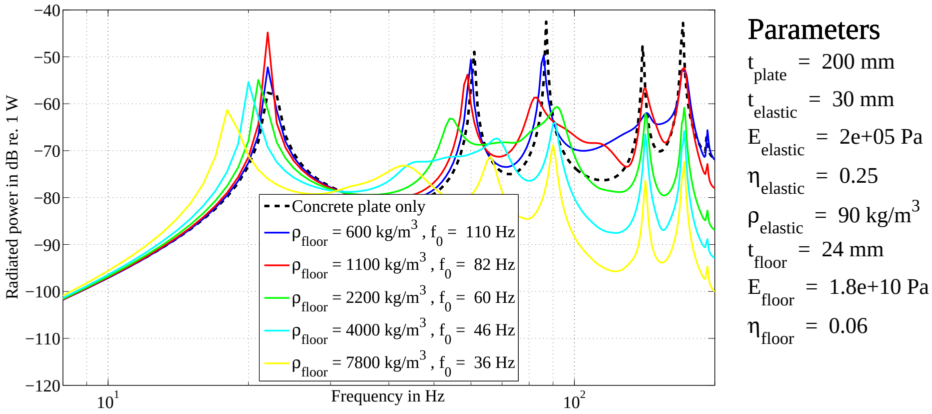

Figure 4.15: Parameter study result from variant 52-56. The density of the floating floor is varied and radiated sound power is calculated for the different cases along with plate only case.

The density has the expected effect about changing f_0 downwards as increasing the mass. For the frequency range studied this has large impact on the improvement. The general rule of thumb here is that larger density implies a much better impact sound insulation.

4.2 CLT base floor

The parameter study results from the case when having a CLT base floor is shown and discussed here. Except from the first three variants, only the radiated sound power is shown. Separate figures for each individual variant with both radiated sound power as well as efficiency is shown in Appendix A.2. Most tendencies observed in the concrete base floor cases are repeated here although some differences can also be seen.

Thickness plate

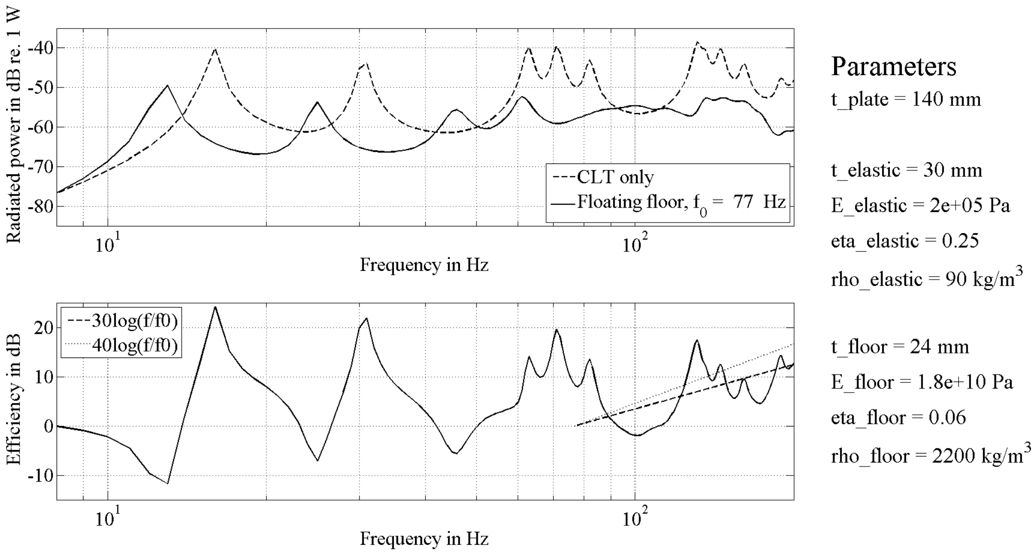

Figure 4.16: Parameter study result from variant 1. The thickness of the CLT plate is varied and radiated sound power is calculated for the floating floor case along with plate only case. See Figure 4.17 and 4.18 for the other thicknesses.

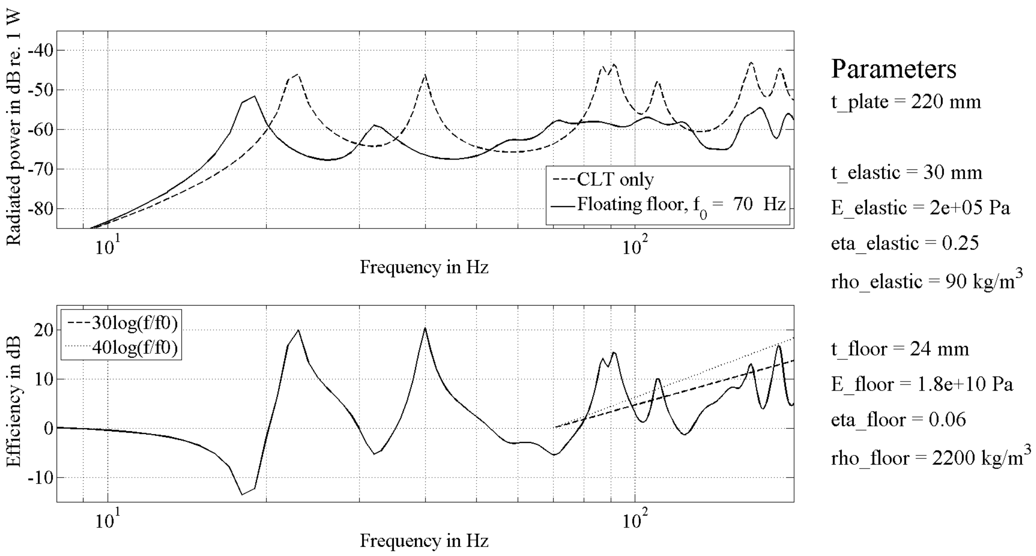

Figure 4.17: Parameter study result from variant 2. The thickness of the CLT plate is varied and radiated sound power is calculated for the floating floor case along with plate only case. See Figure 4.16 and 4.18 for the other thicknesses.

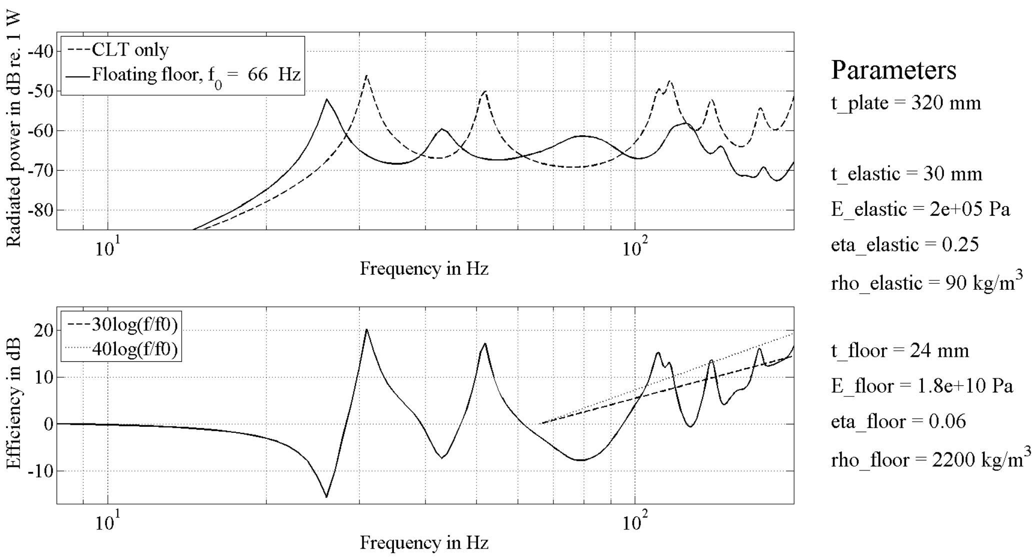

Figure 4.18: Parameter study result from variant 3. The thickness of the CLT plate is varied and radiated sound power is calculated for the floating floor case along with plate only case. See Figure 4.16 and 4.17 for the other thicknesses.

Compared to the case when having a concrete structural plate, the first three cases show larger changes in the radiated sound power. The resonance peaks below the double resonance f_0 is shifted down in frequency to a larger extent. This is because the relative increase in mass is larger compared to the concrete cases causing lower resonance in the total construction. Hence the efficiency is heavily affected both positively and negatively as seen in Figure 4.16-4.18. Since the CLT plate is lighter the double resonance ends up higher in frequency compared to the concrete case, causing the sound insulation improvement to start higher up in frequency.

Thickness interlayer

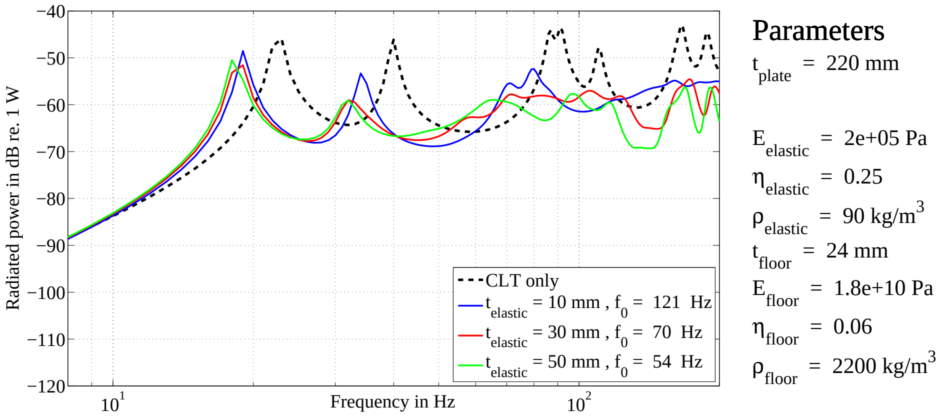

Figure 4.19: Parameter study result from variant 4-6. The thickness of the interlayer is varied and radiated sound power is calculated for the different cases along with plate only case.

Changing the thickness of the interlayer does not have very significant effects when having the floating floor on a CLT plate compared to the concrete case. The efficiency benefits from having a thicker interlayer as the double resonance goes down in frequency. It can also be observed that the amplitudes at the second lowest resonance is attenuated when going from a 10 mm to a 30 mm interlayer.

Stiffness interlayer

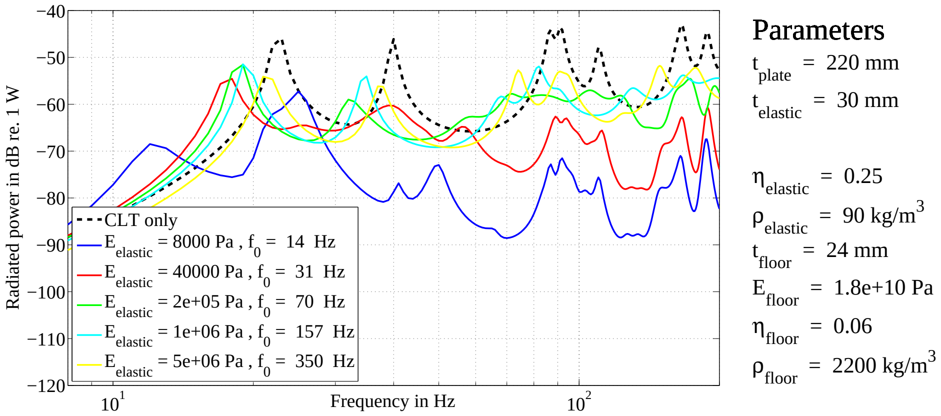

Figure 4.20: Parameter study result from variant 7-11. The stiffness of the interlayer is varied and radiated sound power is calculated for the different cases along with plate only case.

When the stiffness of the interlayer is lowered to the slightly unpractical value of 8000 Pa the efficiency gets really good in most of the studied frequency range. The resonance at 14 Hz is although causing a negative efficiency at the lowest frequencies. The general observation is hence that an interlayer with as small stiffness as possible is wanted. As discussed in the corresponding concrete case, the practical issues when having such a soft interlayer should be considered.

Damping interlayer

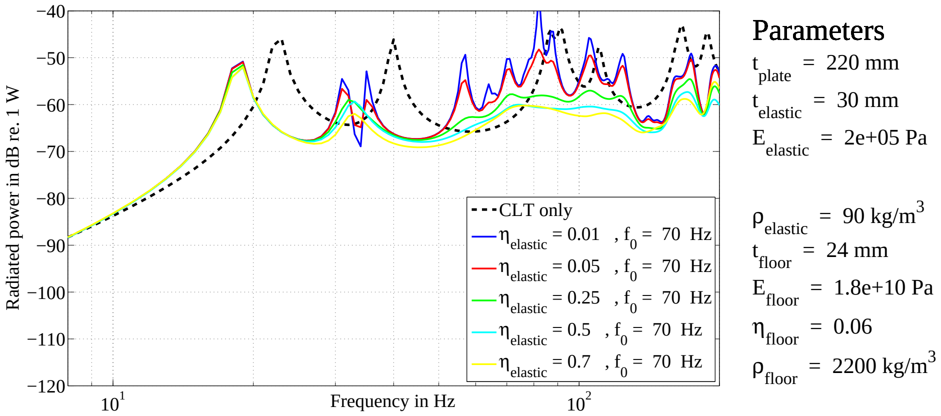

Figure 4.21: Parameter study result from variant 12-16. The damping of the interlayer is varied and radiated sound power is calculated for the different cases along with plate only case.

As for the result in the concrete case, the damping of the interlayer controls the amplitudes at the resonances, where as high damping as possible is wanted.

Density interlayer

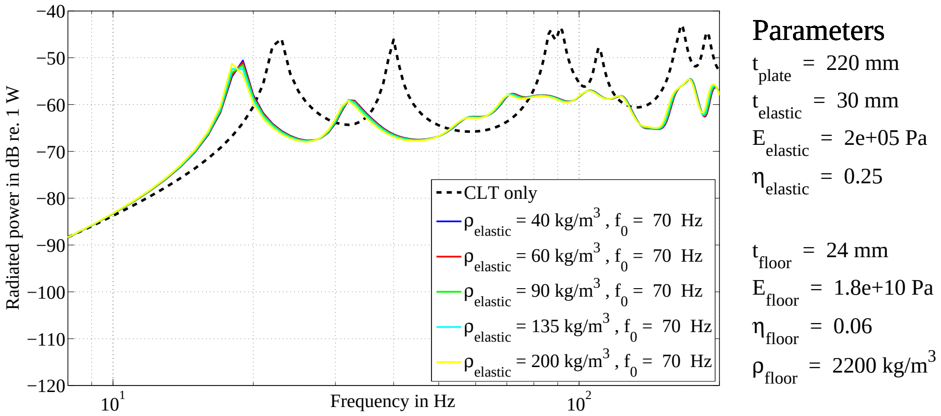

Figure 4.22: Parameter study result from variant 17-21. The density of the interlayer is varied and radiated sound power is calculated for the different cases along with plate only case.

The density of the interlayer is as in the concrete case not at all important for the efficiency of the floating floor. This indicate that the mechanical function of the interlayer is probably an ideal spring that does not act as a mass at all.

Stiffness floor for t_{floor} = 6 mm

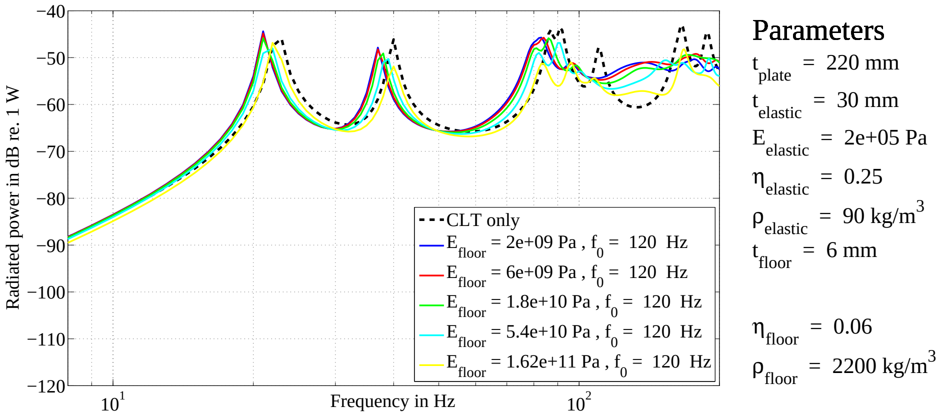

Figure 4.23: Parameter study result from variant 22-26. The stiffness of the floor is varied and radiated sound power is calculated for the different cases along with plate only case.

When using a thin floating floor the general efficiency is low for the frequency range studied. However the result is improved when having a stiffer floor as the amplitudes at the resonances tend to go down. The same discussion holds for the following cases shown in Figure 4.24 and 4.25.

Stiffness floor for t_{floor} = 12 mm

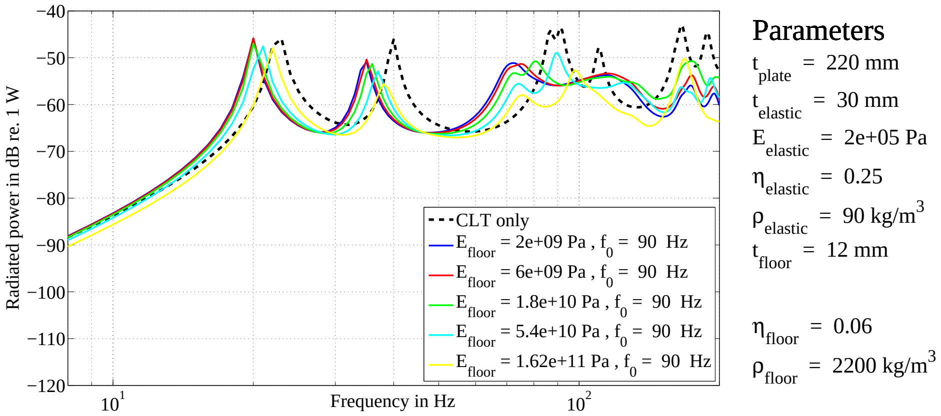

Figure 4.24: Parameter study result from variant 27-31. The stiffness of the floor is varied and radiated sound power is calculated for the different cases along with plate only case.

Stiffness floor for $t_{floor} = 24$ mm

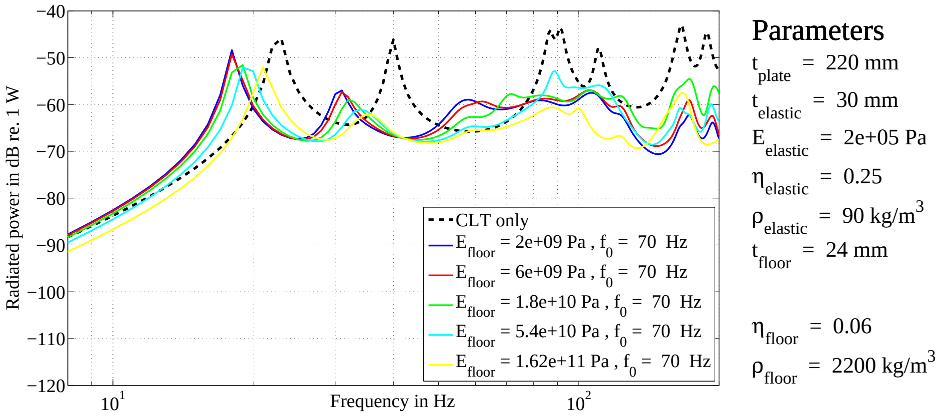

Figure 4.25: Parameter study result from variant 32-36. The stiffness of the floor is varied and radiated sound power is calculated for the different cases along with plate only case.

Stiffness floor for $t_{floor} = 48$ mm

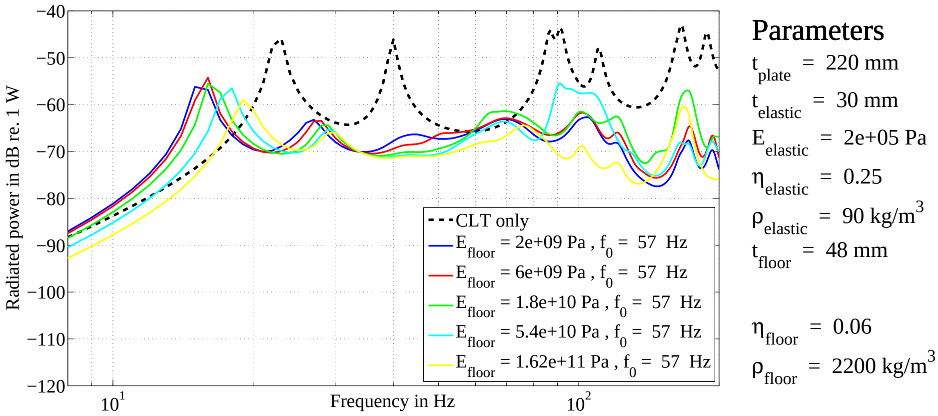

Figure 4.26: Parameter study result from variant 37-41. The stiffness of the floor is varied and radiated sound power is calculated for the different cases along with plate only case.

When increasing the thickness of the floor to 48 mm a significant effect is seen at the lowest frequencies where the modal content of the floor construction is both lowered in frequency and in amplitudes. In fact the amplitudes at the lowest mode is as low as for the concrete case. When increasing the frequency the improvement is not as good as for the concrete case, although the resonances are more damped for this case.

Stiffness floor for $t_{floor} = 96$ mm

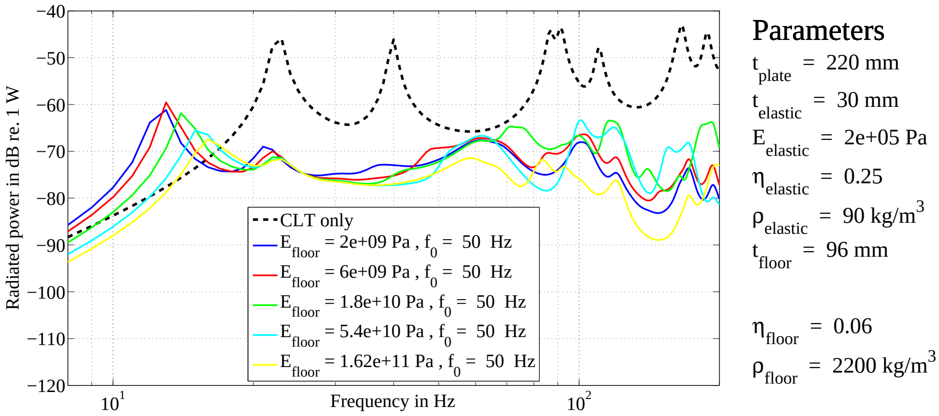

Figure 4.27: Parameter study result from variant 42-46. The stiffness of the floor is varied and radiated sound power is calculated for the different cases along with plate only case.

The overall best result from the calculations in the thesis is obtained when using the thickest floating floor on a CLT plate, where a total efficiency of 24.5 dB is obtained in the studied frequency range. This is partly due to that the double resonance is shifted down in frequency but also because the amplitudes below this frequency is lowered. Again the amplitudes are almost as low as for the concrete case.

As in the concrete case, it is not obvious whether a stiffer floor is better for the sound insulation. For frequencies at and below the double resonance a stiffer floor gives a better attenuation. However for frequencies above the double resonance either a very stiff or very soft floor gives the best attenuation.

Damping floor

The expected influence of the damping of the floor would be to see the difference between a locally or globally reacting floor. It can be concluded that a higher damping in the floor is beneficial for the attenuation especially above the double resonance. E.g. at 200 Hz the difference in radiated sound is about 10 dB when comparing the cases $\eta = 0.01$ and $\eta = 0.4$. Although when comparing these variants with theoretical expectations the attenuation is in the most damped case follows just about the 9 dB/oct slope above f_0. One reason could be the chosen damping model with a complex stiffness is not relevant, that instead another damping model should be used. It could also be that the damping is more important for frequencies above the studied range in the thesis and that a larger effect would be observed there.

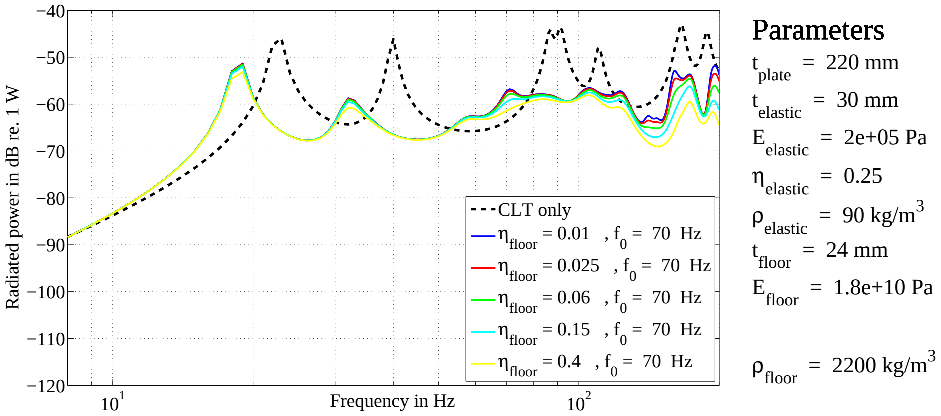

Figure 4.28: Parameter study result from variant 47-51. The damping of the floating floor is varied and radiated sound power is calculated for the different cases along with plate only case.

Density floor

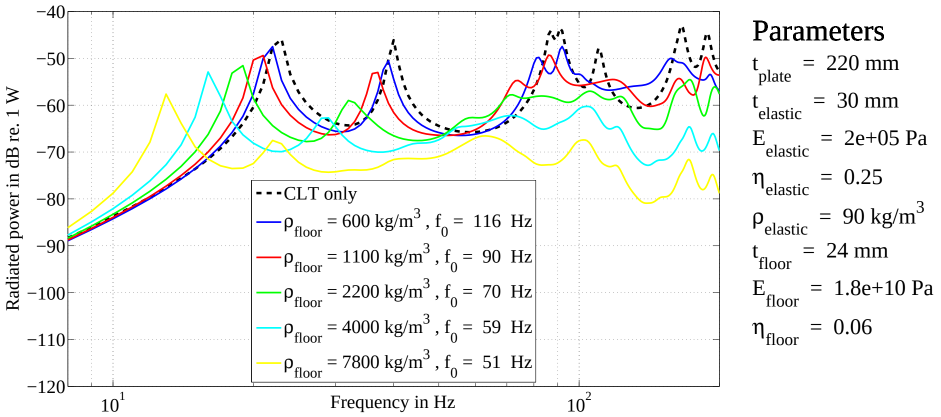

Figure 4.29: Parameter study result from variant 52-56. The density of the floating floor is varied and radiated sound power is calculated for the different cases along with plate only case.

The intuitive expectation that the efficiency increases with increased mass of the floating floor is fulfilled, partly because of the lowered double resonance. The amplitude is generally decreased when increasing the density. The general tendency in the lowest frequencies is that the first resonance in the floor is lowered both in frequency and amplitude when increasing the density of the floor.

4.3 Concrete vs. CLT - general discussion

When having a structural plate of concrete, the radiated sound power show more dynamic differences between modal resonances and anti-resonances compared to the CLT cases. Even though the amplitudes at the resonances are almost the same except at the lowest mode in the two cases, in between the resonances the amplitudes are significantly lower in the concrete case. This is believed to be due to the lower damping in the concrete plate.

Appendix A shows the radiated sound power for all variants individually in addition to the efficiency, with the corresponding theoretical expectation when it comes to vibration isolation above the mass-spring-mass resonance. When the resonance is located relatively high in frequency in the studied range, the agreement with theory is not possible to determine properly. The general observation is that for the CLT cases the efficiency agrees better with an increase of 9 dB/oct, whereas for the concrete cases a steeper slope is obtained.

Adding mass and/or thickness to the floating floor is in both cases attenuating the radiated sound power to a higher extent. Although the relative improvement of the impact sound insulation is higher for the CLT plate which is easier to affect at the lowest frequencies ($f < 30$ Hz). This is interesting from a practical point of view since the footfall frequency spectrum has its peak energy at and around these frequencies. If the main concern of poor impact sound insulation is the thumps and thuds from footsteps, using thick or heavy enough floating slab enables the use of CLT as a structural material. However the study show that not as low levels are obtained above the double resonance for the CLT cases.

5

Conclusions

Applying a floating floor to a structural plate of either cross laminated timber, CLT, or concrete changes the radiated sound power from the floor in different ways. Below the mass-spring-mass resonance frequency created by the three layers, the efficiency of the floating floor is mainly controlled by how the modal content of the floor is changed. Above the resonance the efficiency of the floating floor follows expected theoretical improvements to different extent. The study shows that it is of great importance to be aware of where the modes in the floor are located spectrally and where they will end up when applying the floating floor construction. This in addition to the expected source spectrum along with room modes in the receiving room, will be crucial to the sound isolating properties of the floor at low frequencies.

At the lowest frequencies ($f < 30\,\text{Hz}$) the CLT plate is more easily affected when increasing the thickness or the mass of the floating floor, attenuating the radiated sound power to almost the same amplitudes as for the corresponding concrete case. Above the resonance the slope of the sound insulation improvement is in general steeper for the concrete cases. However no other general tendency can be seen when studying the difference between applying the same floating floor construction to different structural plates.

The most important physical parameters in a floating floor construction is according to this study the stiffness of the interlayer as well as the density and thickness of the floating floor slab. The parameters that do not affect the efficiency of the floating floor is according to the study the density of the interlayer as well as the damping of the floating floor slab.

Future work suggestions

Improvements

The correlation between the model and measurements is not satisfying, both when considering vibration response in the CLT plate as well as when including a floating floor construction. The FEM model needs refinement. In order to get a more precise response in the CLT plate model, each layer of the plate should be modelled separately in e.g. FEM software Abaqus or similar, that can be expected to give more precise results. In addition a modal analysis to larger extent with a higher number of excitation and response points should be conducted.

The boundary conditions should also be studied further. It is not investigated in what way the interlayer and the floating floor are affected when applying them on a structural plate.

The modelling of the materials in the different layers should be done more sophisticated, e.g. frequency dependence of dynamic stiffness and damping. Different damping models can be evaluated such as viscous damping or Rayleigh damping.

Extensions

Although the purpose of this thesis is not to make a tool for prediction of impact sound levels for a given construction, several extensions could be made in order to get there. The input force in the thesis is throughout a frequency independent unit force. To include a modelled force spectrum of a footfall or the ISO tapping machine would be necessary in that case. When studying the radiated sound power from the plate, it can be observed that the spectrum of the source will be crucial to the outcome.

The thesis focuses only on the floor itself and no consideration has been made regarding a possible room modelled below the floor. For a prediction tool to be established this would be needed, especially for low frequencies where a diffuse sound field not can be expected. In addition the effects of in room impact noise is not considered in the thesis, for which no regulations exist in Sweden. However it is known that the radiated sound in the sending room is highly affected when exciting a floating slab compared to a heavy structural plate.

Bibliography

[1] Andersson, P. Kropp, W. (2015) *Introduction to sound and vibration, Lecture 6.* Chalmers University of technology, Göteborg, Sweden.

[2] Andersson, P. Kropp, W. (2015) *Introduction to sound and vibration, Lecture 7.* Chalmers University of technology, Göteborg, Sweden.

[3] Backman, E. et al. (2011) *Akulite - Acoustical Performance of Apartment Buildings – Resident's Survey and Field Measurements.* Borås: SP Sveriges tekniska forskningsinstitut. SP Report 2011:58.

[4] Blazier, W.E., DuPree, R.B. (1994) *Investigation of low-frequency footfall noise in wood-frame, multifamily building construction*, Journal of the Acoustical Society of America, vol. 96, no. 3, pp. 1521-1532.

[5] COMSOL Multiphysics 5.2a. (2016) *Structural Mechanics Module User´s Guide*

[6] Cremer, L., Heckl, M. & Petersson, B.A.T. (2005) *Structure-borne sound: structural vibrations and sound radiation at audio frequencies.* 3rd edition, Springer, New York; Berlin.

[7] Fahy, F. Gardonio, P (2007) *Sound and structural vibration. Radiation, Transmission and Response.* 2nd edition. Oxford: Academic press.

[8] Forssén, J. et al. (2008) *Acoustics in wooden buildings, State of the art 2008.* Stockholm: SP Technical Research Institute of Sweden. SP Report 2008:16.

[9] Gudmundsson, S. (1984) *Sound insulation improvement of floating floors. A study of parameters.* Lund Institute of Technology, Department of Building Acoustics.

[10] Hagberg, K. et al. (2009) *Design of light weight constructions - risks and opportunities.* Internoise. August 23-26, 2009, Ottawa, Canada.

[11] Hoever, C. (2016) *Technical Acoustics II, The boundary element method (BEM) for radiation problems.* Chalmers University of technology, Göteborg, Sweden.

[12] Hopkins, C. (2012) *Sound insulation.* 1st edition, Elsevier / Butterworth-Heinemann, Amsterdam.

[13] Hybrid build solutions. (2013) *CLT - Cross laminated timber.* Hybrid build solutions. http://hybrid-build.co/solutions/clt/. (2016-08-18).

[14] Jarnerö, K. et al. (2013) *Akulite - Sammanställning av resultat för industrin.* Borås: SP Sveriges tekniska forskningsinstitut. SP Report 2013:26.

[15] Kropp, W. (2015) *Technical Acoustics 1, Lecture notes.* Chalmers University of technology, Göteborg, Sweden.

[16] Ottosen, N. Petersson, H. (1992) *Introduction to the finite element method.* Harlow: Prentice Hall Europe.

[17] Park, H.S. et al. 2015, *Low-frequency impact sound transmission of floating floor: Case study of mortar bed on concrete slab with continuous interlayer*, Building and environment, vol. 94, pp. 793-801.

[18] Stora Enso. (2013) *CLT - Massive Wood System.* Stora Enso. http://www.clt.info/en/product/clt-massive-wood-system/. (2016-08-18).

[19] Swedish Wood. (2015) *Design of timber structures, Volume 1.* Swedish Wood, Stockholm.

[20] Vigran, T.E. (2008) *Building Acoustics.* New York: Taylor & Francis.

A

Appendix 1

This appendix contain all results from the parameter study.

A.1 Concrete parameter study results

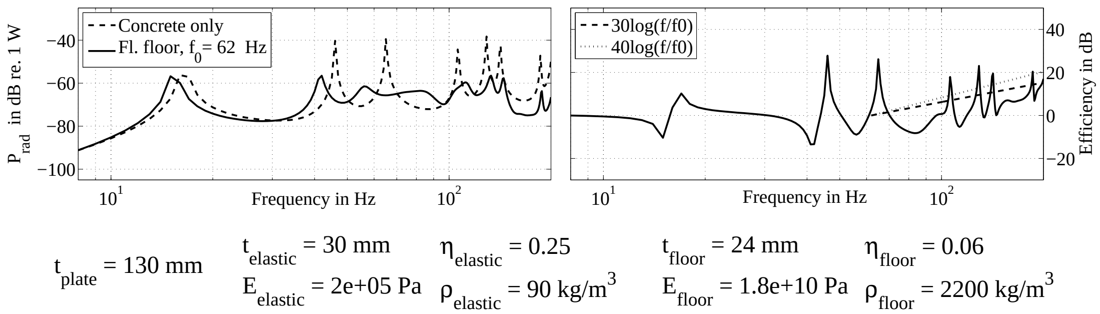

Parameter study result from variant 1.

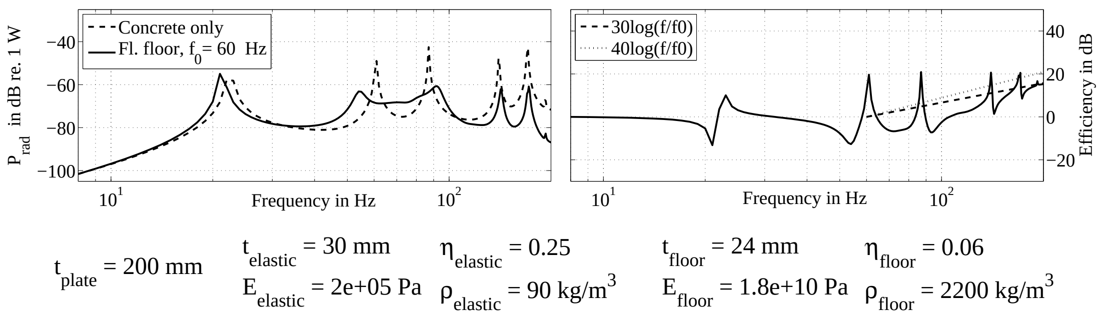

Parameter study result from variant 2.

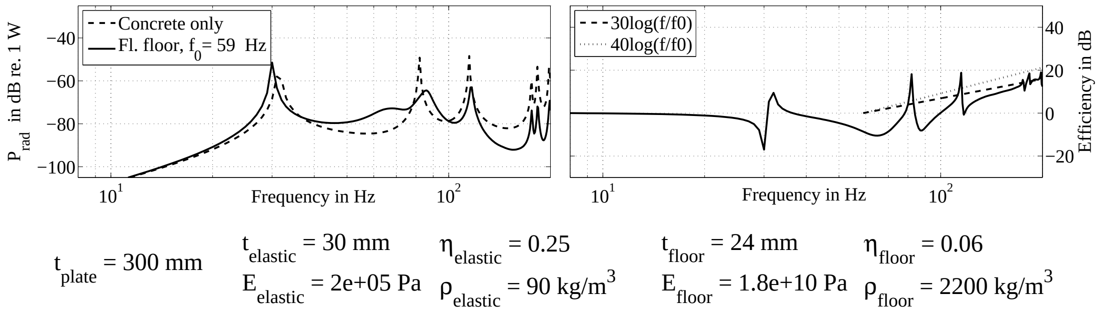

Parameter study result from variant 3.

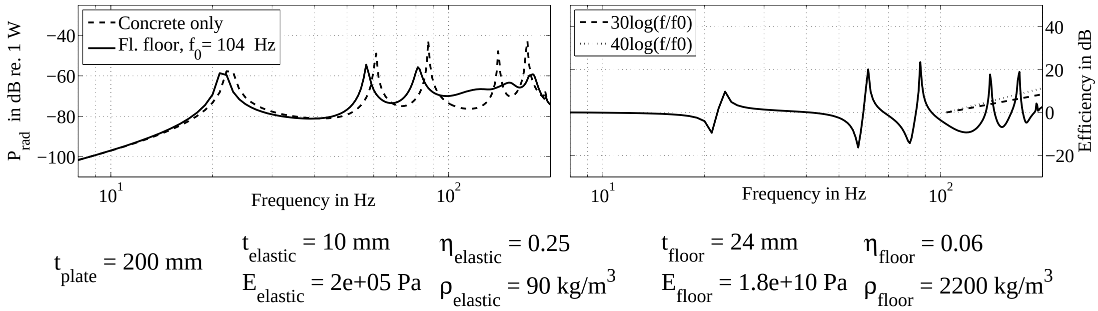

Parameter study result from variant 4.

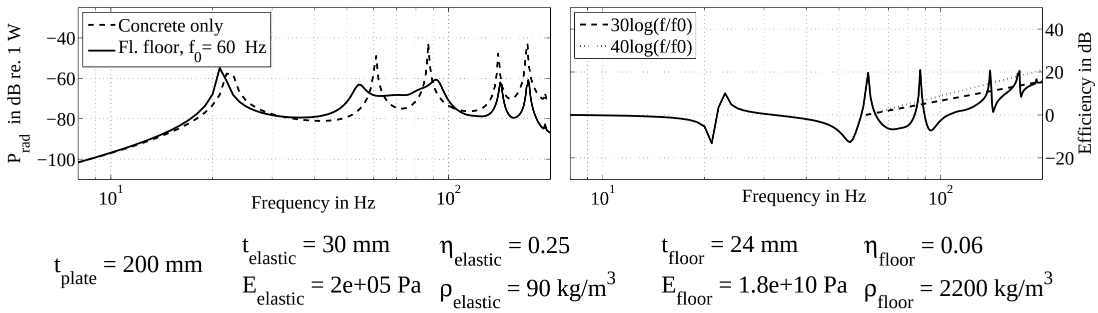

Parameter study result from variant 5.

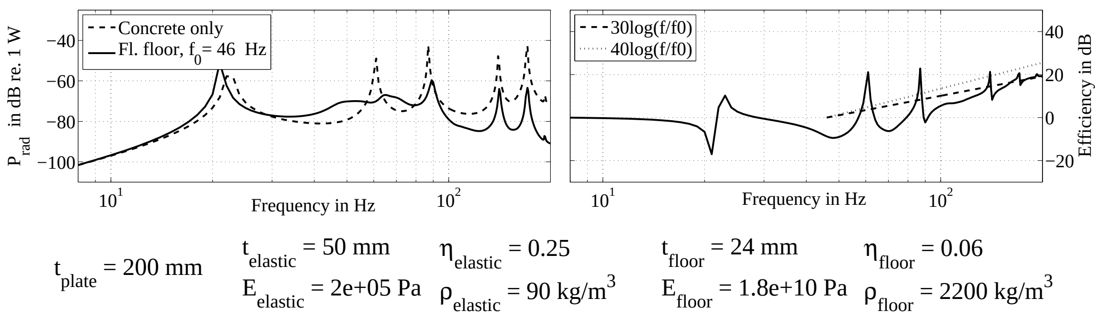

Parameter study result from variant 6.

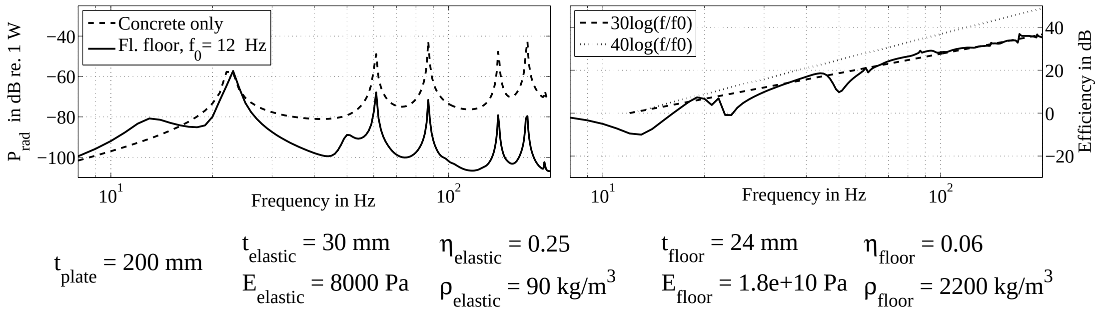

Parameter study result from variant 7.

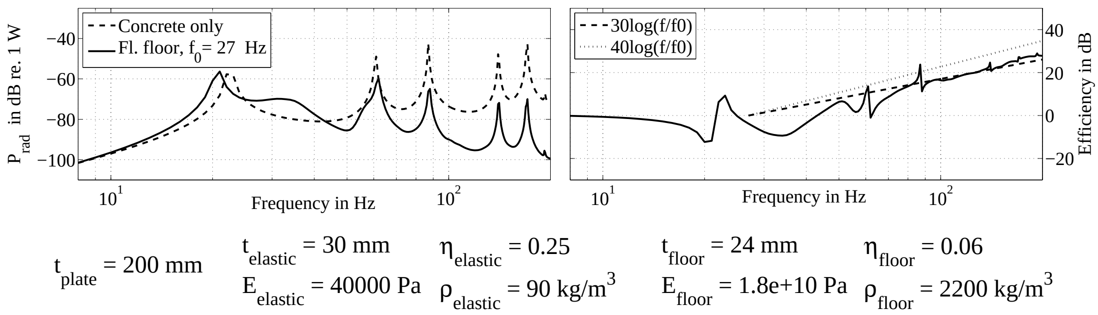

Parameter study result from variant 8.

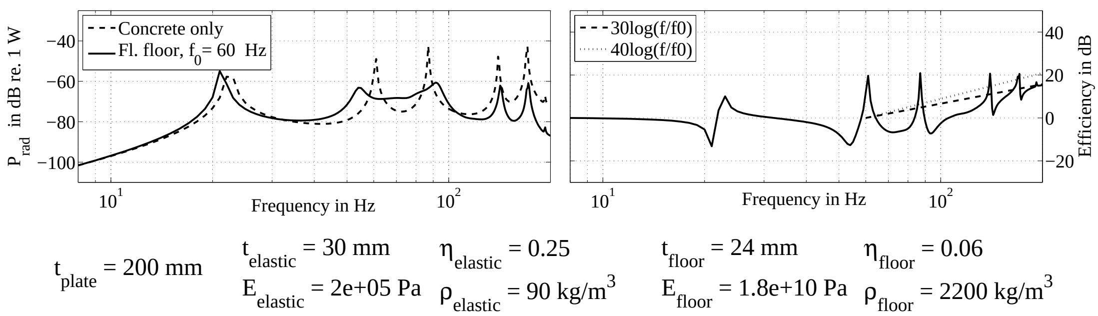

Parameter study result from variant 9.

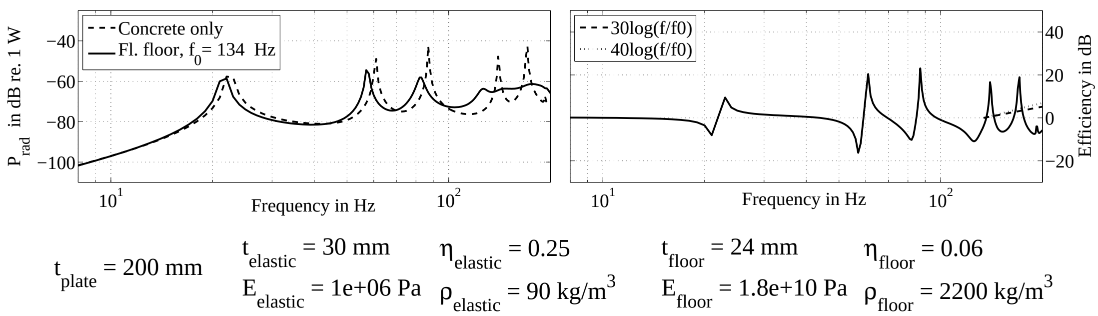

Parameter study result from variant 10.

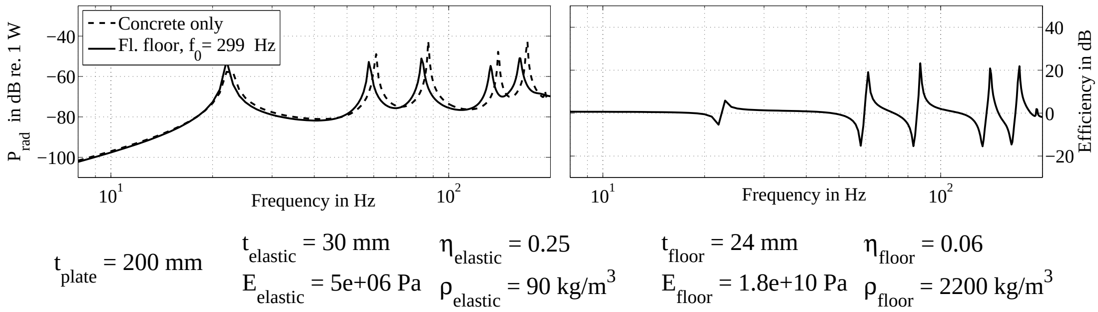

Parameter study result from variant 11.

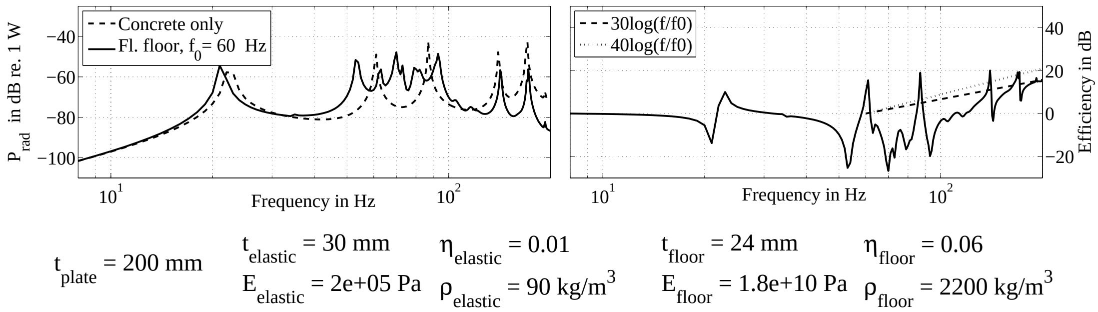

Parameter study result from variant 12.

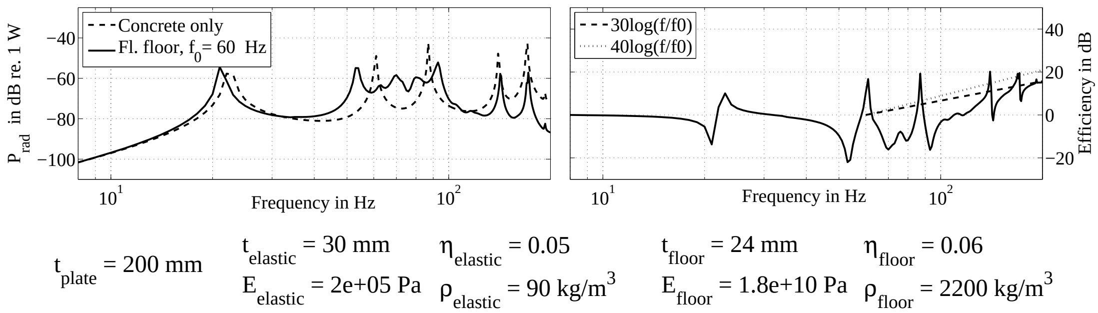

Parameter study result from variant 13.

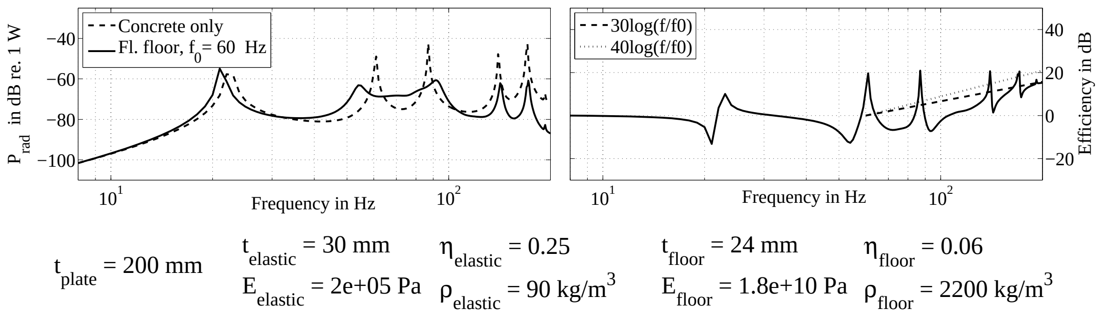

Parameter study result from variant 14.

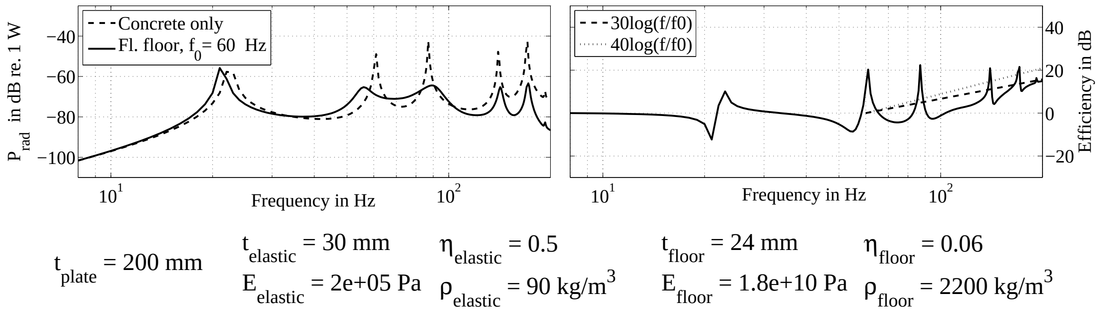

Parameter study result from variant 15.

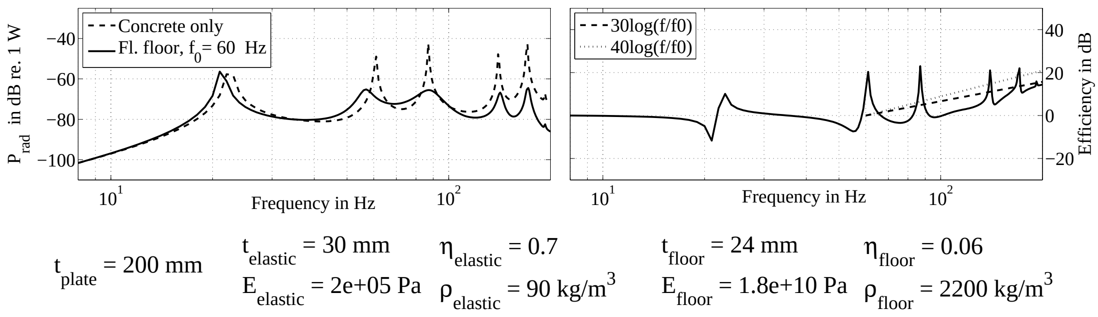

Parameter study result from variant 16.

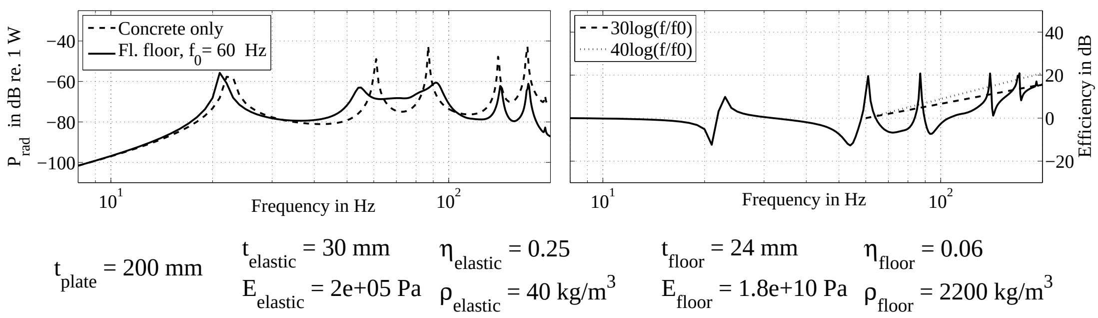

Parameter study result from variant 17.

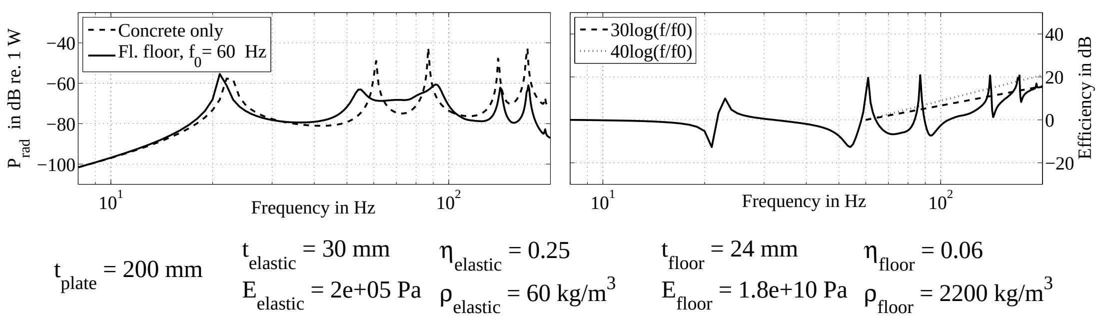

Parameter study result from variant 18.

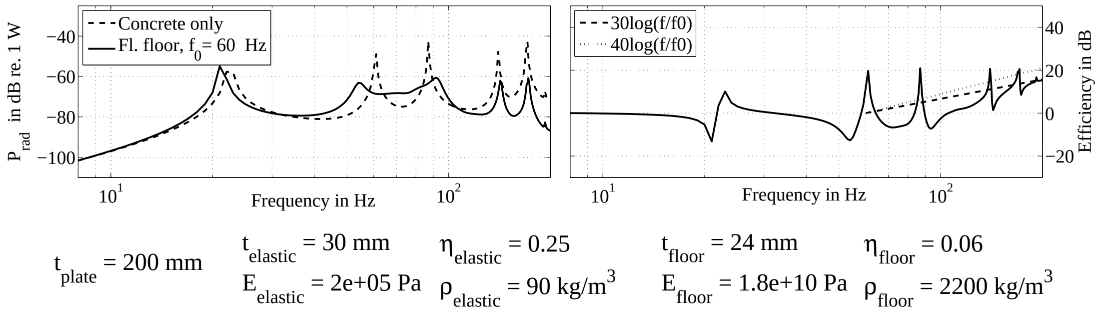

Parameter study result from variant 19.

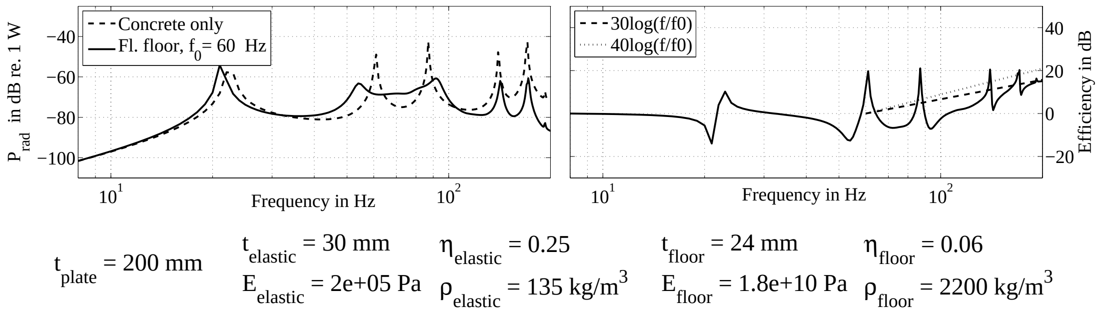

Parameter study result from variant 20.

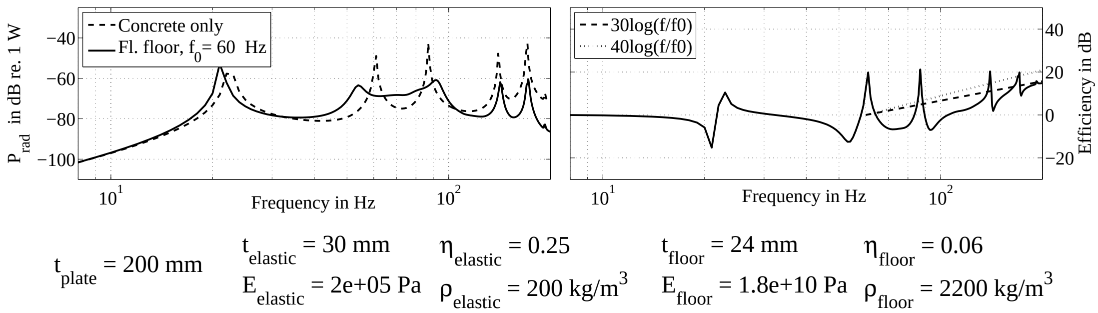

Parameter study result from variant 21.

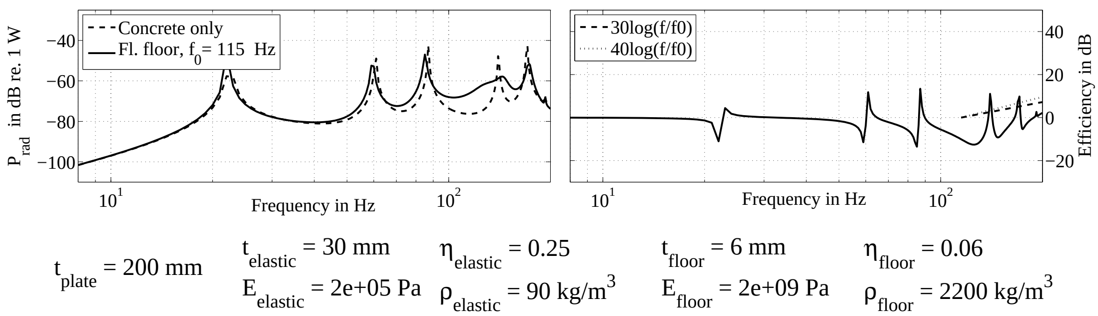

Parameter study result from variant 22.

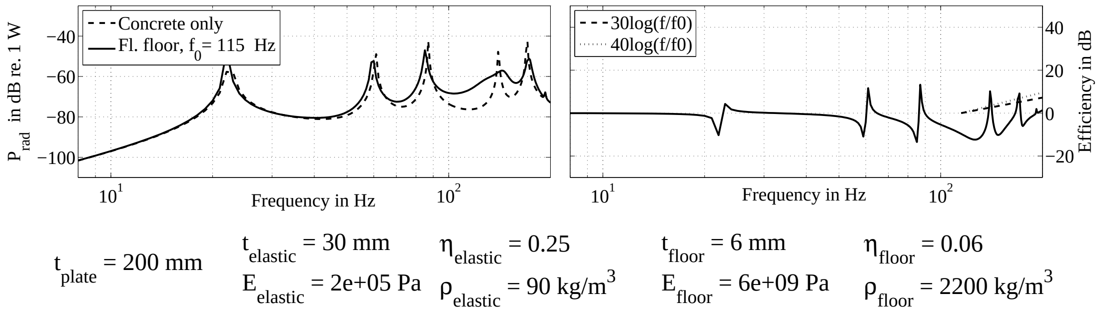

Parameter study result from variant 23.

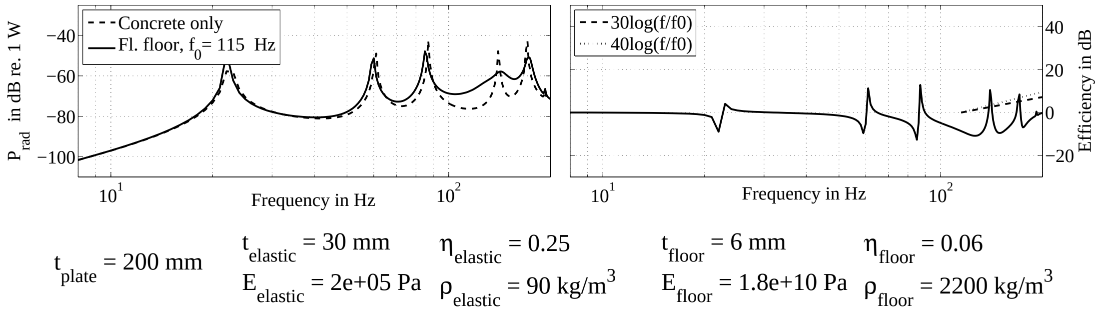

Parameter study result from variant 24.

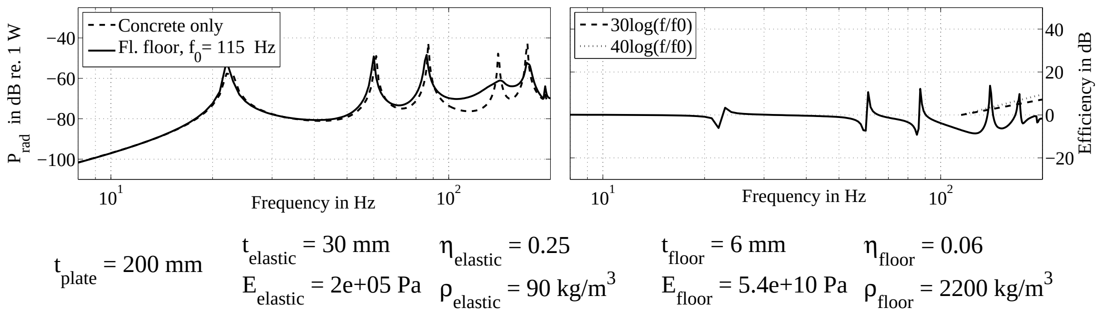

Parameter study result from variant 25.

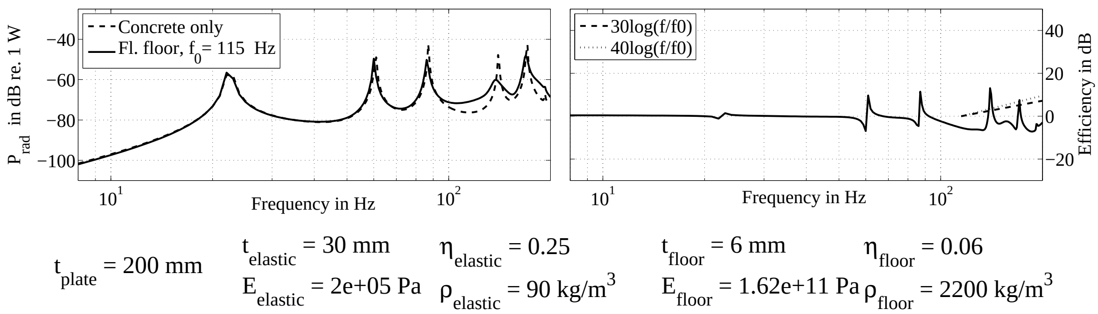

Parameter study result from variant 26.

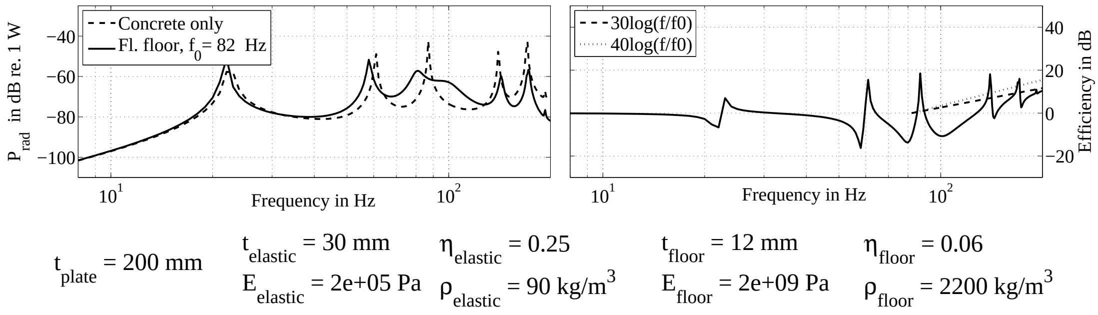

Parameter study result from variant 27.

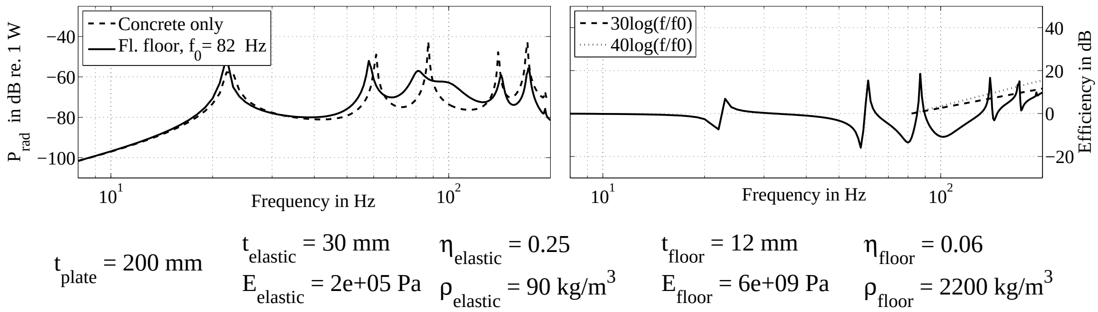

Parameter study result from variant 28.

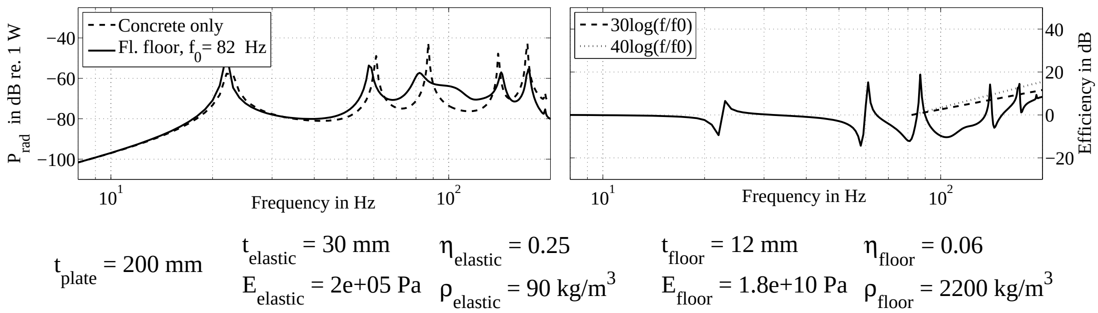

Parameter study result from variant 29.

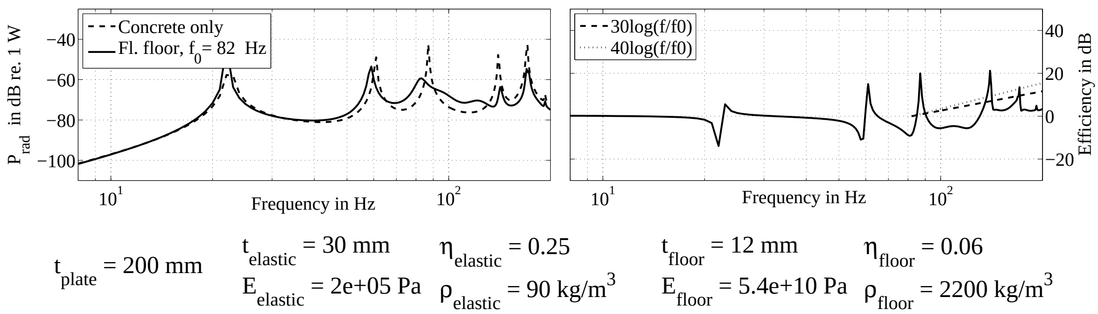

Parameter study result from variant 30.

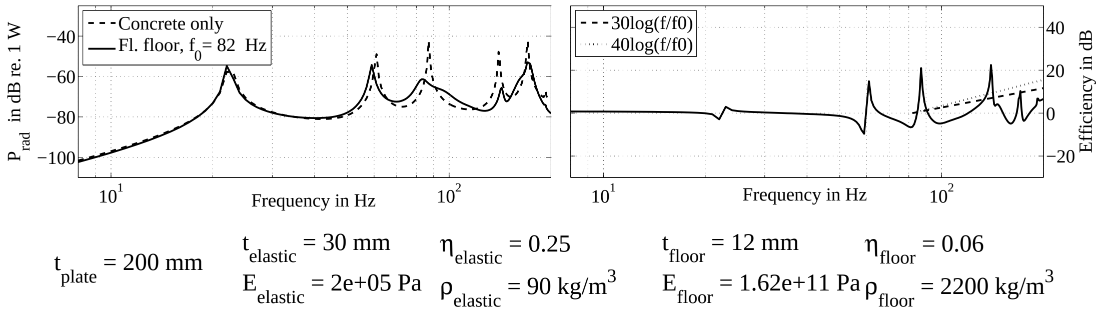

Parameter study result from variant 31.

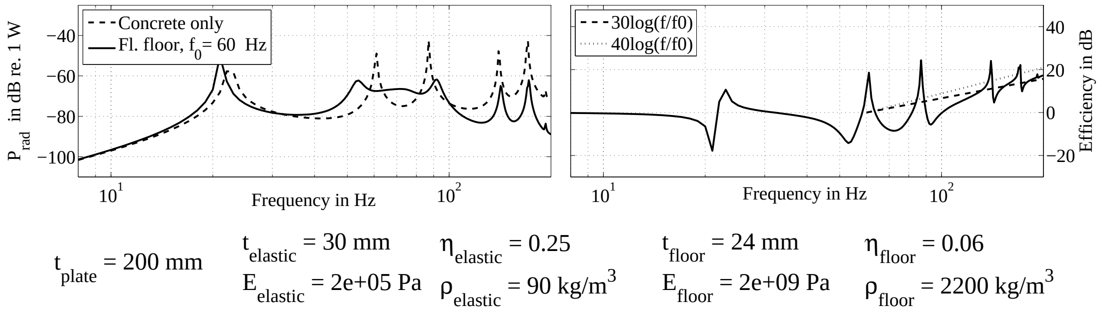

Parameter study result from variant 32.

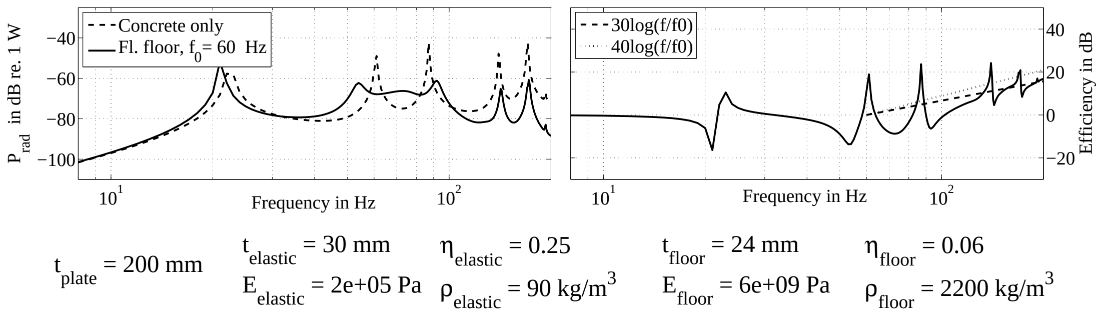

Parameter study result from variant 33.

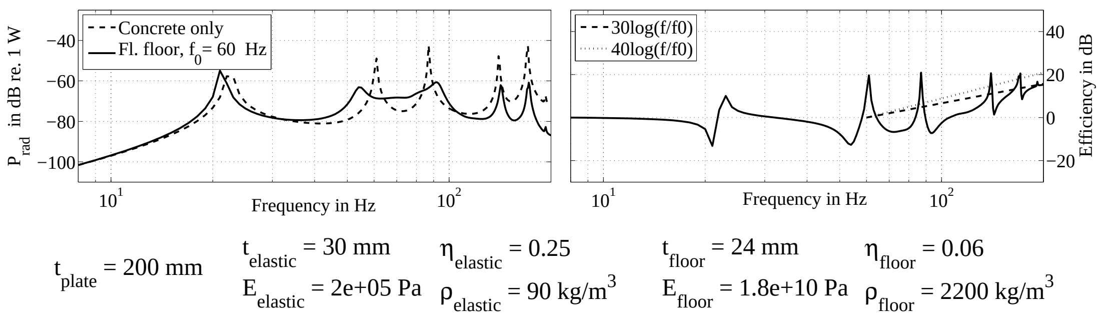

Parameter study result from variant 34.

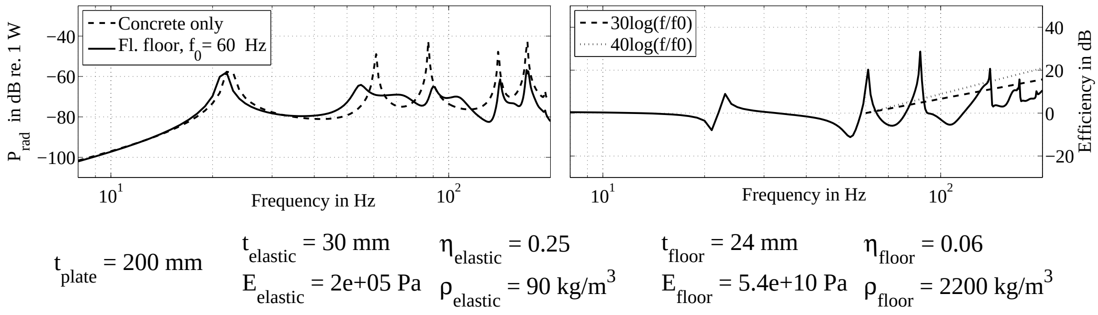

Parameter study result from variant 35.

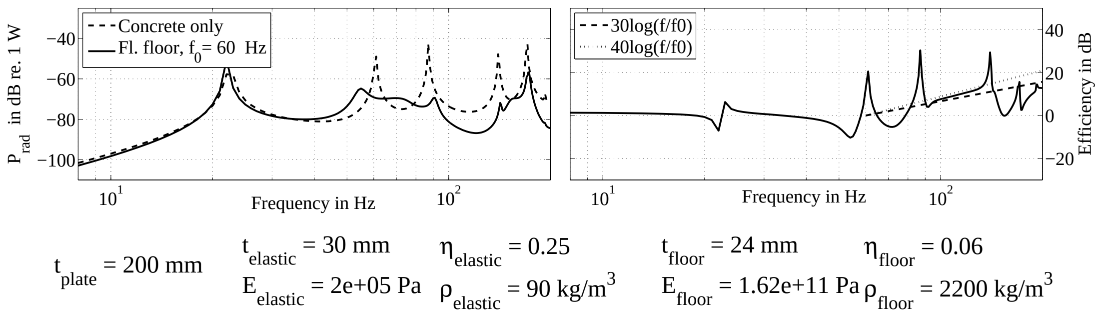

Parameter study result from variant 36.

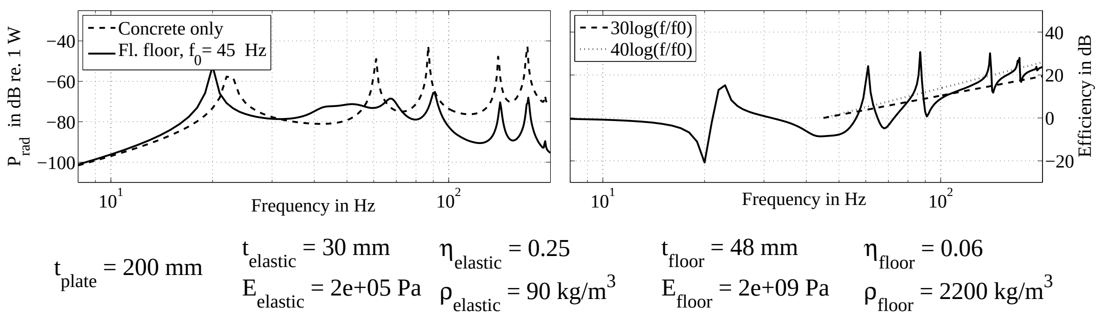

Parameter study result from variant 37.

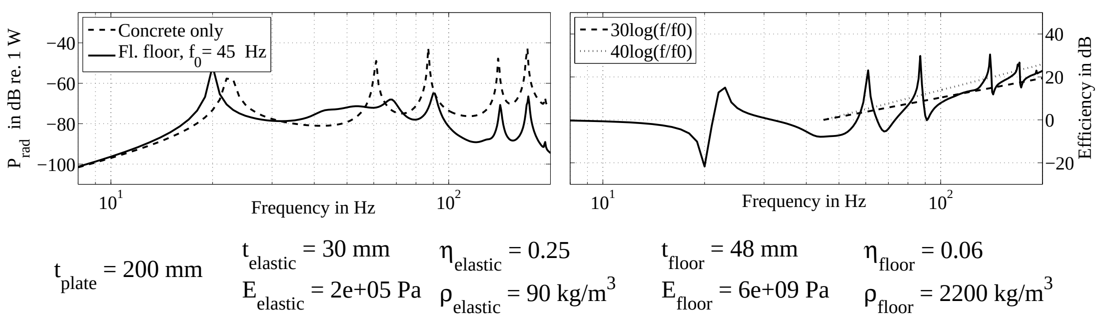

Parameter study result from variant 38.

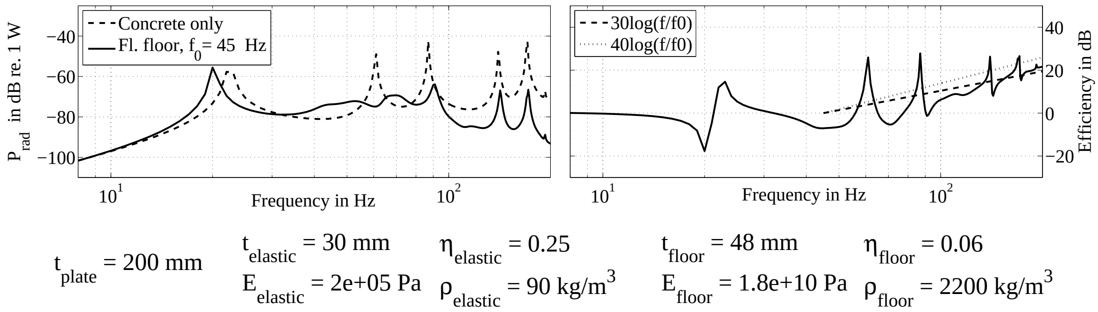

Parameter study result from variant 39.

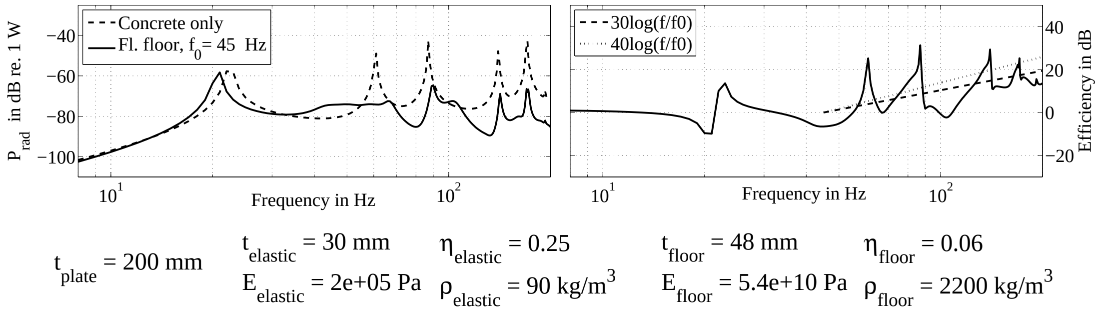

Parameter study result from variant 40.

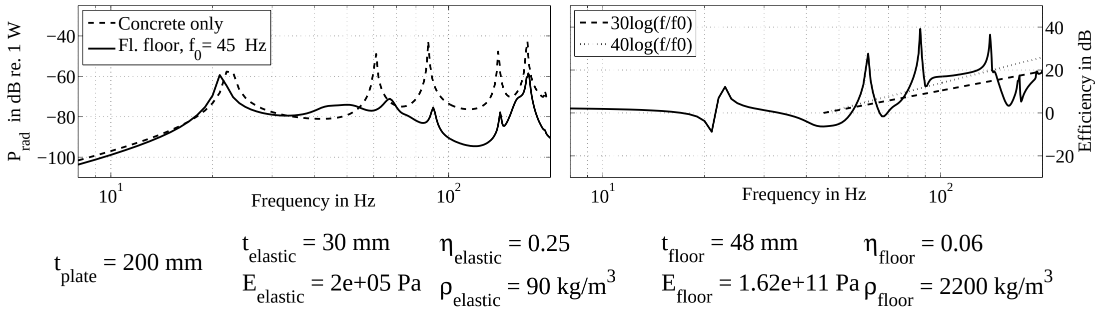

Parameter study result from variant 41.

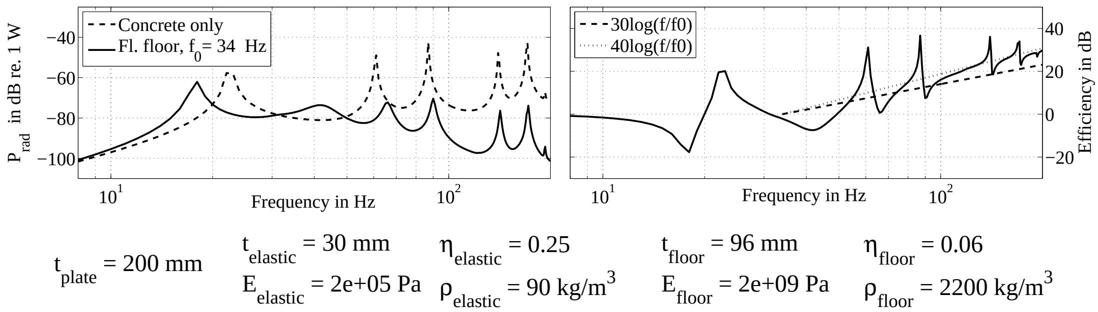

Parameter study result from variant 42.

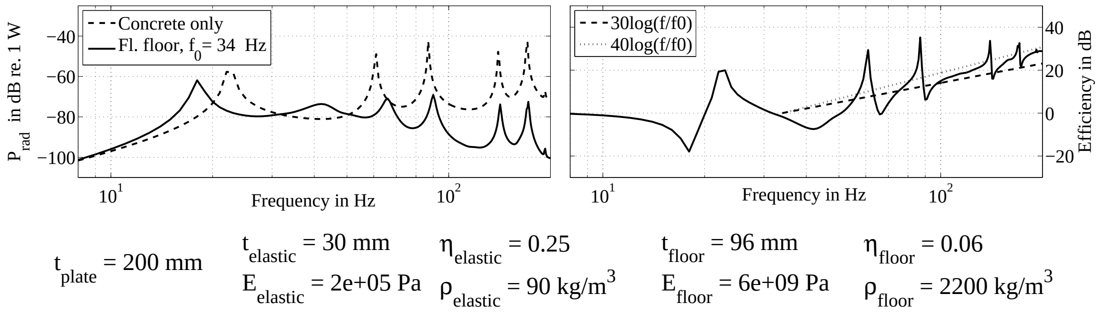

Parameter study result from variant 43.

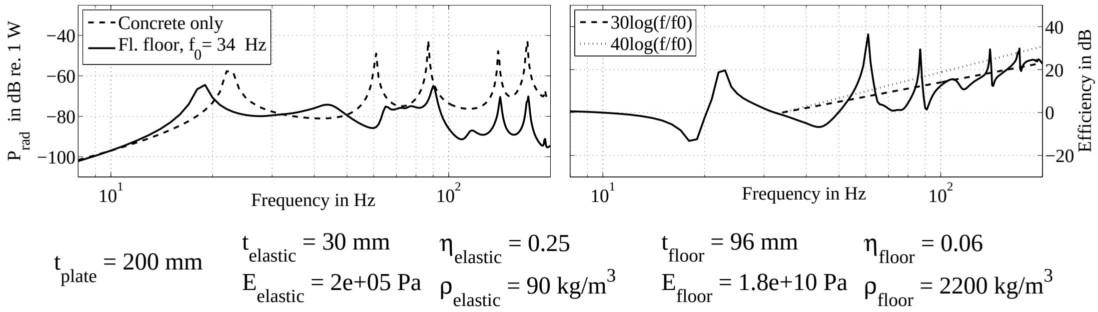

Parameter study result from variant 44.

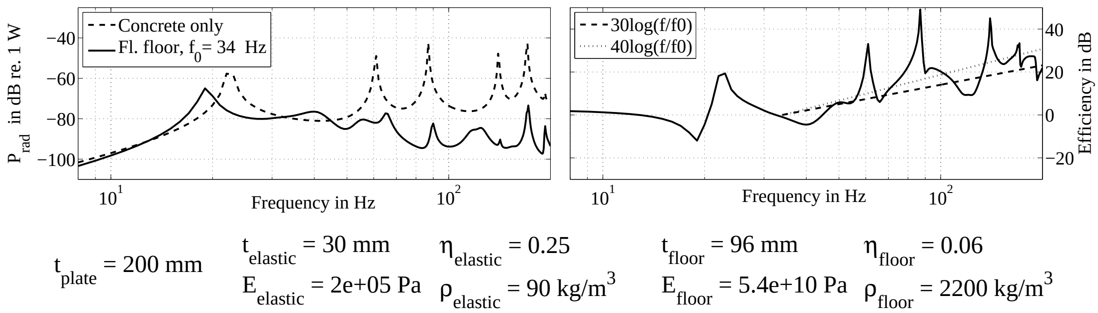

Parameter study result from variant 45.

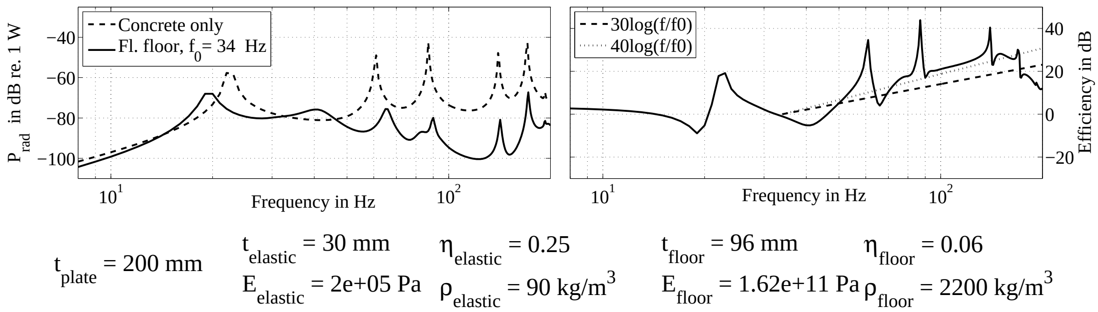

Parameter study result from variant 46.

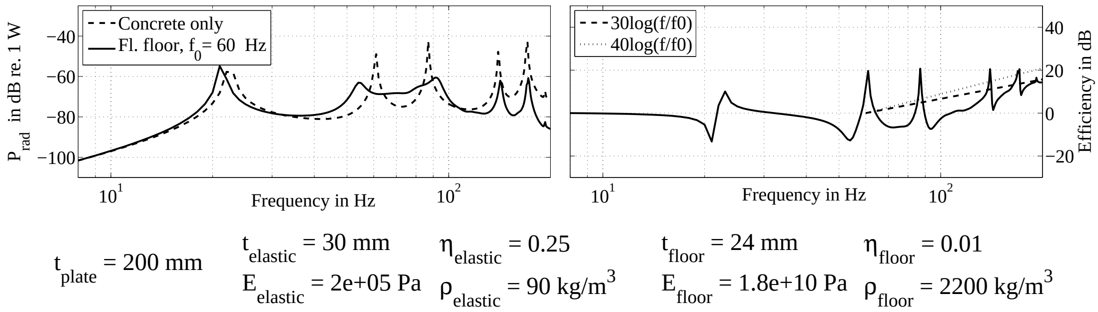

Parameter study result from variant 47.

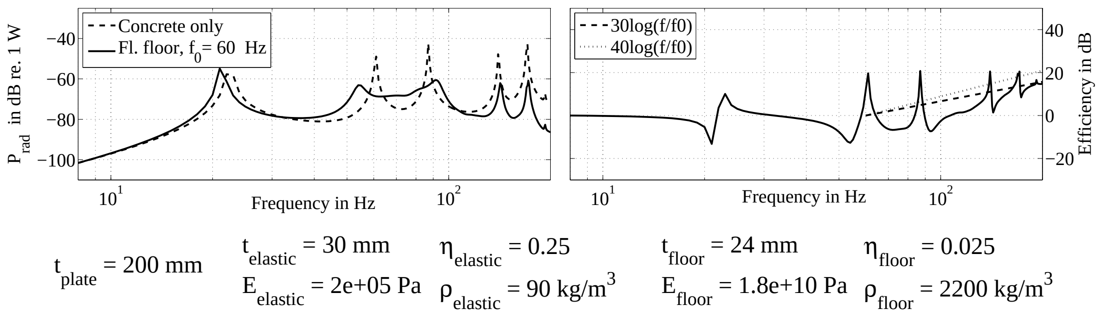

Parameter study result from variant 48.

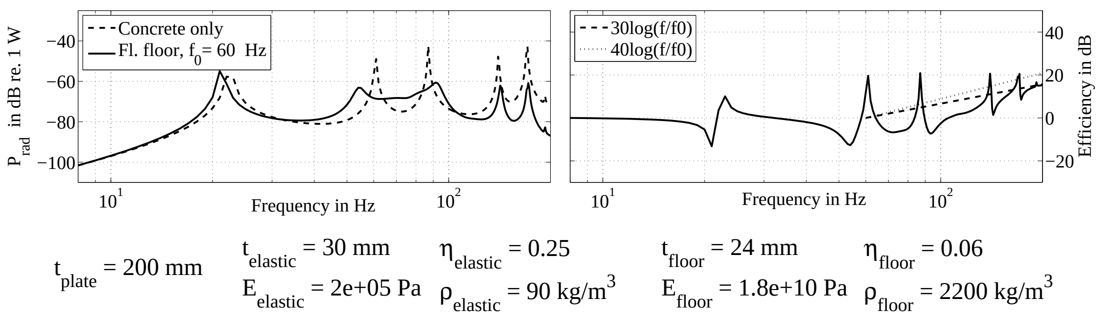

Parameter study result from variant 49.

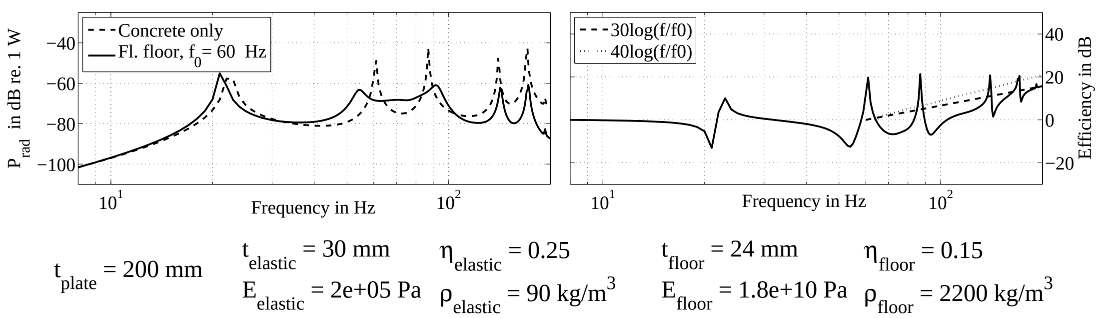

Parameter study result from variant 50.

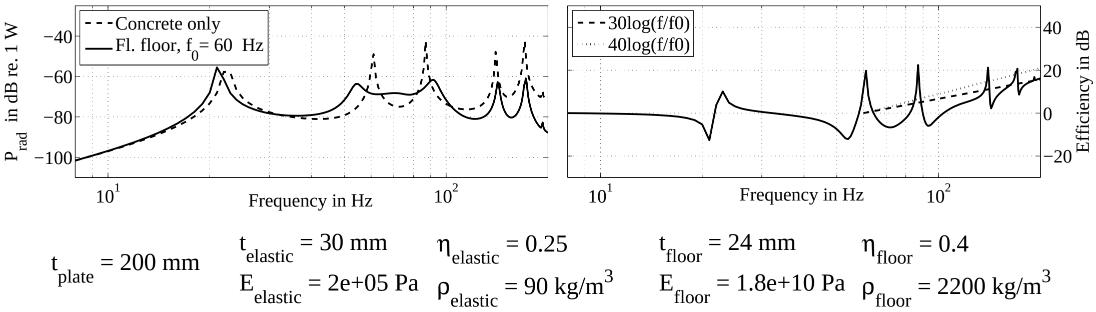

Parameter study result from variant 51.

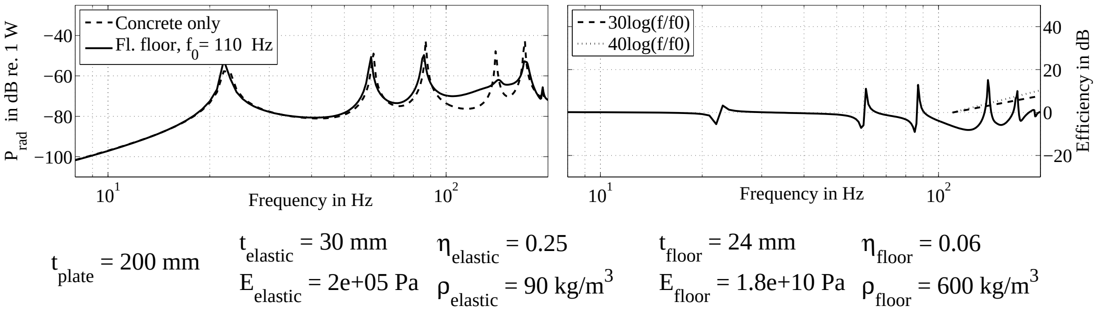

Parameter study result from variant 52.

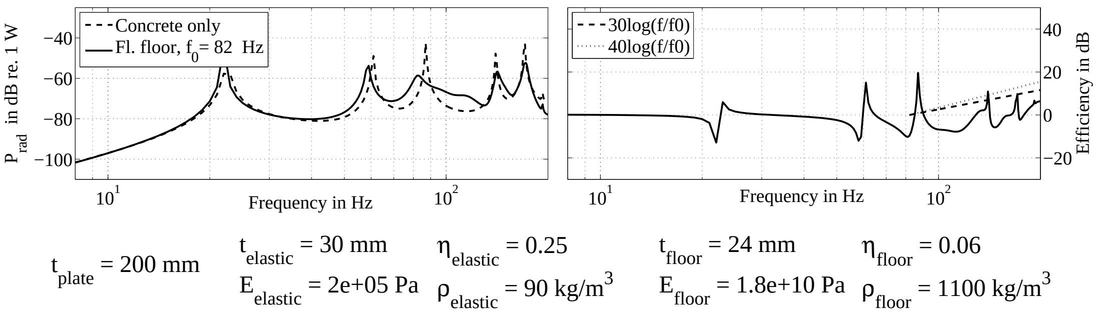

Parameter study result from variant 53.

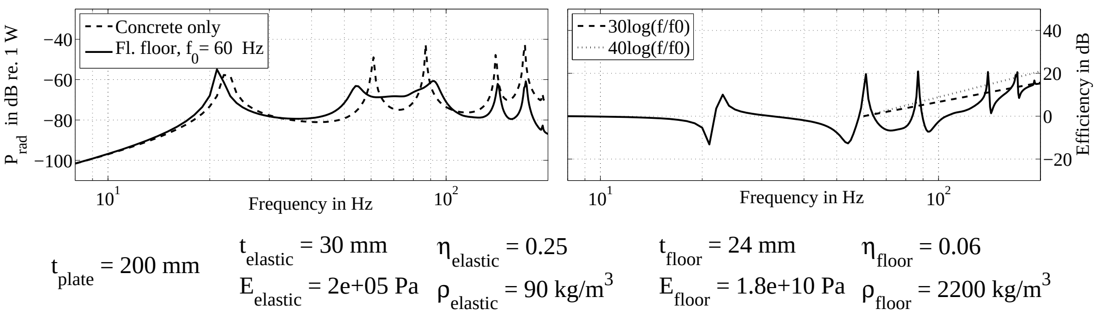

Parameter study result from variant 54.

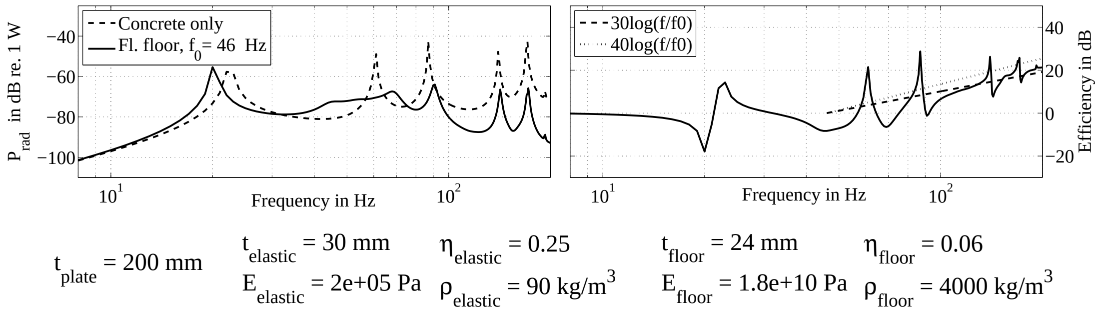

Parameter study result from variant 55.

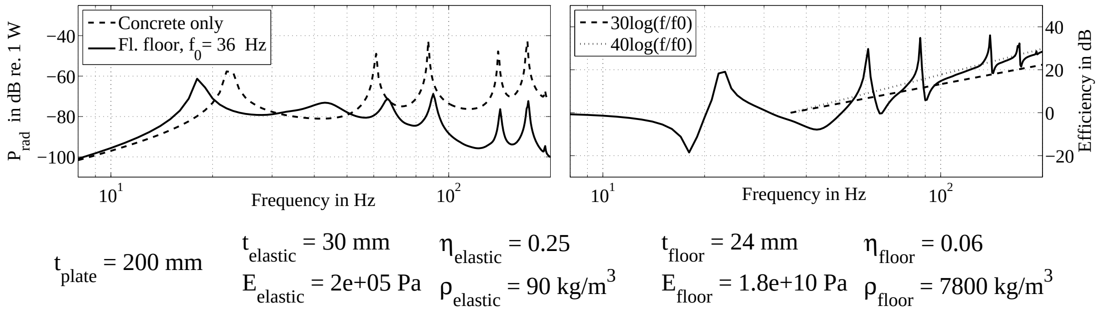

Parameter study result from variant 56.

A.2 CLT parameter study results

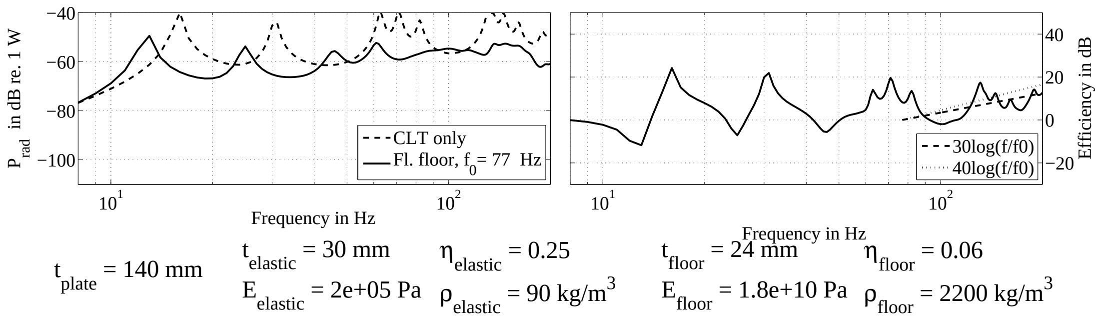

Parameter study result from variant 1.

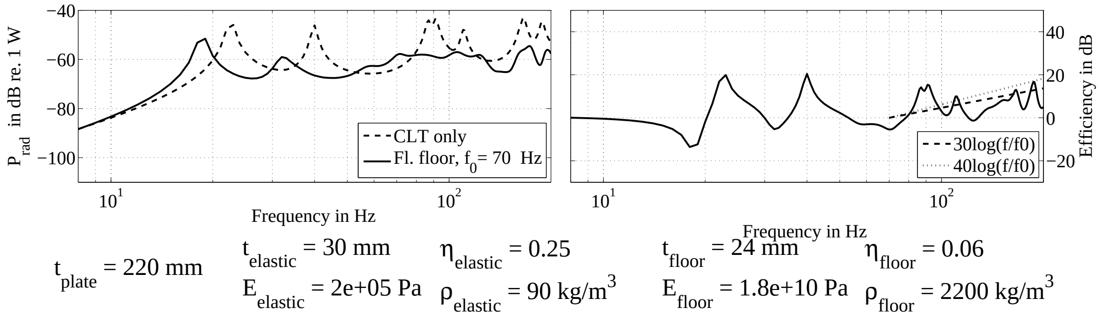

Parameter study result from variant 2.

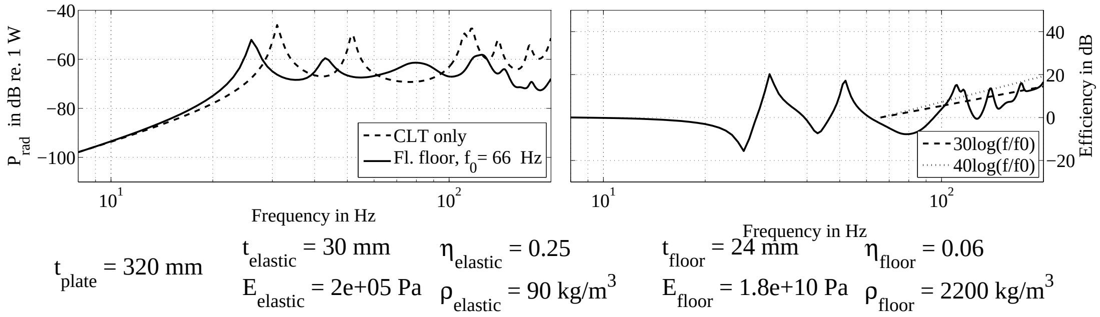

Parameter study result from variant 3.

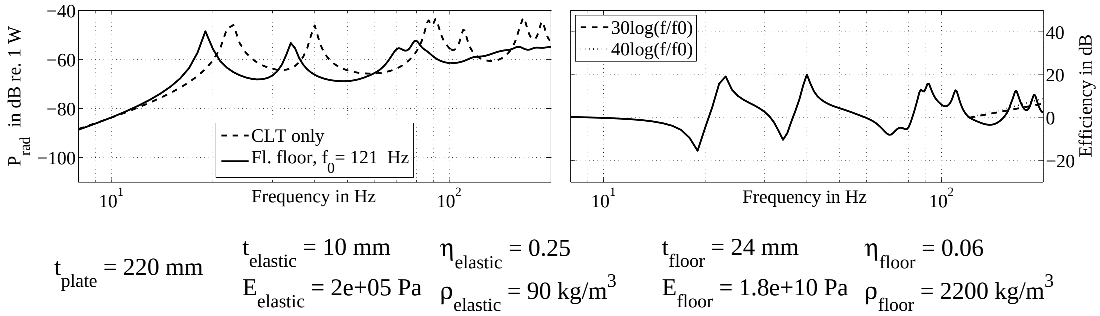

Parameter study result from variant 4.

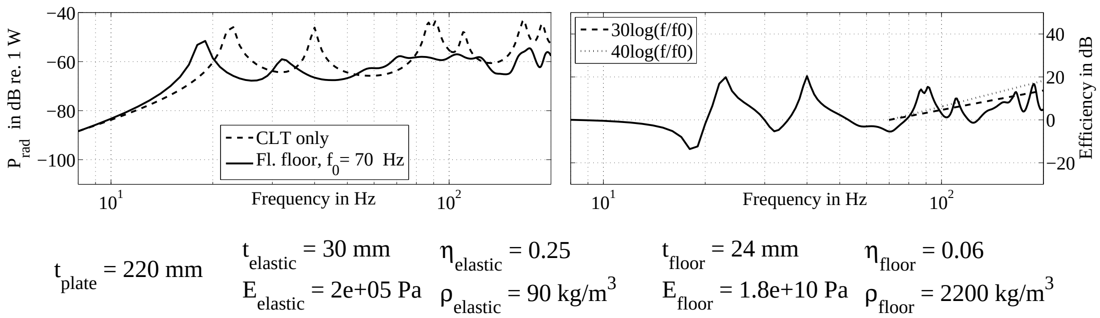

Parameter study result from variant 5.

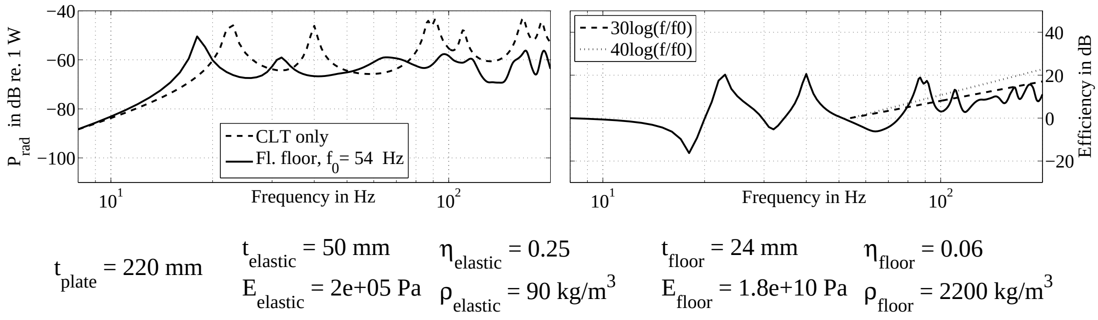

Parameter study result from variant 6.

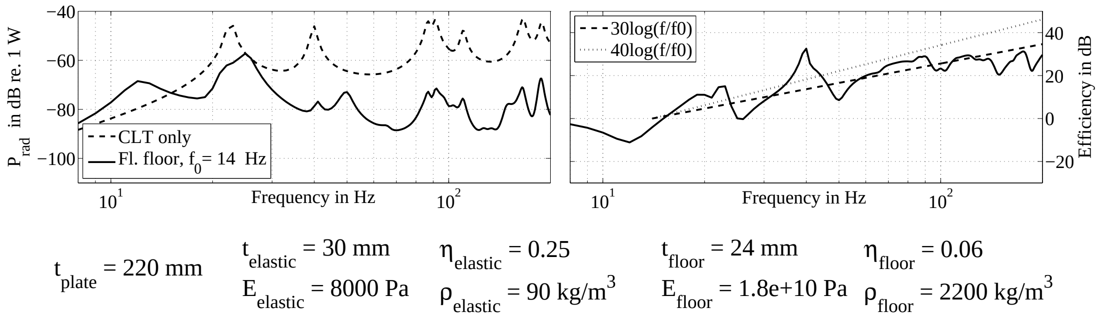

Parameter study result from variant 7.

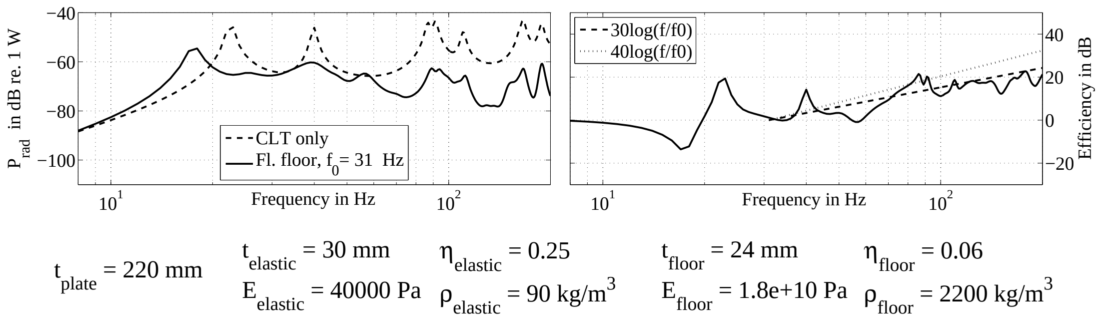

Parameter study result from variant 8.

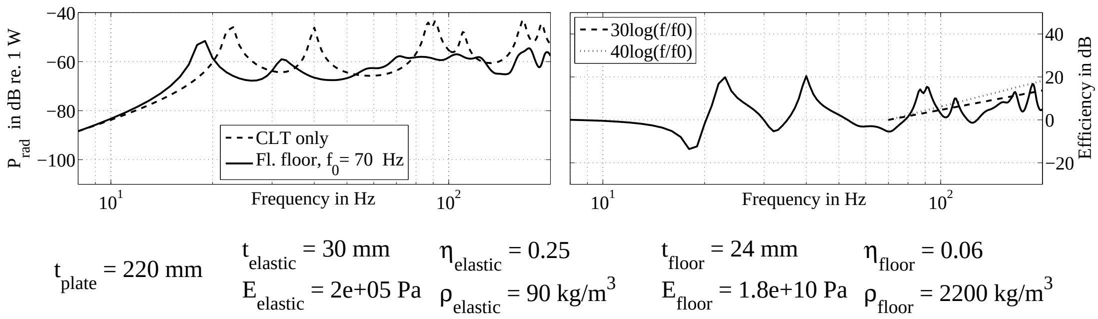

Parameter study result from variant 9.

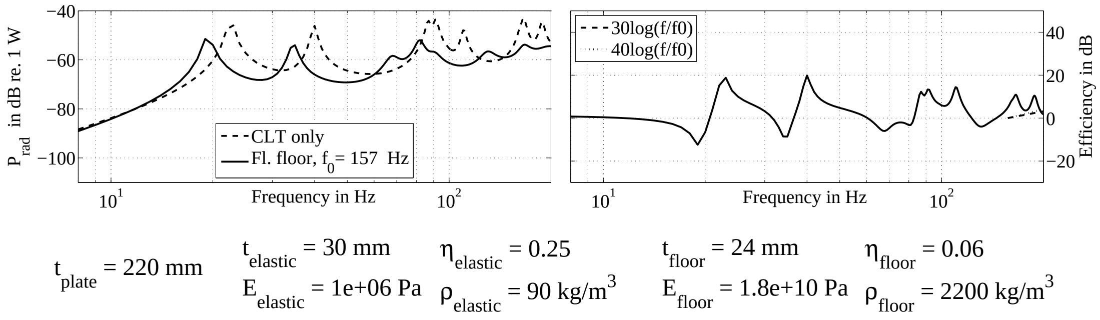

Parameter study result from variant 10.

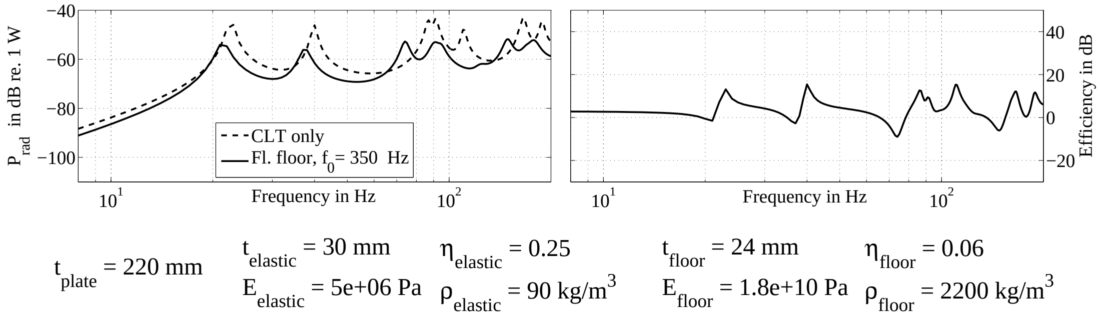

Parameter study result from variant 11.

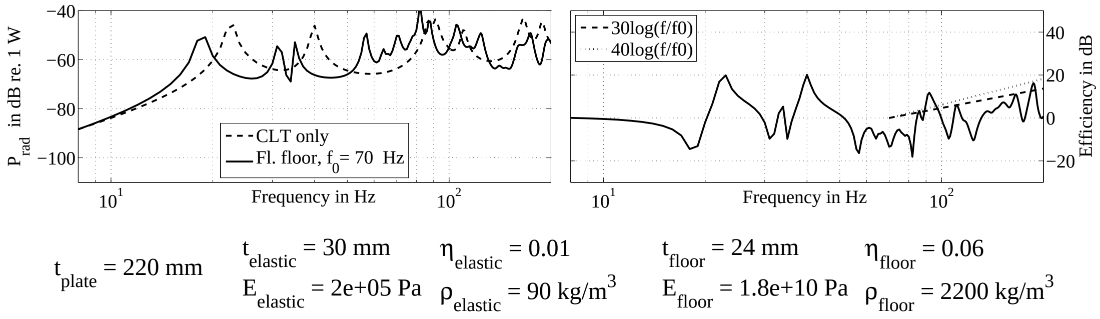

Parameter study result from variant 12.

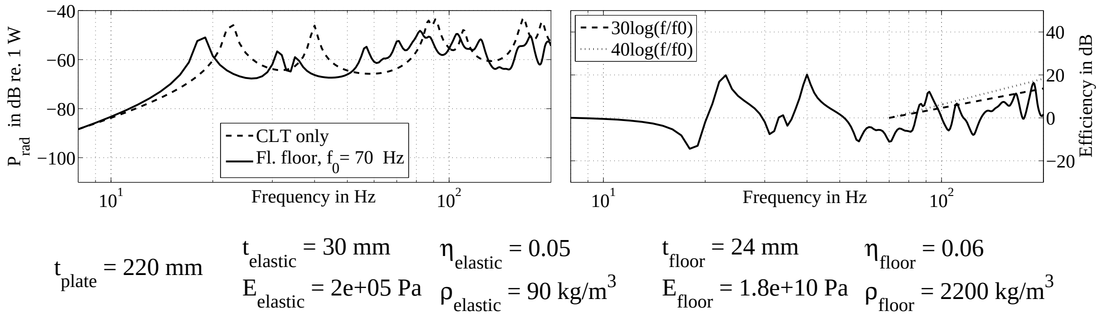

Parameter study result from variant 13.

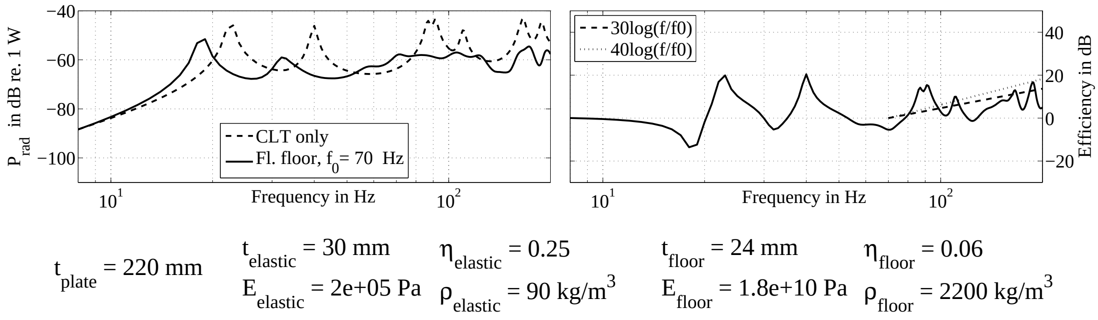

Parameter study result from variant 14.

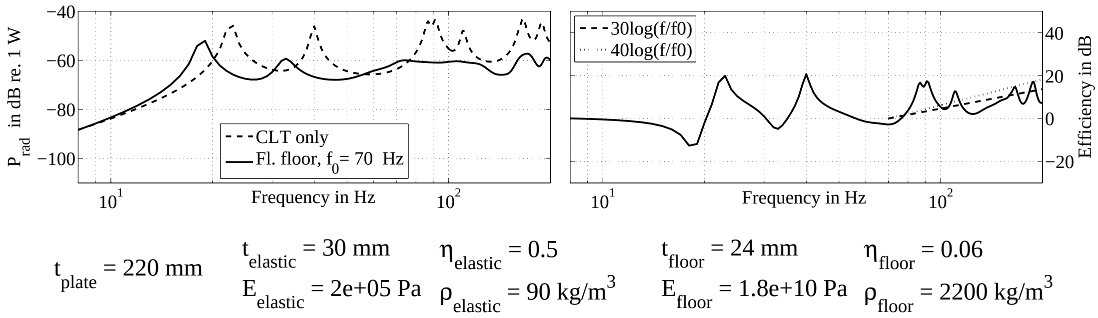

Parameter study result from variant 15.

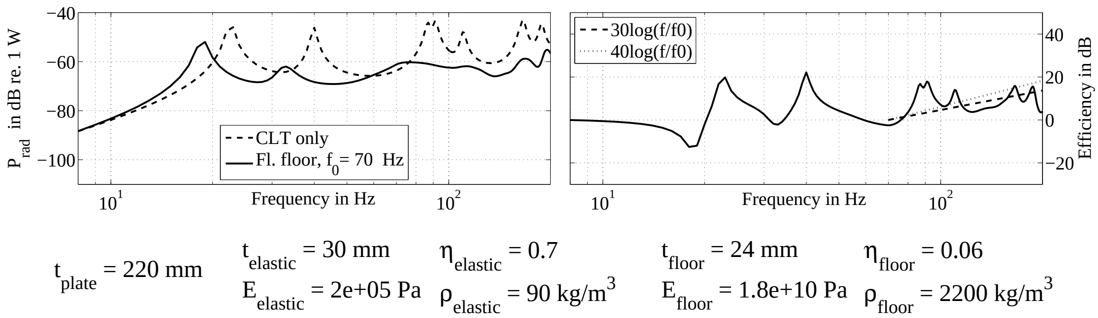

Parameter study result from variant 16.

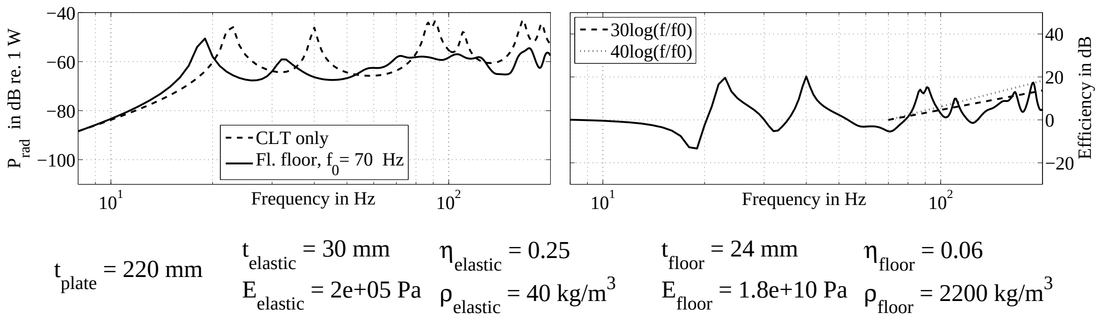

Parameter study result from variant 17.

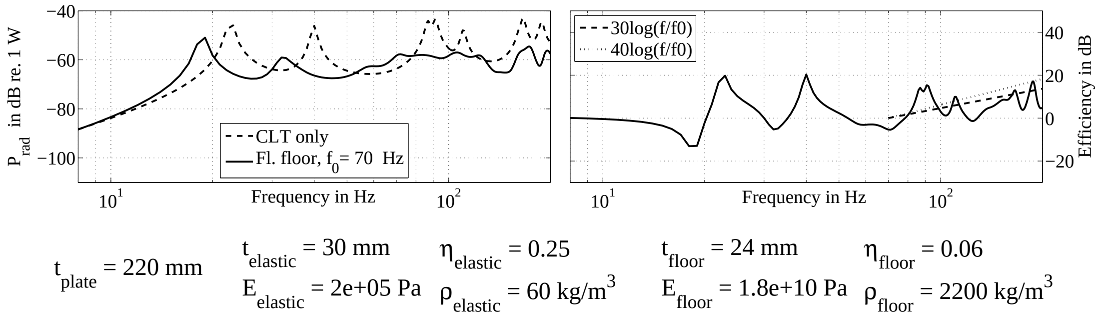

Parameter study result from variant 18.

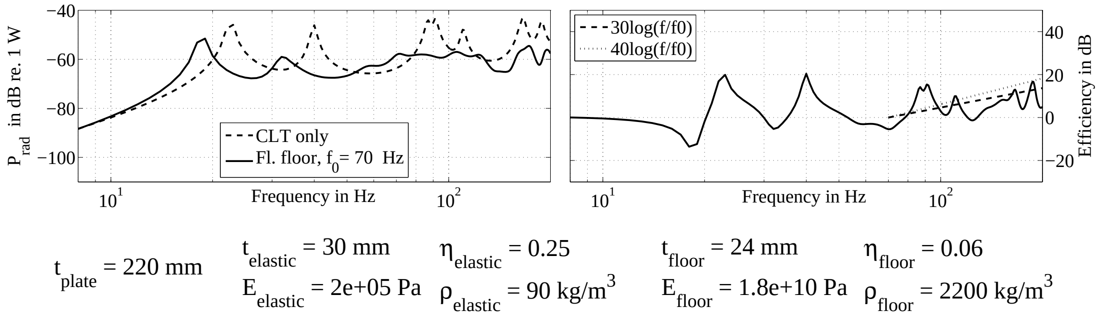

Parameter study result from variant 19.

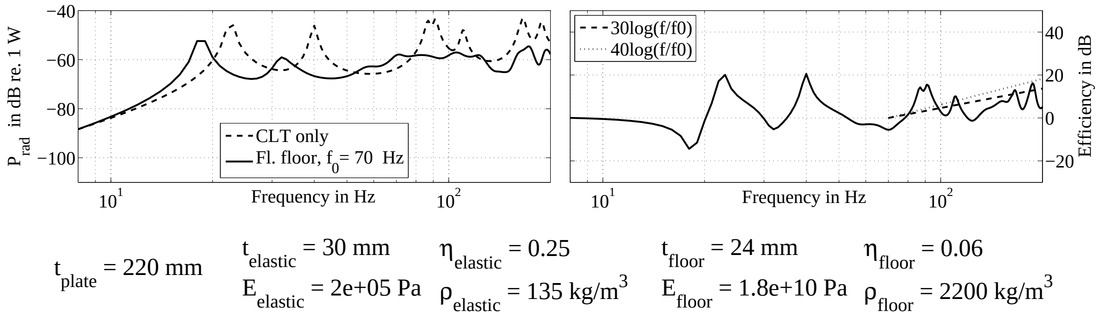

Parameter study result from variant 20.

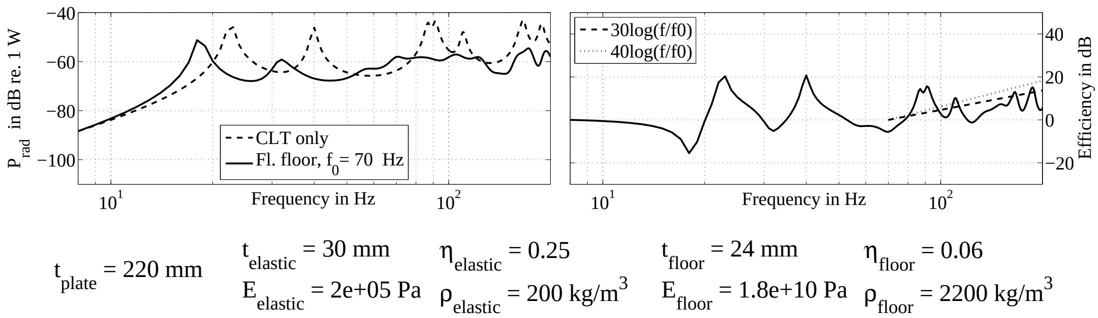

Parameter study result from variant 21.

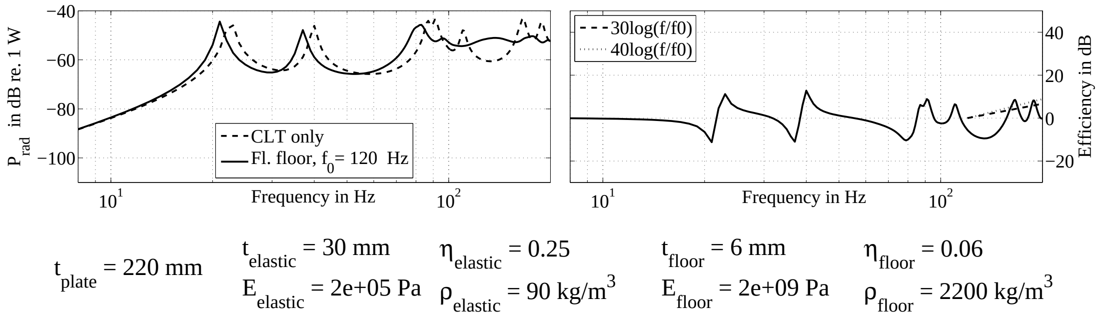

Parameter study result from variant 22.

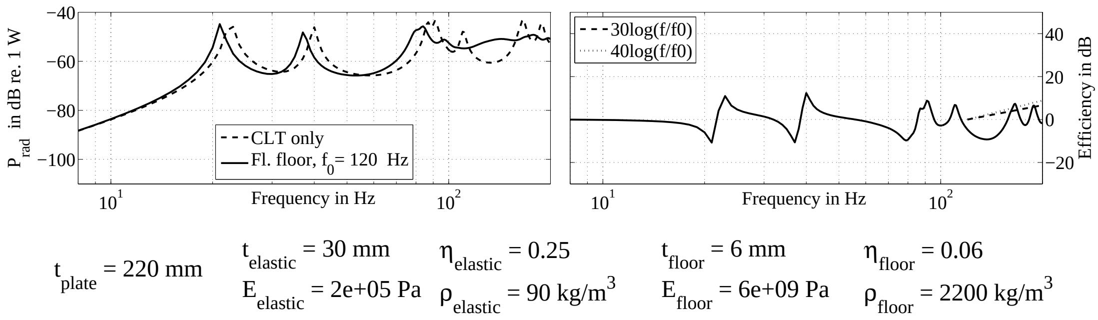

Parameter study result from variant 23.

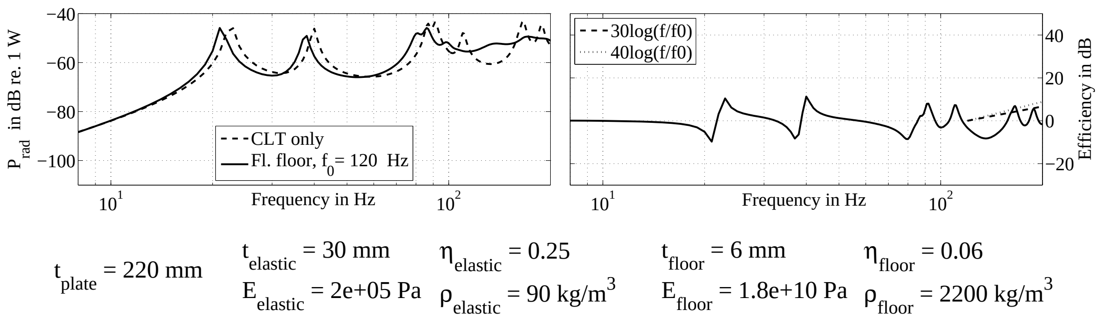

Parameter study result from variant 24.

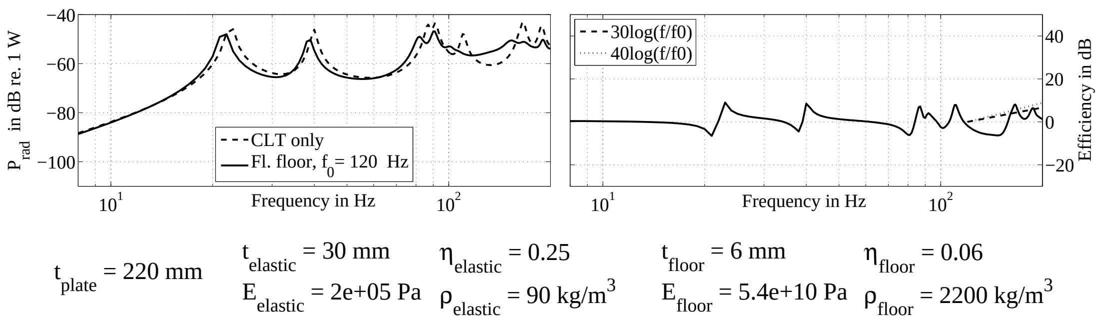

Parameter study result from variant 25.

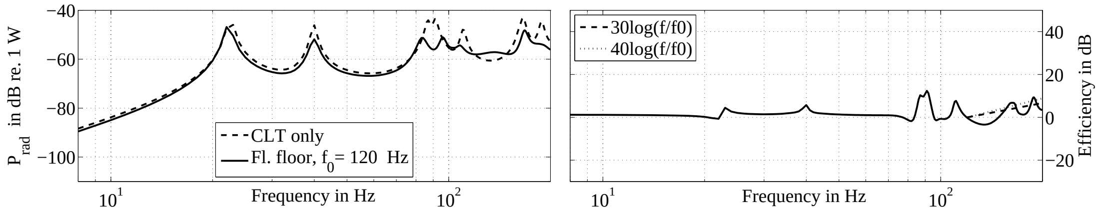

t_{plate} = 220 mm
$t_{elastic}$ = 30 mm $\eta_{elastic}$ = 0.25 t_{floor} = 6 mm η_{floor} = 0.06
$E_{elastic}$ = 2e+05 Pa $\rho_{elastic}$ = 90 kg/m^3 E_{floor} = 1.62e+11 Pa ρ_{floor} = 2200 kg/m^3

Parameter study result from variant 26.

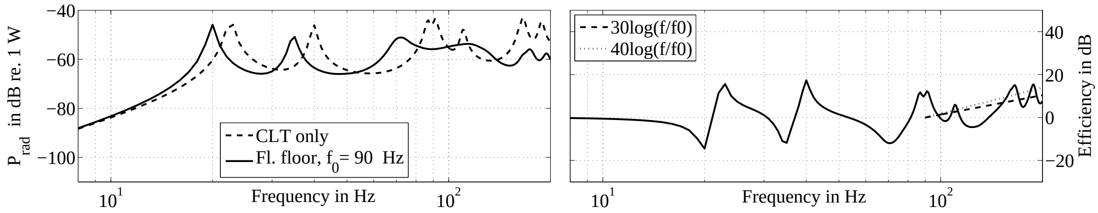

t_{plate} = 220 mm
$t_{elastic}$ = 30 mm $\eta_{elastic}$ = 0.25 t_{floor} = 12 mm η_{floor} = 0.06
$E_{elastic}$ = 2e+05 Pa $\rho_{elastic}$ = 90 kg/m^3 E_{floor} = 2e+09 Pa ρ_{floor} = 2200 kg/m^3

Parameter study result from variant 27.

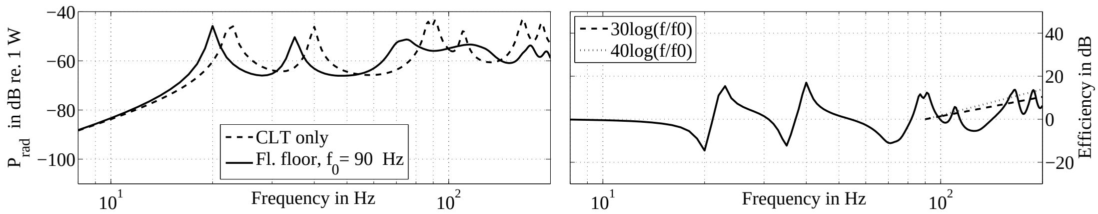

t_{plate} = 220 mm
$t_{elastic}$ = 30 mm $\eta_{elastic}$ = 0.25 t_{floor} = 12 mm η_{floor} = 0.06
$E_{elastic}$ = 2e+05 Pa $\rho_{elastic}$ = 90 kg/m^3 E_{floor} = 6e+09 Pa ρ_{floor} = 2200 kg/m^3

Parameter study result from variant 28.

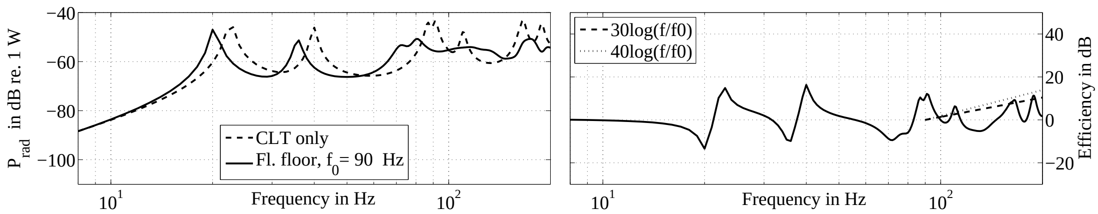

t_{plate} = 220 mm
$t_{elastic}$ = 30 mm $\eta_{elastic}$ = 0.25 t_{floor} = 12 mm η_{floor} = 0.06
$E_{elastic}$ = 2e+05 Pa $\rho_{elastic}$ = 90 kg/m^3 E_{floor} = 1.8e+10 Pa ρ_{floor} = 2200 kg/m^3

Parameter study result from variant 29.

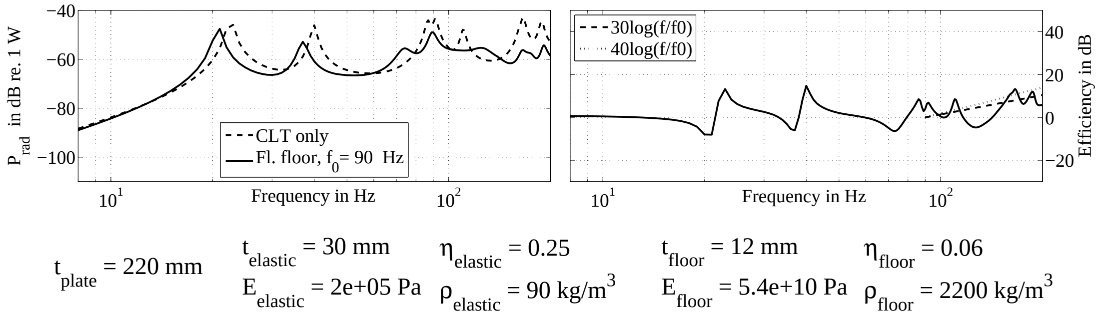

Parameter study result from variant 30.

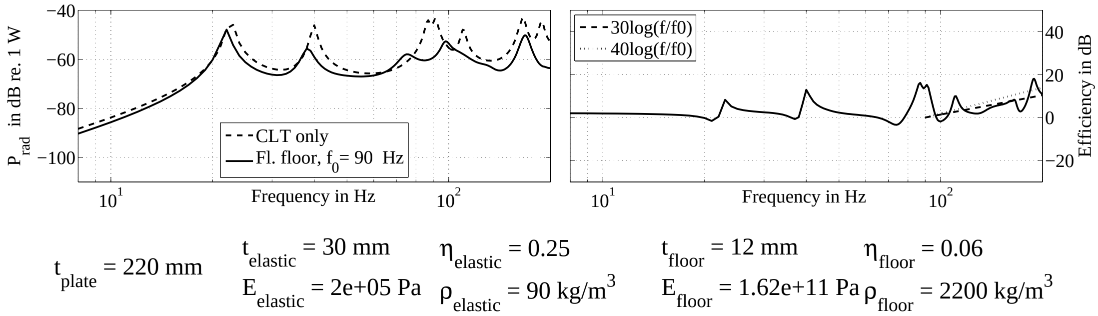

Parameter study result from variant 31.

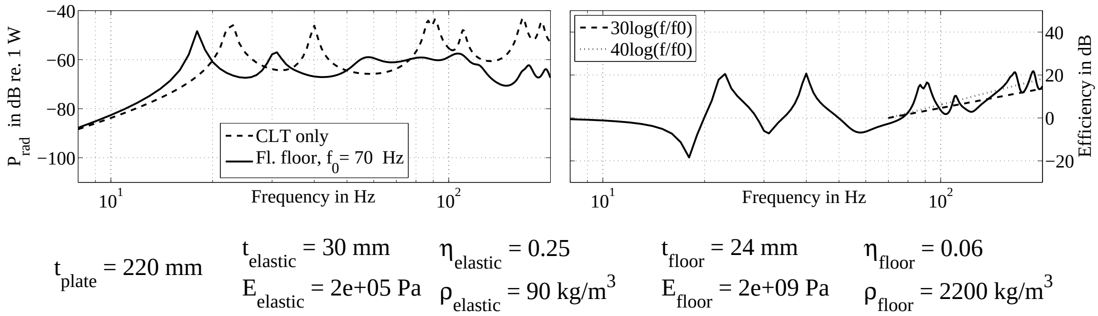

Parameter study result from variant 32.

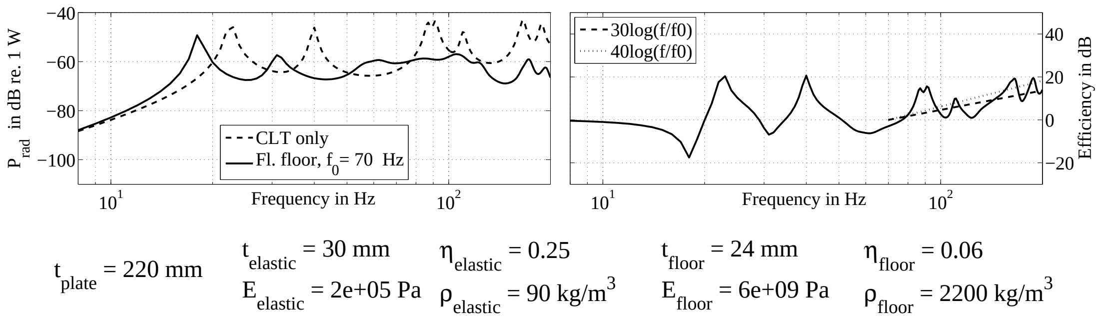

Parameter study result from variant 33.

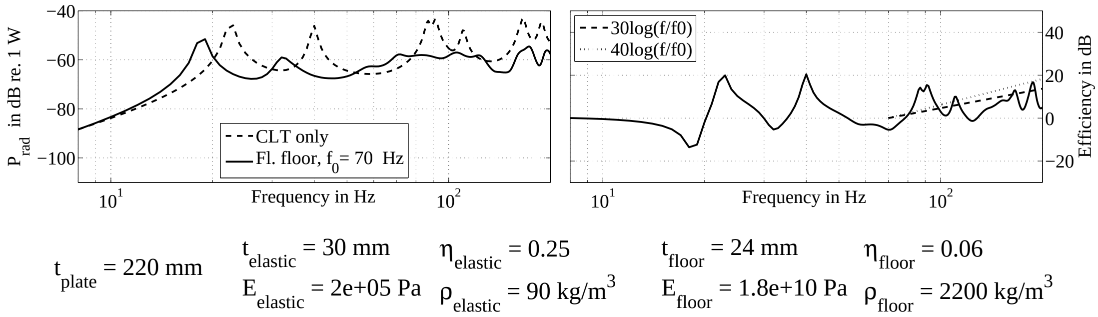

Parameter study result from variant 34.

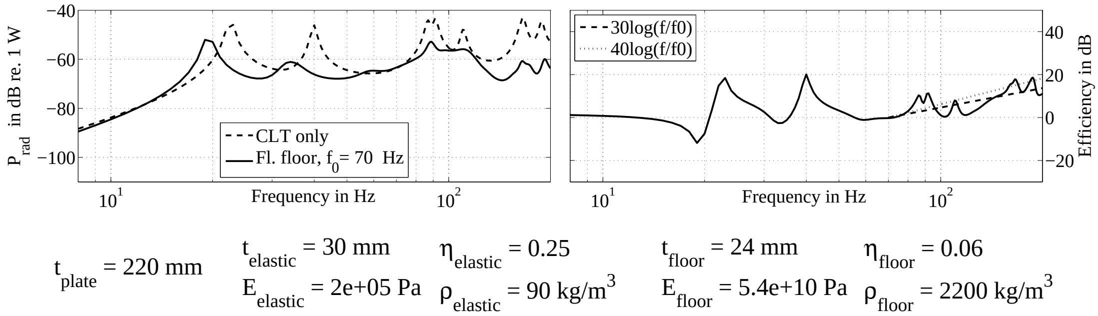

Parameter study result from variant 35.

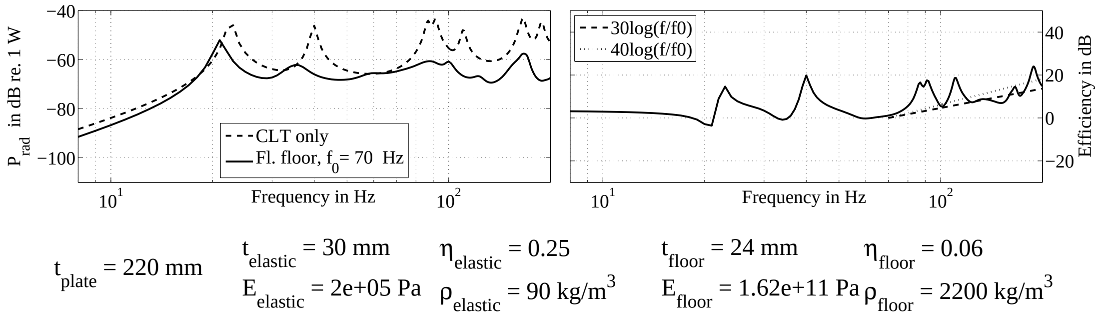

Parameter study result from variant 36.

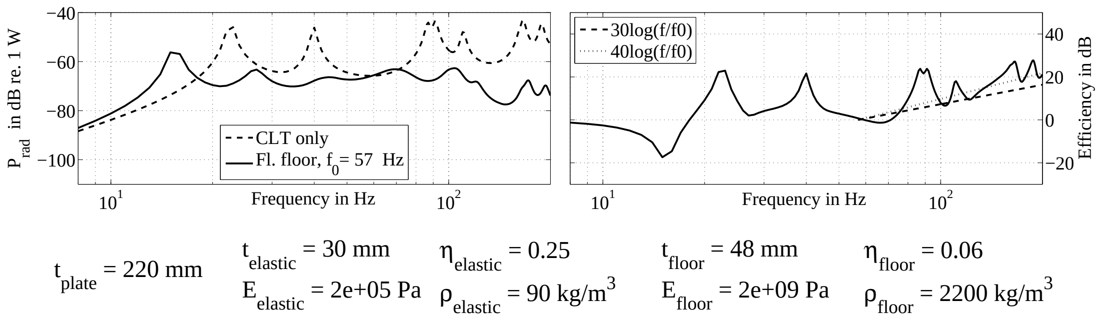

Parameter study result from variant 37.

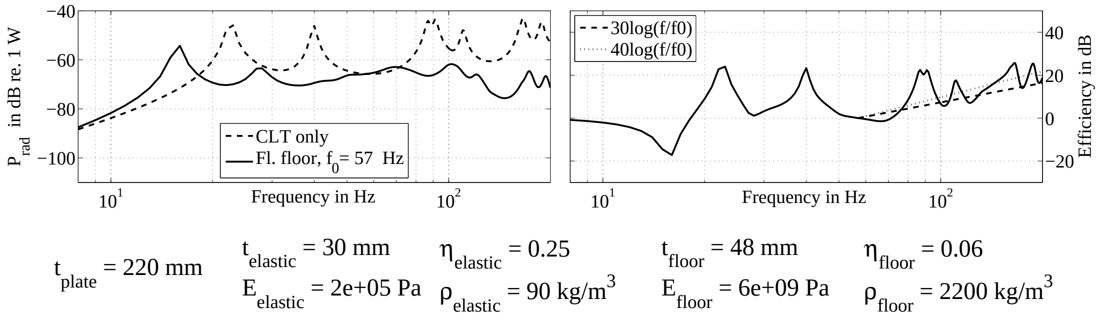

Parameter study result from variant 38.

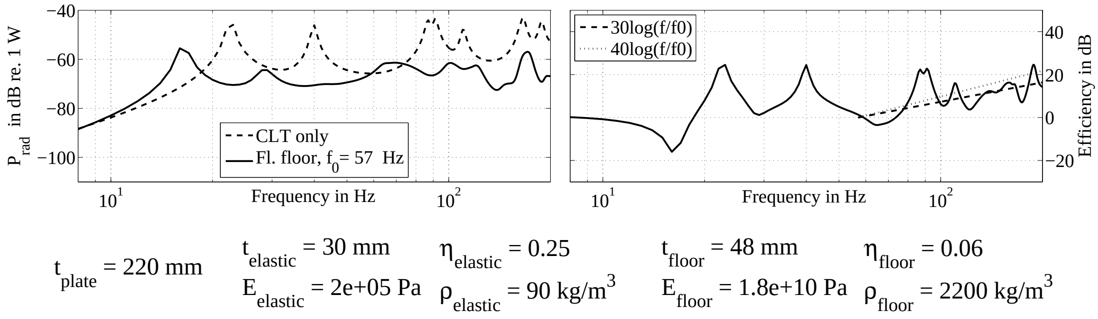

Parameter study result from variant 39.

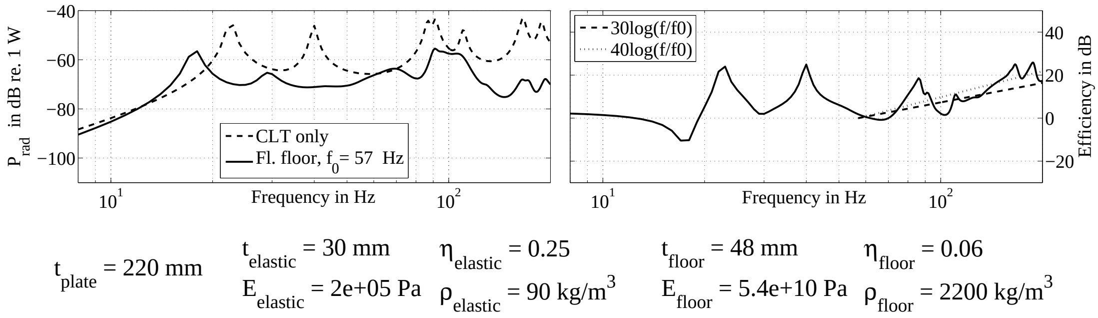

Parameter study result from variant 40.

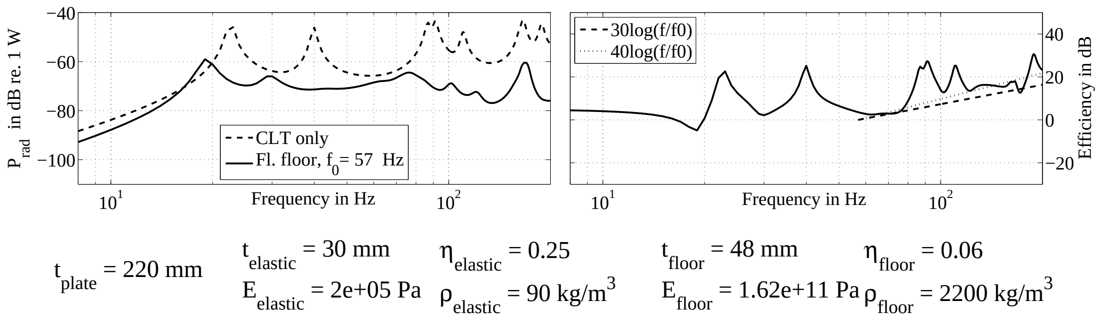

Parameter study result from variant 41.

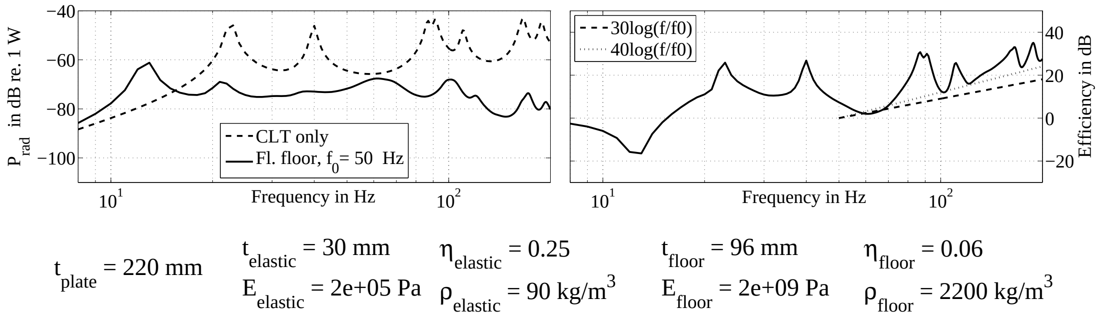

Parameter study result from variant 42.

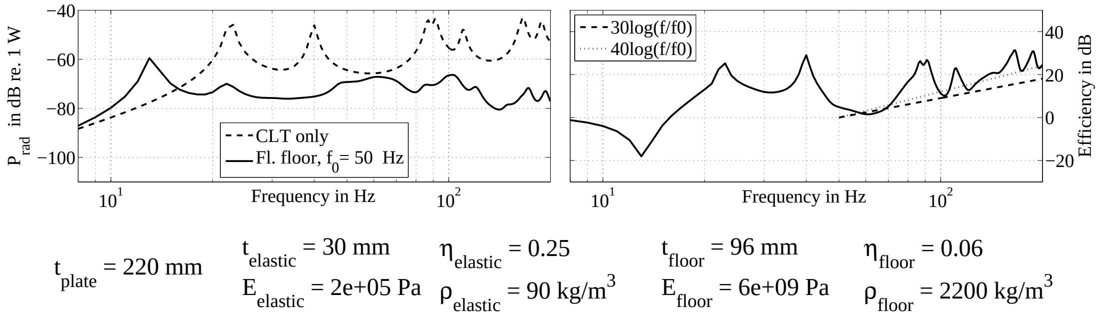

Parameter study result from variant 43.

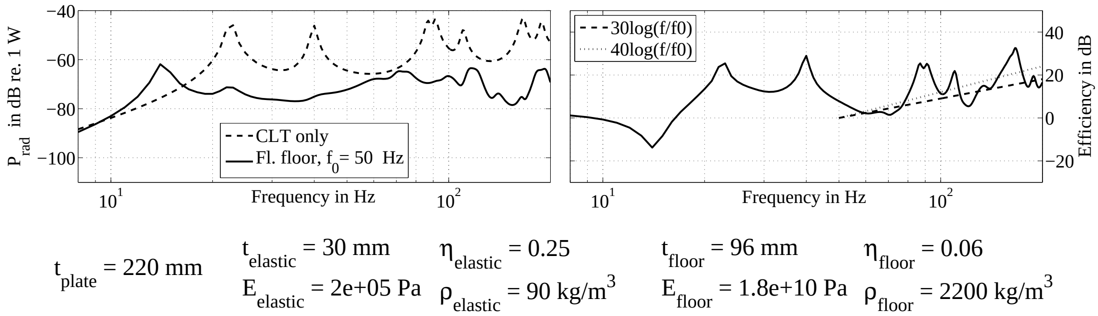

Parameter study result from variant 44.

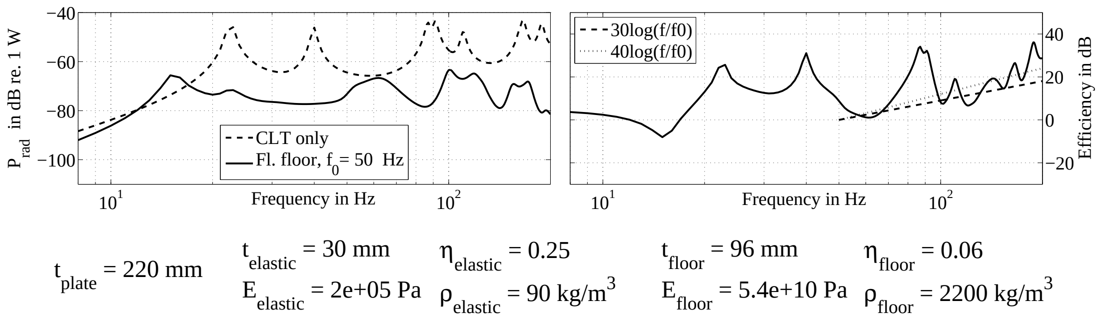

Parameter study result from variant 45.

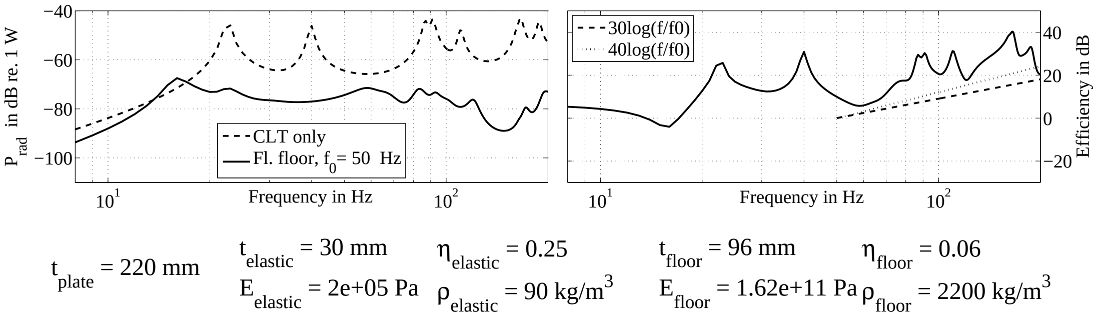

Parameter study result from variant 46.

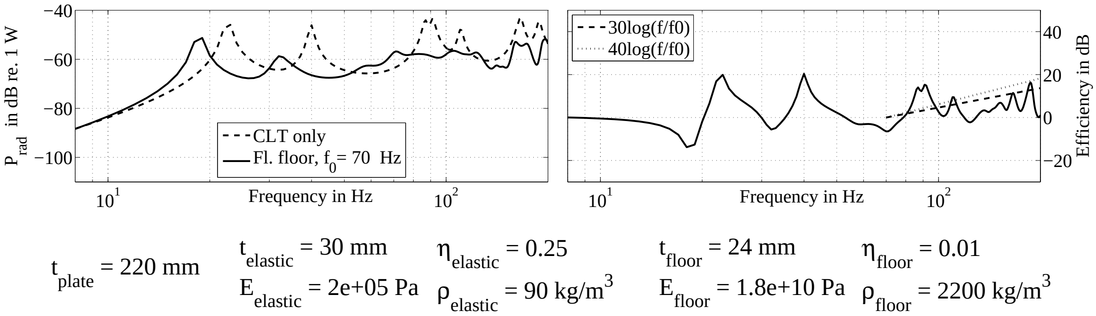

Parameter study result from variant 47.

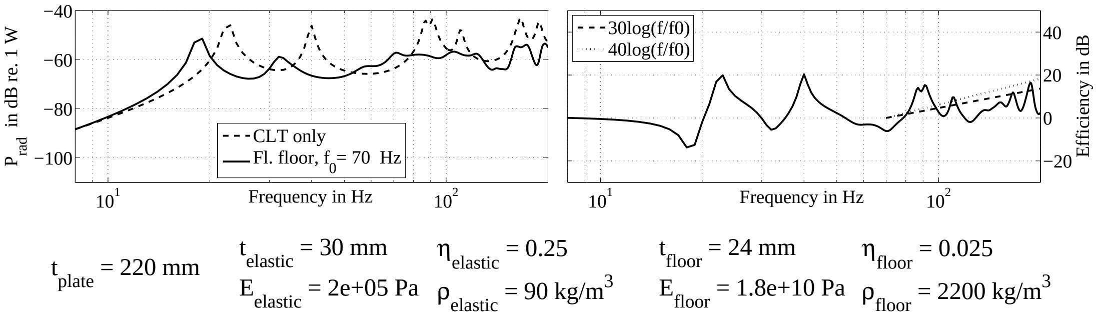

Parameter study result from variant 48.

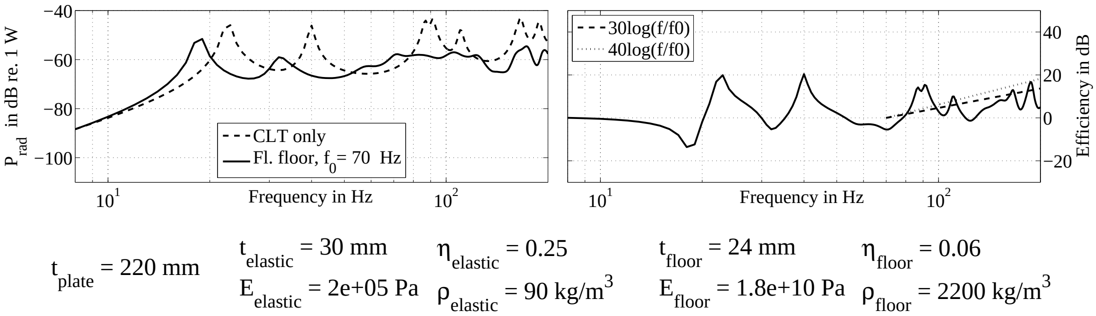

Parameter study result from variant 49.

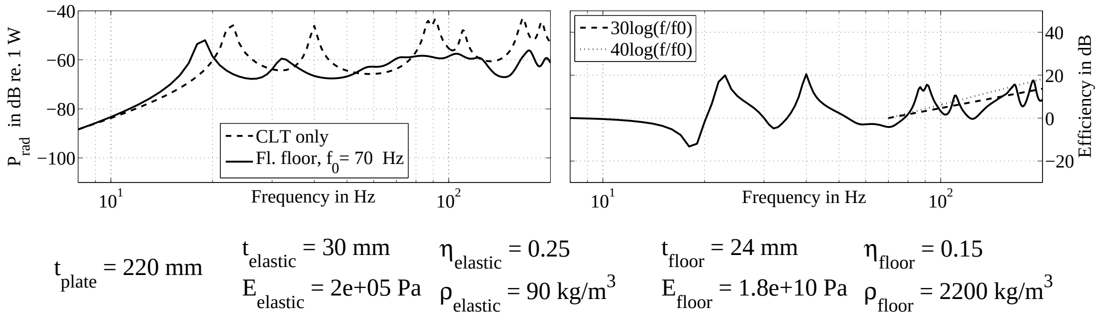

Parameter study result from variant 50.

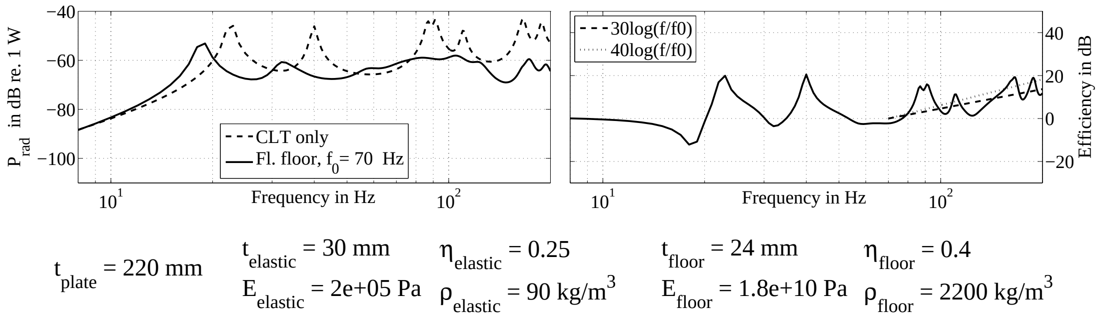

Parameter study result from variant 51.

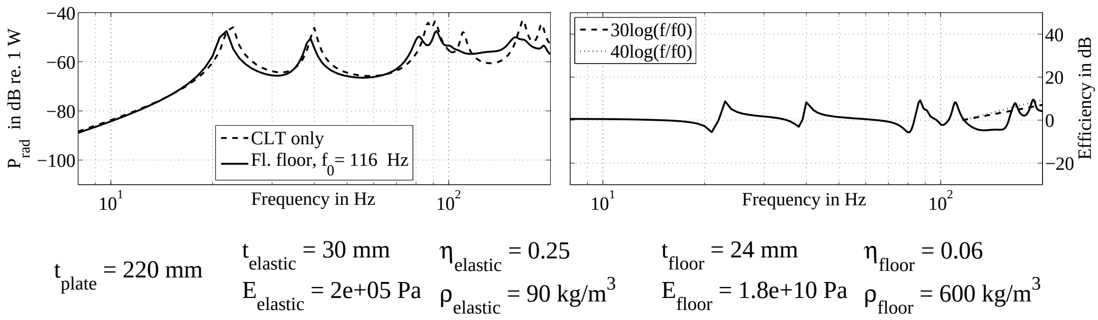

Parameter study result from variant 52.

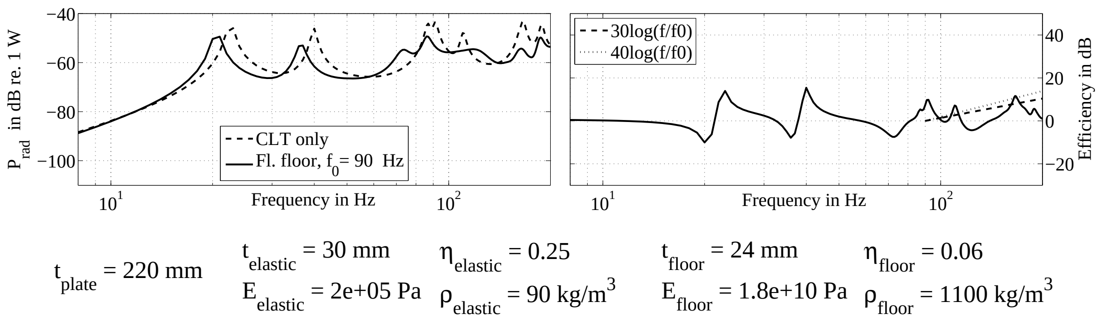

Parameter study result from variant 53.

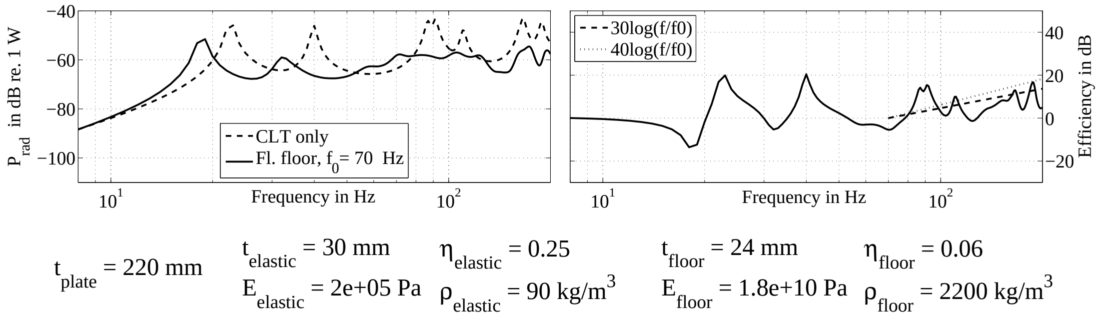

Parameter study result from variant 54.

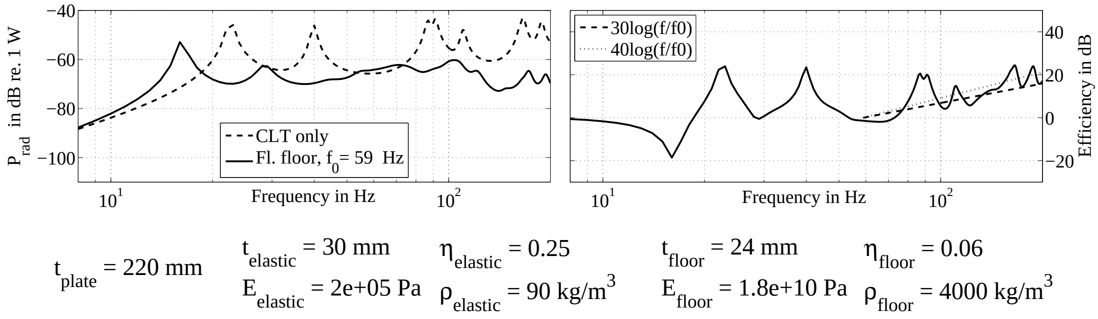

Parameter study result from variant 55.

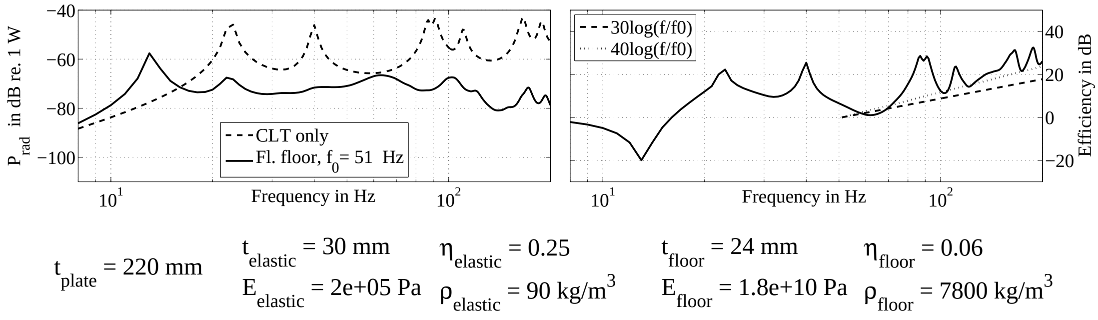

Parameter study result from variant 56.